University of Kerbala

College of Education for Pure Sciences

Department of Chemistry

Theoretical and Experimental Study of the Properties of ZnSe Semiconductor Nanostructures

A Thesis

submitted to the Council of the College of Education for Pure Sciences / University of Kerbala as part of the requirements for obtaining a Master's Degree in Chemistry Sciences

By

Sharemen Sahib Hussein

Supervised by

Assist. Prof. D
Dr. Aula M. AL-Hindawi

Assist. Prof. Dr.
Dr. Jihan Hamid Abul Ameer

2025 A.D

1446 A.H

بِسْمِ اللَّهِ الرَّحْمَنِ الرَّحِيمِ

﴿ وَلَا تَيْأَسُوا مِن رَّوْحِ اللَّهِ ۖ إِنَّهُ لَا يَيْأَسُ مِن رَّوْحِ اللَّهِ إِلَّا الْقَوْمُ الْكَافِرُونَ ﴾

صدق اللَّهُ الْعَلِيُّ العَظِيم

(سورة يوسف –الآية (87))

(Supervisor's Declaration)

I hereby certify that this thesis, entitled: (Theoretical and Experimental Study of the Properties of ZnSe Semiconductor Nanostructures), was prepared under my supervision in the Chemistry Department, College of Education for Pure Sciences, University of Kerbala, as part of the requirements for a Master's degree in Chemistry.

Signature:

Supervisor: Dr. Aula Mahdi AL-Hindawi

Academic Rank: Assistant Professor

Signature:

Supervisor: Dr. Jihan Hameed Abdulameer

Academic Rank: Assistant Professor

Address: University of Kerbala / College of Education for Pure Sciences

Date: 20 / 3 / 2025

Date: 20 / 3 / 2025

(Chemistry Department Head's Declaration)

Referring to the above recommendation submitted by the supervisor, I refer this thesis to the discussion committee for review and approval.

Signature:

Name: Asst. Prof. Dr. Shatha Abdal Amir Jawad

Academic Rank: Assistant Professor

Address: University of Kerbala, College of Education for Pure Sciences

Date: 20/3 / 2025

(First Scientific Approval)

I certify that this thesis, entitled **(Theoretical and Experimental Study of the Properties of ZnSe Semiconductor Nanostructures)**, submitted by (Sharmeen Sahib Hussein), College of Education for Pure Sciences, Department of Chemistry, University of Kerbala, has been scientifically reviewed and is now eligible for discussion.

Signature:

Name: Dr. Hamida Edan Salman

Academic Rank: Professor

Address: University of Kerbala, College of Education for Pure Sciences

Date: 20/3/2025

(Linguistic Evaluator's Declaration)

certify that this thesis, entitled (**Theoretical and Experimental Study of the roperties of ZnSe Semiconductor Nanostructures**), (College of Education for Pure ciences, Department of Chemistry, University of Kerbala), submitted by the student (harmeen Sahib Hussein) , has been linguistically reviewed and any linguistic and rammatical errors have been corrected. Therefore, the thesis is eligible for discussion s far as the integrity of the style and correctness of expression are concerned.

Signature:

Name: Dr. Muayyad Omran Chiad

Academic Rank: Professor

Address: University of Kerbala, College of Education for Humanities

Date: 20 / 3 / 2025

(Second Scientific Criterion Declaration)

certify that this thesis, entitled (**Theoretical and Experimental Study of the operties of ZnSe Semiconductor Nanostructures**), submitted by the student harmeen Sahib Hussein) , from the College of Education for Pure Sciences, epartment of Chemistry, University of Kerbala, has been scientifically reviewed and is w eligible for discussion.

gnature:

me: Majida Hameed Obaid Jassim

cademic Rank: Professor

ddress: University of Kufa - College of Education for Girls

ate: 20/3/2025

(Discussion Committee Approval)

e, the undersigned members of the examination committee, certify that we have reviewed the ıster's thesis entitled (Theoretical and Experimental Study of the Properties of ZnSe miconductor Nanostructures) from the College of Education for Pure Sciences, Department ' Chemistry, University of Karbala, submitted by the student (Sharmeen Sahib Hussein) as ırt of the requirements for the master's degree. After a public examination, it was found to eet the requirements of the degree, and we therefore recommend the thesis be accepted with a rade of "Excellent."

Discussion Committee Chair,

Signature:

Name: Dr. Mohammad N. Bahjat

Academic Rank: Professor

ddress: University of Kerbala / College of Education for Pure Sciences **Date:20/3/2025**

Committee Member

ignature:

ame: Dr. Asmaa Kadim Ayal

cademic Rank: Professor

ddress: University of Baghdad / College Science for Women

ate:20/3/2025

Committee Member

Signature:

Name: Dr. Shatha Abdul Amir Jawad

Academic Rank: Assistant Professor

Address: University of Kerbala / College of Education for Pure Sciences

Date:20/3/2025

lember and Supervisor

ignature:

Name: Dr. Aula Mahdi Al-Hindawi

cademic Rank: Assistant Professor

Member and Supervisor

Signature:

Name: Dr. Jihan Hameed Abdulameer

Academic Rank: Assistant Professor

Address: University of Kerbala / College of Education for Pure Sciences

ate:20/3/2025 **Date:20/3/2025**

pproval of the Deanship of the College of Education for Pure Sciences

pprove the above committee decision.

gnature

me: Dr. Hamida Edan Salman

:ademic Rank: Professor

ddress: University of Kerbala / College of Education for Pure Sciences **Date: 20/3/2025**

Dedication

In the name of Allah, the Most Gracious, the Most Merciful.

“And say, ‘My Lord, increase me in knowledge.’

With deep gratitude and appreciation, I dedicate this work to Allah, the source of all blessings, whose mercy and guidance have illuminated my path. I extend my utmost reverence to the Ahlulbayt (peace be upon them), whose teachings and inspiration have been a constant source of strength in my life.

To my dear familyTo the soul of my beloved father,

whose support was the foundation of my life. Though he is physically absent, his spiritual presence in every achievement continues to give me strength. May Allah have mercy on him and grant him eternal peace.

To the soul of my dear brother, Mahdi Sahib,

who left us in body but never left my heart. His memory has been an inspiration for me to continue striving and dedicating myself. May Allah have mercy on you and bless your resting place.

To my beloved mother,

To my dearest mother, the epitome of sacrifice and unconditional love. Her endless prayers, unwavering support, and profound wisdom have been the foundation of my strength and success. She has given her all for my dreams, and her encouragement has been a beacon through every challenge.

And to my dear sister, Shahnaz Sahib,

To my cherished sister, Shahnaz Sahib, whose tireless efforts and selfless sacrifices have been a pillar of support in my life. She has always been a source of love and strength, and her belief in me has been an invaluable source of motivation.

To my beloved husband, Engineer Wisam Bahra,

who has been my partner every step of the way? Your unwavering support and encouragement have been essential to my success. Balancing my studies with managing our home was not easy, but with your love and support, I was able to achieve my dreams. Thank you from the depths of my heart.

To my dear daughter Asma Wisam Bahra,

who illuminated my life during my master's journey, and who has been a beacon of hope that brightened my path in difficult times? You came into this world despite all the challenges I faced during my pregnancy, yet I managed to maintain my studies because you were always in my heart and mind. Your arrival was like a light that brightened my life, and you are my little angel who gave me the strength and motivation to keep going. I promise to always be a role model for you in striving for success and to work hard to make you proud, just as I am proud of you.

Acknowledgements

First and foremost, I thank Allah for His countless blessings, guidance, and mercy throughout this journey. Without His grace and help, none of this would have been possible. I am forever grateful for the strength He provided me in facing every challenge.

To Dr. Aula Mahdi Al-Hindawi,

who has truly been a source of inspiration for me, providing me with unlimited support and valuable guidance that significantly contributed to my academic development. Your presence was not only in easy times, but you were also my support in the toughest circumstances, and your standing by my side has given me hope and strength to face challenges. I thank you from the depths of my heart for everything you have done for me.

To Dr. Jihan Hamid,

who has never hesitated to provide support and assistance throughout my journey. Your kindness and understanding have had a profound impact on overcoming difficulties, as your insightful guidance has been crucial in improving my academic performance. I thank you for your faith in me and for standing by my side in challenging times.

To the Department of Chemistry in the College of Education for Pure Sciences,

I extend my highest gratitude and appreciation for your ongoing support and encouragement. Your diligent efforts have had a significant impact on my academic journey, as the positive environment in the department has helped enhance my knowledge and skills. Thank you all for your cooperation and support.

O Allah, all praise is due to You as befits the majesty of Your Face and the greatness of Your Sovereignty. I thank You at all times and ask You, O Allah, to bless my knowledge and make me among those who benefit from it and benefit others, for You are the Most Generous, the Bestower.

Abstract

Zinc selenide (ZnSe) is prepared by chemical deposition. The formation of ZnSe nanoparticles in the absence and presence of EDTA was confirmed through Field emission Scanning Electron Microscopy (FE-SEM), Energy Dispersive X-ray Spectroscopy (EDX), Fourier transform infrared (FT-IR), X-Ray Diffraction (XRD), and Raman spectroscopy. The UV-visible spectrum was used to estimate the band gap energy and it turned out to be (3.32 ev and 3.54 ev) for both uncapped ZnSe and EDTA capped ZnSe nanoparticles. The optical properties of the prepared nanomaterials covered with the polymer or not covered were also studied. Then the theoretical part of this work was moved using special program Gaussian View 6.0 Gaussian 09W Chem Draw don professional 15.0, In order to the results of the practical part with the theoretical one.

In this study EDTA acting as a capping agent. The samples were prepared and analyzed using a variety of analytical techniques, The results showed that EDTA acts as an effective capping agent, regulating the size of the nanoparticles and preventing aggregation, resulting in enhanced stability of ZnSe. UV-Vis spectroscopy measurements revealed an optical band gap suitable for optoelectronic applications, with EDTA influencing the material's optical properties. XRD analysis revealed the formation of a well-ordered crystalline structure with a significant reduction in crystal size due to the effect of EDTA characteristics of zinc selenium.

The purity of material's was enhanced by the capping, which also stopped the production of unwanted contaminants, as demonstrated by the FTIR and Raman data, which clearly showed an interaction between ZnSe and EDTA. When the prepared sample was subjected to EDS analysis, the elements were distributed uniformly.

Low affinity energy thresholds were precisely tailored into the Zn_3Se_3 cluster's molecular geometry configurations both before and after the addition of ethylenediaminetetraacetic acid (EDTA). Theory of density functionals and the structural and electronic characteristics of the Zn_3Se_3-EDTA composite were examined using DFT/B3LYP calculations using the 6-113G (d, p) basis set. Comprehensive vibrational mode frequencies were methodically examined using potential energy distribution as a basis for analysis. Theoretical conclusions regarding the active peaks of the O–H, N–H, C=O, and Zn–Se functional groups were evaluated using the FTIR spectra of the designated compounds. The energy

gap ($E_{\boldsymbol{g}}$) resulting from the difference between those orbitals was computed and plotted using the frontier high occupied and low unoccupied molecular orbitals (HOMO&LUMO). Before and after adding EDTA, the promising indicator was achieved at increasing $E_{\boldsymbol{g}}$ from 0.03833 eV to 0.1379 eV, highlighting the capping agent effect of the organ compound on the Zn_3Se_3 surface. In addition, the molecular electrostatic potential is surface and contour diagram of Zn_3S_3 and Zn_3S_3_EDTA were determined, along with electronic properties of the stated structures, including Ionization potential (IP), Electron affinity (EA), Ef, Energy Gap ($\boldsymbol{Eg}$), Chemical Potential ($\boldsymbol{Cp}$), Electronegativity (χ), Global Hardness (η), Chemical Softness (S), Electrophilicity ($\boldsymbol{\omega}$) and Nucleophilicity (ε),

The study concluded that the properties of the nanomaterial, such as stability and size control are much improved when EDTA is used as a capping agent during the manufacture of ZnSe.

Table of Contents

Abbreviation form	Abbreviation meaning
A	Absorbance
D	The average crystallite size
Ec	Connecting band energy
EDX	Energy dispersive X-ray spectroscopy
Eg	energy band Gap
Eph	The energy of the auxiliary phonon
e V	Equivalence band energy
ZnSe _ EDTA	Zinc selenide - Ethylenediaminetetraacetic acid
FE-SEM	Field Emission Scanning Electron Microscope
FTIR	Fourier Transform Infrared Spectrophotometer
H	Planck constant.
ICDD	Center International Data Diffraction

I^0	Incident Light Intensity
LCAOs	Linear Combination of Atomic Orbitals
IA	Absorbance Light Intensity
IR	Reflected Light Intensity
IT	Transmitted Light Intensity
$K_{\circ}$	Extinction Coefficient
N	Complex refractive index.
STOs	Slater-Type Orbitals
N	An integer called the order of reflection
n_o	The real part of the complex refractive index.
NPs	Nanoparticles
R	Reflectivity
T	Transmittance
T	The thickness of the sample
UV-Vis	UV. Visible spectrometry
XRD	X- Ray Diffraction
A	Linear absorption coefficient
Θ	Bragg angle
λ	Wavelength

$Ylm\ (\theta, \Phi)$	A spherical harmonic
R (r)	Radial part of the atomic functions $Rnl(\vec{r})$
N	Normalization constant
n*	Active principal quantum number

Chapter One

Introduction

1.1 Nanotechnology

The term nanotechnology deals with materials at the nanoscale, or one billion times smaller than a meter. This technology has received potential attention in last decade due to its ability to create and manipulate materials at nano-scale range, leading to produce materials with incredible features. These features, including chemical physical, and biological, are quit differ from their counterpart bulk material. For instance, bulk gold is known to be chemically inert and unsuitable for the use as a catalyst, however, when the size of gold reduces to 1 nm, it exhibits exceptional catalytic properties. Moreover, the movement of copper atoms leads to making bulk cupper bend easily while as the cupper size reduced to less than 40 nm, the copper becomes super-hard materials, and they differ from bulk copper in their characteristics.

The term nanotechnology was referred to the 4th century, when the king ancient Roman cup (Lycurgus Cup) illuminated different color when exposed to light. The cup appears green in natural light and red when a candle or other light source is placed inside the cap. Recent studies showed that the cup contains 50–100 nm gold and silver nanoparticles and these particles absorb and scatter green and blue colors because they have shorter wavelengths of light. [1] .This cup also transmits longer wavelength such as red and orange. The choice of gold and silver nanoparticles is essential for creating a dichroic effect, which occurs due to the fact that their electrons can oscillate at frequencies that correspond to visible light. X-ray analysis was also used to examine these nanoparticles and the result showed that the romain cap had an alloy of silver and gold (Ag-Au) with an Ag:Au ratio of about 7:3 in its composition. [2,3]

In 1959, the term nanotechnology was first introduced by Richard Feynman (an American physicist who earn Nobile prize) in his talk in American Physical Society. He said that the bottom contains a large number of rooms. That is, objects at the atomic size can be easily manipulated.[4]

Researchers are moving more quickly to advance the field of nanotechnology as a result of the development of electrical and probe microscopic techniques in the 1980.[5]

1.2 Applications of nanotechnology

Numerous applications can be identified or have been proposed in numerous areas due to the potential chemical and physical properties of nanomaterials, as shown in Figure 1.1 One such instance is the discipline of medicine, or nanomedicine, which deals with the prevention, diagnosis, and treatment of various illnesses, including cancer, Parkinson's disease, Alzheimer's disease, and many more. [6]The diagnosis and treatment of cancer cells could be greatly enhanced by nanomaterials. The use of nano-based medicines and diagnostics has advanced significantly, and many more interventions are being developed, despite the fact that scientists and engineers only began investigating these technologies in the 1980. This could be because their ability to increase the sensitivity of these cancer cells to radiation therapy, they may also be used as carriers to deliver treatments to the cancer cells.[7] This is done through the functionalization of ligands (antibodies, and peptides) that bind to receptors on the surface of the cancer cell.[8]This receptor-ligand-nanoparticle complex then enters the cell through endocytosis and leads to gene expression and cellular effects.[9]Gold nanoparticles were the most important nanomaterials used in cancer treatment, they have been shown to absorb near infra-red (NIR) light and convert it into heat, this heat can destroy cancer cells

when they accumulate in the tumour cell, and this is done without damage to the surrounding tissue.[10]

Owing to their tunable physicochemical properties such as melting points, electrical and thermal conductivities, light absorption and scattering characteristics, optical sensitivity, (photo) catalytic activity, and wettability, they can be used in the production of solar cells and optoelectronic devices. Furthermore, advances in nanotechnology are being made in the fields of agriculture, nanoelectronics, nanomedicine, sensor development, energy storage devices, catalysts, and other areas. [11-13]

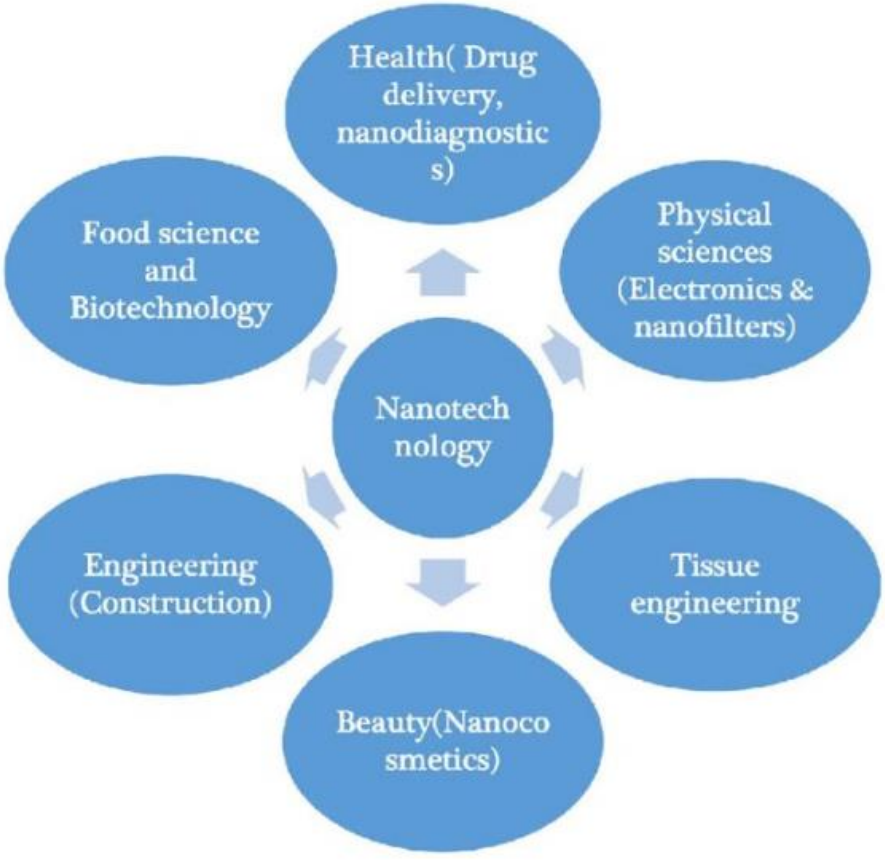

Figure (1.1): Interesting applications of nanotechnology.[12]

1.3 Classification of Nanostructure Types

Nanomaterial's have different shapes, sizes, and crystal structures. They can be spherical, conical, spiral, cylindrical, tubular, flat, hollow, or irregular in shape and be from 1 to 100 nm in size. Nanomaterials can be generally classified into four material-based categories:

1. Inorganic-based nanomaterials: the fundamental constituent of these materials is metal or metal oxide particles with a size of less than 100 nm. They are made of pure precious metal nanoparticles, like Au or Ag, or they can be metallic oxides, like ZnO and TiO_2. Ceramics and silicon are also examples of semiconductors that fall within this group.
2. Organic-based nanomaterials: are materials that are mostly made of organic substances with nanoscale dimensions. These substances are renowned for having distinct chemical and physical characteristics that can be adjusted for a range of uses. They can be used in encapsulating drugs for targeted and controlled release, improving therapeutic efficacy while minimizing side effects. Dendrimers and nanofibers are examples for these nanomaterials class.
3. Polymeric Nanomaterials are made of polymers that have undergone nanoscale engineering; their usual size ranges from 1 to 100 nanometers. They are useful in a variety of applications because of their distinctive qualities and capabilities. They can be utilized in coatings, packaging, and drug delivery.[13] They can be formed of polymers (polylactic acid, polyvinyl alcohol, etc.).
4. Carbon-based nanomaterials are a broad class of materials that are mostly made of carbon and have special qualities because of their nanoscale size. Because of their remarkable mechanical, electrical, and thermal qualities,

they are becoming more and more significant in a variety of disciplines. Graphene, carbon nanotubes, and fullerenes are examples of nanomaterials with remarkable mechanical, electrical, and thermal capabilities. [14]

Nanostructured materials are also classified according to their dimensions into (see Figure 1.2):

1. Zero-dimension materials (0D) are materials, such as nanoparticles, fullerenes, and quantum dots, whose dimensions are all on the nanoscale scale. These structures can be made of ceramic or metal.
2. One-dimensional structures (1D) are structures with a single dimension falls with the nanoscale rangs. Thin films, nanorods, and other materials that are needle-like and exist outside the nanoscale additionally to nanowires. They could be ceramic, metallic, or polymeric [.15]
3. Two-dimensional (2D) structures: structures with an exterior two-dimensional dimension falls in the nanoscale range and possess geometries resembling plates, including nanofilms, and nano walls.
4. Three-dimensional (3D) structures: structures with no dimension fall to the nanoscale range, thus, sometimes called bulk material (they are composed of discrete blocks that are in the nanometer scale (1–100 nm)). This broad class includes multilayer structures, aggregates of nanowires and nanotubes, dispersions of nanoparticles, and bulk powders. A wide range of uses are possible because these materials combine the unique features of nanoparticles with the behaviors of bulk materials.

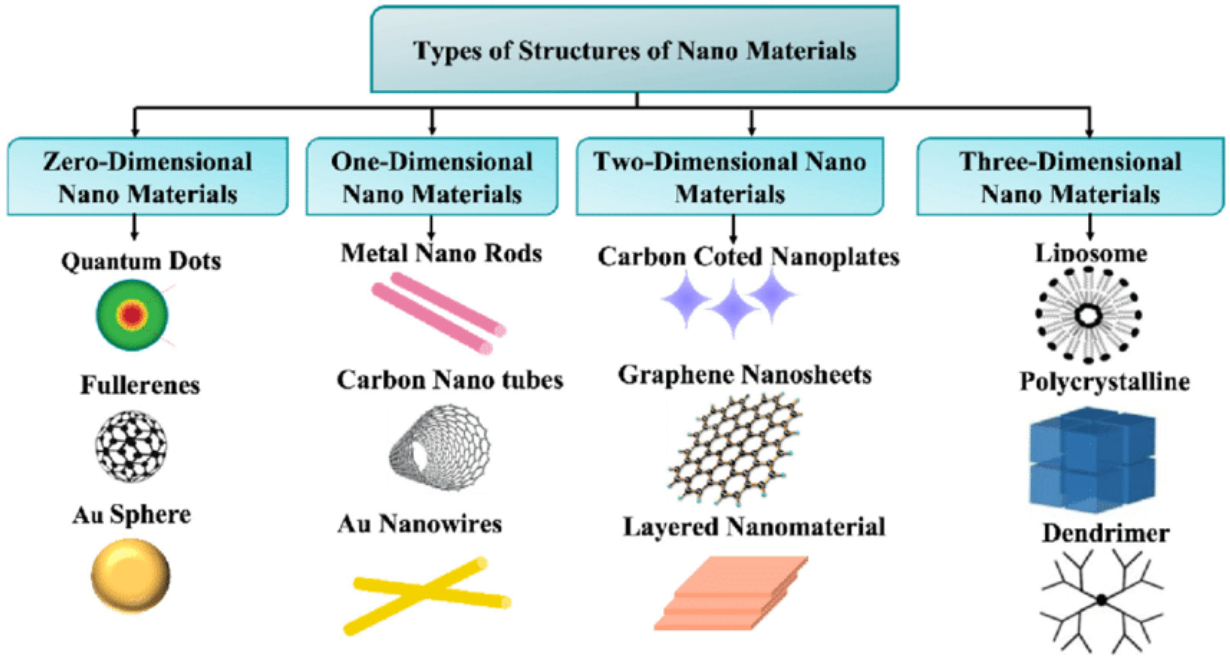

Figure (1.2): Classification of nanoscale structures according to their dimensions. [16]

1.4 Nanoparticle Synthesis

Physical, chemical, and biological techniques have all been proposed and employed to create nanoparticles. These methods fall into two primary categories, as illustrated in Figure 1.3: (1) the top-down approach and (2) the bottom-up approach.

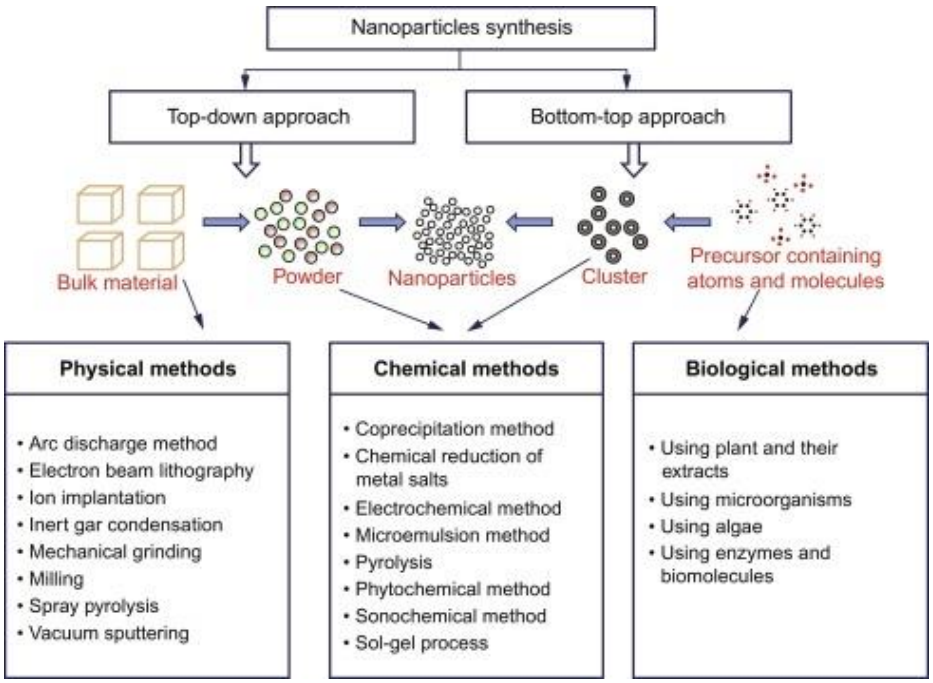

Figure (1.3): Illustration showing the top-down and bottom-up technology concepts: different approaches to nanoparticle synthesis. [17]

In top-bottom methods, the desired bulk materials is broken down into tiny particles using mechanical, chemical, or other energy sources. Techniques include mechanical milling/alloying and sputtering have been used for crushing the particles. [18] This technique may lead to surface defects in the final product that provide a serious safety issue because a material's surface structure is essential to its surface chemical and physical properties. Tiny sizes are almost tough to reach, therefore size is a persistent problem.

Bottom-up approaches depend on the self-assemble of atoms or molecules into nuclei to start the synthesis process, which then proceed to produce nano-sized particles. [19] These methods rely on biological and chemical processes to produce nanomaterials. Atomic condensation, sol-gel, and chemical precipitation are all included in this technique.

Even though all of the physical and chemical methods have been utilized extensively to manufacture nano-sized materials, they have some drawbacks, such as using such dangerous chemicals and solvents that pose a biological risk. Some of them used ultrasonic waves or intense heat, which could affect the produced particles' crystalline structures. [20] Recently researchers have been formed nanostructures depending on the biological materials, which is sometimes known as "green synthesis." The production of nanomaterials relies on the use of bacteria, yeast, or plants as reducing and capping agents [.21, -22] Among the many benefits of this method are its simplicity, affordability, and environmental friendliness.

In this work, the chemical precipitation method was used to produce ZnSe nanostructures, it is considered one of the most popular and common techniques for producing nanomaterials.[23, 24] Three steps are involved in this process to form nanostructures: a chemical reaction, particle nucleation, and particle growth. During the formation process, the resulting particles may group together, which could result in a wide size distribution. Furthermore, it is challenging to control the particle morphology. To solve these issues, stabilizing agents and capping agents should be added to the precursor's solution, which will hopefully prevent further atoms from adhering to the surface of the as-prepared particles.

The idea behind this method is to use inorganic salts (nitrate, acetate, sulfate, etc.) as precursors. To form homogenous solutions that exhibit ions, these salts should be dissolved in water or any other suitable solution. [25]Also, in this technique parameters including pH, reaction temperature, and the concentration of precursors should be adjusted to prevent the agglomeration of nanomaterials. Thereafter, the resulting precipitate will be subjected to filtration and drying.

1.5 Semiconductor nanoparticles

Semiconductors have a crystalline structure and contain few free electrons at room temperature. They fall between conductors and insulators, and act as insulators at room temperature, however, their conductivity increases with increasing temperature and conductivity can be controlled by adding appropriate impurities to the semiconductor. In its unadulterated (intrinsic) form, a semiconductor is not a good insulator or conductor. Antimony (Sb), arsenic (As), astatine (At), boron (B), polonium (Po), tellurium (Te), silicon (Si), and germanium (Ge) are single-element semiconductors. Compound semiconductors, which are widely utilized in many applications, including silicon carbide, silicon germanium, gallium arsenide, indium phosphide, zinc selenide, and gallium nitride. Atoms containing four valence electrons are characteristic of single-element semiconductors.

In semiconductor nanomaterials, as atoms approach one another and start to form bonds, their energy levels will separate into bands made of closely spaced energy levels. The valence band, which is the lowest energy band formed by the valence orbitals, is typically filled with electrons once the atoms have reached equilibrium interatomic spacing. The conduction band is the second band, and it is devoid of electrons. The term band gap energy, which is shown in Figure (1.4) refers to the energy differential between the valence and conduction bands. The band gap energy has a significant impact on the electrical and optical properties of semiconductors.

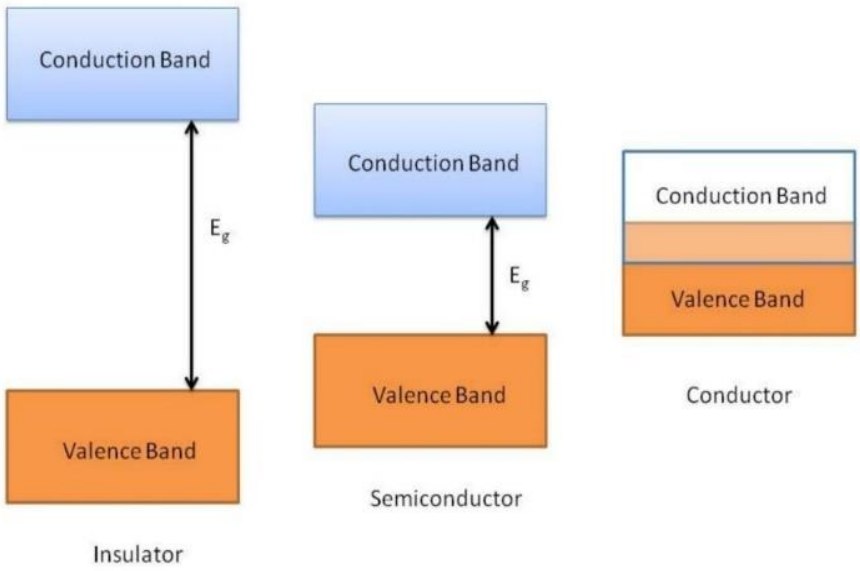

Figure (1.4): Energy band diagram showing the band gap for insulators, semiconductors, and metals. [26]

Because of their special size-tunable optical and electrical capabilities, semiconductor nanoparticles have garnered a lot of attention from the scientific and technological community. Due to its wide band gap and transmittance range, high luminescence efficiency, low absorption coefficient, and outstanding transparency to infrared. When a semiconductor material absorbs light with energy equal to or greater than its band gap energy, the electron in the valance band shifts to the conduction band, leaving a positive hole behind. Because the electron and hole have opposite charges, they unite to produce the exciton, which collapses quickly. A photon with nearly the same energy as the band gap can be released once the excited electron and hole recombine. Due to the exciton's size range of 1 to 100 nm, charges would confine if the particle size dropped below that of the exciton, a phenomenon called the quantum size effect. [27]

These days, it is possible to create nanostructures of semiconducting materials with specific sizes and compositions, which has sparked a lot of interest in studying these structures to find new uses and technologies. The size and form of nanostructures determine a material's physicochemical properties, which differ from those of the material in their bulk form. Therefore, a molecular species that represents the unit cell is needed to construct the nanostructure of materials in order to analyze such structures at the nanoscale level. Because of the wide range of uses for nanostructures, a great deal of theoretical and practical research on several potential materials has been done.

Among semiconductor nanostructures, II-VI semiconductors are fascinating because of their large energy gap, strong photoluminescence, excellent stability, and size dependency. [28]Consequently, they find usage in several applications, including catalysts, solar cells, LEDs, sensors, and biological photoelectrochemical cells. Zinc selenide (ZnSe) is one of the II-VI compounds which has a band gap of 2.7 eV. ZnSe can be used as a good material for doped nanocrystals in manufacturing LEDs, photodetectors, transistors, and photoelectrochemical cells.[29, 30] ZnSe at displays at the nanoscale vastly distinct characteristics from bulk form.

It is well known that the band gap energy of materials in solar cells play an essential role in optimizing solar energy absorption, therefore, ZnSe nanoparticles can be used in improving the efficiency of photovoltaic devices' by enhancing their capacity to harvest light. [31] Furthermore, ZnSe thin films are advantageous for semiconductor devices because of these characteristics. ZnSe thin films are used in a variety of devices, including photovoltaic solar cells, laser and light emitting diodes, in the creation of high-power infrared laser lenses, [32] as buffer layers on

solar cells, and in luminescent devices. Buffer layers in solar cells and luminescent devices serve as intermediate layers to enhance performance.

• In solar cells: They improve charge separation, reduce interface defects, and increase energy conversion efficiency.

• In luminescent devices: They enhance light emission, prevent unwanted reabsorption, and improve electrical and optical properties.

Overall, buffer layers optimize efficiency and reliability in both applications.

1.6 Zinc selenide nanoparticles:

Zinc selenide (ZnSe) is a semiconductor belonging to the II-VI group, it has a band gap of 2.7 eV. This band gap energy paves the way for using ZnSe in a wide range of optical transparency in the visible spectrum, high linear and nonlinear refractive indices, good electronic transport characteristics, a substantial exciton binding energy (21 meV), and a wide band gap. The semiconductor material's particle sizes can be adjusted to modify the ZnSe band gap. Quantum confinement has been demonstrated to be the cause of a feature of a nanoparticle that is different from its bulk group material when its size is lower than its exciton Bohr radius. Zinc selenide (ZnSe) is a significant II–VI semiconductor that was among the first to be discovered. It is also likely one of the most important electronic and optoelectronic materials, with a wide range of applications including logic gates, transistors, light emitting diodes (LEDs), nonlinear optical devices, flat panel displays, and lasers. Due to its significant potential for both fundamental physical study and applications in the construction of nanoscale electric and optoelectronic devices, ZnSe nanostructures have recently attracted a lot of attention.

Because of its new characteristics, structure richness, and advanced applications, nanostructured ZnSe has become one of the most popular optoelectronic materials in recent years. ZnSe nanostructures having potential morphologies and close fundamental physical attributes to their crystal structures and lattice constants.

The Zinc selenide (ZnSe) is a light-yellow binary compound semiconductor having a wide bandgap of 2.7 eV. The ZnSe compound exists in wurtzite (hexagonal) and zinc blende (cubic) crystalline forms Figure (1.5), of which the cubic phase is believed to be stable than others. ZnSe is generally produced as an n-type semiconductor like most of the other II-VI compounds. Zinc Selenide (ZnSe) is one of the most attractive binary wide band gaps semiconducting materials amongst II-VI group materials.

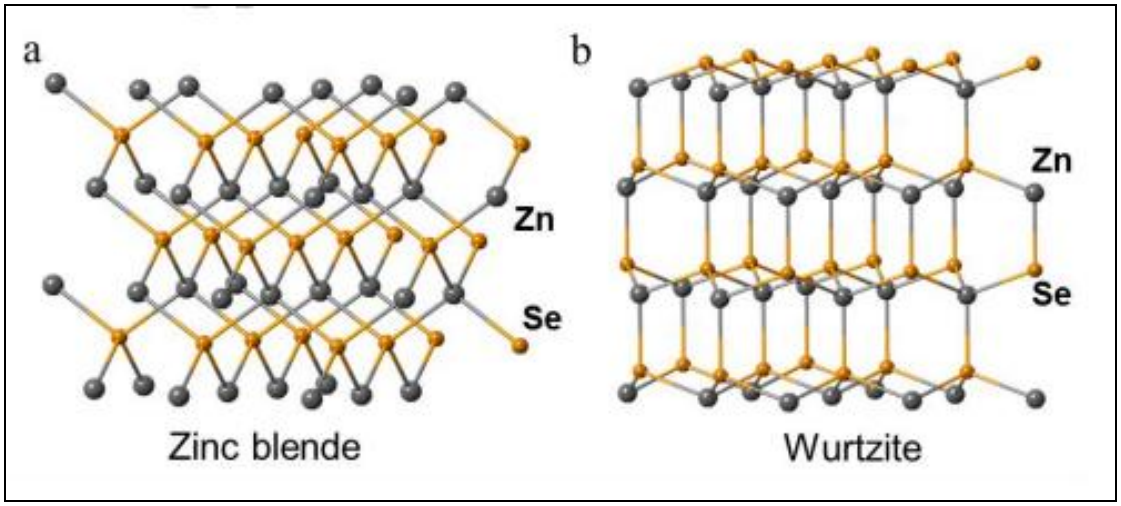

Figure (1.5): Crystal structure of zinc selenide showing zinc blende and wurtzite phases. (33)

ZnSe material can be formed using a variety of methods, including electrodeposition technique, chemical vapour deposition, inert gas condensation method, evaporation method, thermal evaporation, vacuum evaporation, chemical bath deposition (CBD), molecular beam epitaxy, successive ionic Layer adsorption

and reaction (SILAR) , cyclic voltammetry method etc. vacuum deposition technique which is one of the fast synthesis methods to produce high-quality thin films of large scale.

1.7 Capping agents in nanotechnology

Capping agents are materials that are added to nanoparticles during their synthesis in order to regulate their surface properties, stability, size, and shape. They are essential for the colloidal stability of nanoparticles because they keep them from aggregating and guarantee and consequently, keeping their special characteristics. The optical, electrical, and catalytic properties of nanomaterials can be affected by the capping agent utilized; for example, gold nanoparticles are stabilized by thiols, but silver nanoparticles may be stabilized by phosphines.

Furthermore, capping agents can improve their biocompatibility, which qualifies them for use in biomedical applications including imaging and targeted medication delivery. The potential uses of these cutting-edge materials in fields like energy storage, environmental remediation, and sensing are further increased by the ability to precisely control the interface between the capping agent and the surface of the nanoparticles.

Capping agents' inherent capacity to firmly adsorbe on the surface of nanoparticles, establishing a mono- or multi-layered protective covering, controls the size, shape, and geometry of the particles, ensuring their long-term stability. These factors all influence how nanoparticles behave in biological systems; of particular importance is the notable improvement of several biological characteristics that would otherwise be unachievable.[34]

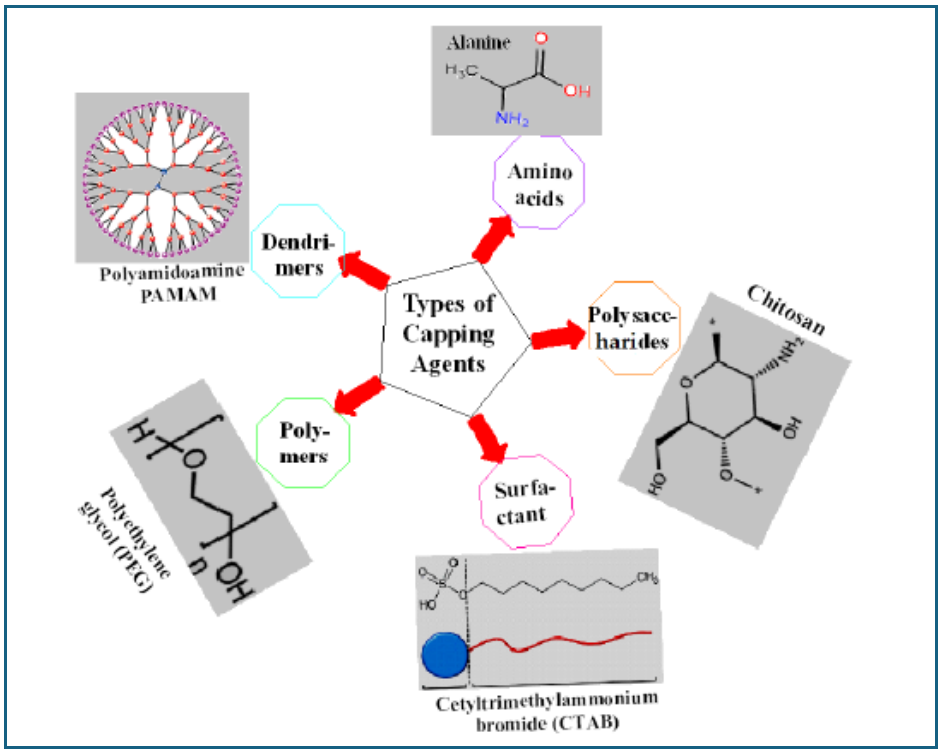

Figure (1.6): Diagram showing different capping agent.

Polysaccharides, proteins, dendrimers, cyclodextrins, organic ligands, amino acids, polymers, and bio-extracts, are examples of capping agents. The capping agents chosen are biocompatible, biodegradable, and non-toxic for the capping of colloidal nanoparticles. The use of capped nanoparticles increases the possibility of building intelligent drug delivery systems that may provide targeted distribution and a slow, continuous release of drugs in the tumor microenvironment. With these nanoparticles, hitherto unheard-of outcomes have been seen in bioimaging, biosensing, and gene delivery. It has been observed that capping agents serve the following main purposes: (1) regulating nanoparticle growth to attain desired size and shape, and (2) reducing the surface energy of each individual nanoparticle to stop it from clumping together, so that the particles remain apart instead of joining forces. Although there is still more work to be done to bridge the current research

gaps, this strategy offers the potential to assuage concerns about nano safety and present opportunities for growth in nanomedicine and other important domains. Different capping agents have demonstrated multifunctional properties and are critical in augmenting the properties of nanoparticles in ways that make them exceptionally well-suited for usage in a variety of nanomedicine applications. It is certainly a difficult work to choose the right surface capping agent for the careful design and synthesis of nanoparticles in order to accomplish the desired breakthrough in nanomedicine. Furthermore, conducting highly optimized, repeatable experiments pertaining to the production of shape/size-controlled nanoparticles seems to be extremely challenging at this point. For instance, the majority of nanotechnology research is currently done on a Due to the low stability of nanoparticles in natural environments or environmental samples, high batch-to-batch variability, and lack of multifunctionality, anomalies in overall performance are observed in laboratory settings. Applying the right capping agents to the surface of the nanoparticles can reduce or prevent these problems. It is challenging to assess the capping agent's pure influence on a particular nanomedicine technique when accounting for other factors, despite research demonstrating the capping agent's remarkable advantages.

The amphiphilic structure of capping agents consists of a non-polar tail submerged in the surrounding medium and a polar head affixed to the surfaces of nanoparticles. The capping agents raise the overall percentile of atoms on the nanoparticle surface even further, giving biological functioning, for example, an increase in reactivity.[35]

1.8 Ethylenediaminetetraacetic acid (EDTA)

EDTA is a multipurpose chelating agent that's often used in biology, medicine, and chemistry. Because of the way it is structured (see Figure 1.7), metals including calcium, magnesium, lead, and iron can be successfully sequestered by binding metal ions through its two amine groups and four carboxylic acid groups. Because of this characteristic, EDTA finds usage in analytical chemistry to assist determine metal concentrations and in water treatment to help avoid scale development by binding hardness ions. In the medical field, EDTA is utilized in chelation therapy to treat atherosclerosis and heavy metal poisoning by lowering calcium deposits.

Moreover, it can be widely used in the food industry to stabilize and preservative food by absorbing metal ions that might cause food products to become spoiled and discolored. EDTA can be also utilized in fertilizers to improve plant uptake of vital nutrients by reducing metal ion precipitation and increasing nutrient availability. Owing to its ability to serve as a chelating agent, EDTA inhibits oxidation and radical reactions by chelating metal ions that are harmful to human health, which is the primary benefit of EDTA in drug delivery systems. EDTA has the ability to attract positive ions in addition to its electronegativity. This characteristic is widely used in chemical and biological applications.

.

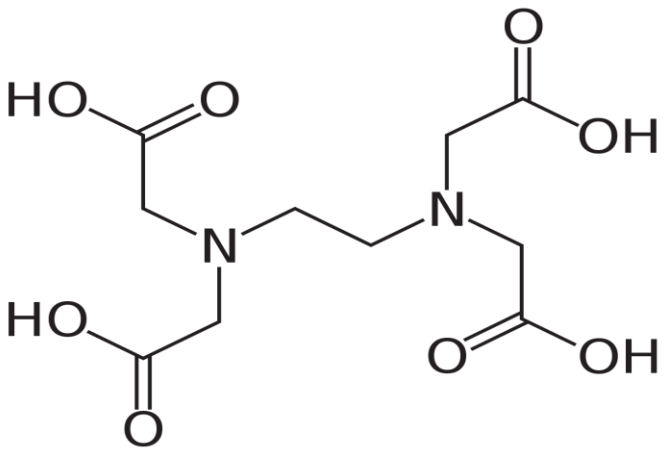

Figure (1.7): The chemical structure of EDTA.

In the field of nanotechnology, EDTA has been used extensively because of its capability to stabilize nanoparticles, which improves dispersion and inhibits agglomeration by encircling the nanoparticles in a protective layer. Therefore, the water soluble EDTA is one of the most important capping agents, which is utilized in the formation of nanoparticles. EDTA helps to avoid agglomeration between the nucleation and growth phases, and then regulate the production of nanoparticles in term of their sizes and shapes.

EDTA was chosen in this work, for the first time, as a capping agent for the formation of ZnSe nanostructures because the tetraacetate ions is able to form strong complexes with zinc ions. The zinc cation in the complex is surrounded by six strong donor atoms (two nitrogen and four oxygen) in EDTA, obtaining the maximum number (6) of feasible donor–acceptor interactions. However, the anionic nature of the ligand plays a role in the complex's stabilization in addition to these charge transfer interactions. Strong electrostatic attraction can be established

between the trapped zinc cation and the four carboxylate oxygens, in particular, as they each carry a negative charge.

1.9 Literature Review

Ethylenediaminetetraacetic acid (EDTA) was utilized as a capping agent for preparing nickel oxide (NiO) nanoparticles prepared using coprecipitation method. The findings showed that EDTA plays a role in controlling the size and the shape of the resulting nanoparticles comparing with uncapped NiO nanoparticles. Their XRD patteren showed that the prepared particles have Face-centered cubic (FCC) phase and their crystallite sizes ranged from 28 to 33 nm. [.36]

In 2008, ZnSe nanoparticles capped with Thioglycolic were prepared using low temperature (~ 80 °C) wet chemical technique that is easy to use and reasonably priced. The effect of capping on the optical properties of ZnSe particles was studies. TEM images showed that the shape of the samples was spherical with an average size of about (6-18 nm) for all the nanoparticles. It was found that the size of capped particles is strongly affected by changing the concentration of thioglycolic. Due to their high luminescence and monodispersed nature, the resulting particles have a wide range of potential uses. [37]

In 2010, the hydrothermal method was used to prepare ZnSe and ZnS nanoparticles. The authors were used EDTA to tuning the properties of the synthesized particles. The resulting nanoparticles were characterized by ultraviolet spectroscopy, X-ray spectroscopy, photoluminescence emission spectra, and surface area measurement. It is revealed that emission peaks with PL efficiencies of 4.0 (for ZnSe-EDTA) and 2.4% (for ZnS:Mn-EDTA) were seen in the solution PL spectra at 390 and 597 nm, respectively.[38]

DFT calculation was used to study the vibrational frequencies of Zn_xSe_y clusters (x = 1, 2, 3 and 4 y = 1, 2, 3, and 4) and the authors found that the clusters of ZnSe oscillate at 137.6 cm^{-1} and the bond length for Zn-Se is 2.247.[39]

Nano-sized ZnSe particles were successfully synthesized via chemical co-precipitation using Sodium borohydride as capping agent. The authors found that the capping agent plays a vital role in enhancing the optical and electrical properties of ZnSe. The absorption wavelength of bulk ZnSe is 460 nm, whereas the ZnSe nanoparticles absorbed UV-Vis light with wavelengths less than that. According to the analysis of the XRD patterns single-phase ZnSe was effectively synthesized, and the TEM-based particle size verified that the particles were nano-sized.[40]

ZnSe nanoparticles were synthesized using a simple and cost-effective chemical coprecipitation method with ethylenediaminetetraacetic acid (EDTA) as a capping agent. EDTA's role was to stabilize the nanoparticles against aggregation and provide chemical passivation. Utilizing Scherrer's equation to calculate XRD patterns, the average size of the cubic zinc blende structure particles was approximately 3-5 nm. Verifying the cubic phase of ZnSe, the SAED pattern revealed three rings that corresponded to the (111), (220), and (311) planes. The optical band gap energy of EDTA-capped ZnSe nanoparticles was significantly higher than that of uncapped and bulk ZnSe, as demonstrated by the UV-Vis absorption measurements, which also indicated a substantial quantum confinement effect. Fluorescence spectra showed that ZnSe nanoparticles capped with EDTA had a greater photoluminescence intensity than uncapped nanoparticles. The Raman examination of the ZnSe nanoparticles with EDTA caps showed many Raman peaks in resonance, suggesting a satisfactory level of optical quality.[41]

Using theoretical calculations from first principles, one can carefully examine how one-coordinated atoms affect the properties of ZnSe clusters. The coordination states and local bond lengths of the remaining surface atoms are altered by the addition or removal of one-coordinated atoms. The HOMO, and LUMO plots demonstrated that the changes only marginally impact the states at the Fermi level region. The significance of the cluster core is shown by the fact that the states close to the band gap margins are primarily ascribed to the internal Zn and Se atoms. The ZnSe clusters' computed absorption spectra provide more evidence that the cluster core's electron excitation is essential to the clusters' optical characteristics. [42]

An experimental work by Sridevi's group has showed that the catalytic activity of ZnSe can be improved by introducing Mercaptothion (C_2H_6OS), and hydrazine hydrate (N_2H_4) to the growth process of ZnSe. With the use of UV-visible diffuse reflectance spectroscopy, the optical band gap (Eg) value of ZnSe NPs was examined and determined to be approximately 2.6 eV. Researchers expect that capped- ZnSe particles will provide an exciting new opportunity for enhancing semiconductor performance in the field of removing dyes from aqueous solutions.[43] Very recently Gupta et al. have prepared both ZnSe nanorods and nanoparticles nanoparticles through co- co-precipitation method.[44]

1.10 Aims of the Study

The Study aim to:

The aim of this work is to show the chemical precipitation approach to explain the growth process of zinc selenide nanostructures. One objection of the key aim is to demonstrate the use of capping agent to see whether this allows access to particles with larger band gap than observed without agents. This study therefor included the addition of a EDTA to the starting materials, which will hopefully control the growth of ZnSe nanostructures, reduce the aggregation of particles and form small particles with wide band gap. These may have a number of uses including optical applications where the scattering of light plays a role in enhancing signals.

This study also intended to use the density functional theory (DFT) to study the electronic features of ZnSe nanoparticles. This would be a promising study to compare results experimentally and theoretically. Thus, a quantitative prediction of a research case made and confirmed through experiment shows that the theoretical study of that particular experiment is comparable to the theoretical study using DFT theory.

1.11 THEORETICAL METHODS

1.12 Introduction

One of the most well-known and frequently applied theories to study and understand the electrical characteristics of molecules is the density functional theory. The quantum states of atoms, molecules, and solids, as well as ab-initio molecular dynamics, may now be computed with great efficiency. Thomas and Fermi presented an early, approximative version of density functional theory in 1927, not long after quantum mechanics was established. After that, a density functional theory of the quantum ground state was developed by Hohenberg, Kohn, and Sham, which outperformed the theories of Thomas-Fermi and Hartree-Fock and allowed a multitude of applications involving real physical systems. [45]

Molecular computing techniques, electronic characteristics, and the Schrödinger equation ara all be covered in this chapter. The methods of density functional theory, semi-empirical theory, and HF are also discussed.

1.13 Schrödinger Equation

A system of interacting particles has a total energy that, according to classical mechanics, is equal to the product of its kinetic and potential energies; this may be found in:[46]

$$E = T + V \qquad (2\text{-}1)$$

T: represents the kinetic energy, which is the energy associated with the motion of particles or a system.

V: represents the potential energy, which is the stored energy in the system due to forces such as electrostatic, nuclear, or elastic forces.

Exchange of the classical kinetic and potential energy is Schrödinger's correct explanation for the wave nature of particles.

$\{T\hat{}+V\hat{}\}\psi=E\hat{}\ \psi$

Or

$H\hat{}\ \psi=E\hat{}\ \psi$

Alternatively, where PEO is the potential energy operator, Potential Energy Operator (PEO) and Eigenvalues

• The potential energy operator $V\hat{}$ represents the potential energy in the system.

• The eigenvalue $\mathbf{D}\hat{}$ (which seems to be a notation issue, and it is likely referring to E) corresponds to the total energy of the system, obtained from the Hamiltonian operator $H\hat{}$.

• ψ is the eigenfunction (wave function) that describes the motion of the electron in the system.

$\mathbf{D}\hat{}$ is the eigenvalue of the Hamiltonian $H\hat{}$, and ψ is the eigenfunction that characterizes the electron motion of the system. To grasp the essence of density-functional theory, it is useful to step back and review some basic quantum physics. We can in quantum mechanics that a system's wave function contains all of the information we could ever know about it. Schrodinger's equation is used to obtain this wave formula nonrelativistic ally. For a single electron moving in a potential (r), this equation can be expressed as:[47]

$$\cdot\left[-\frac{\hbar^2}{2^m}\nabla^2+V_{(r)}\right]\psi(\gamma)=E\psi(r) \qquad (2\text{-}3)$$

Here:

• ∇^2 is the Laplacian operator, representing the spatial variations of the wave

function.

- $\hbar$ is the reduced Planck's constant.
- m is the mass of the electron.
- E is the energy of the electron.

The total Hamiltonian of the system, which includes n electrons and N nuclei, can be expressed as follows:

$$\hat{H}=\hat{T}N(R)+\hat{T}e(r)+\hat{V}eN\ (r,R)+\hat{V}NN(R)+\hat{V}ee(r) \quad (2\text{-}4)$$

Atoms have kinetic energy operators $\hat{T}(R)$ while electrons have kinetic energy operators $\hat{T}e(r)$. Nuclei-nuclei, electron-electron, and electron-nuclei have the following potential energy operators: $\hat{V}$ ($\boldsymbol{U}$, R), $\hat{V}NN(R)$, and $\hat{V}ee(\boldsymbol{U})$, respectively. whereas r represents electron coordinates, R stands for nuclear coordinates.

So, equation (2-4) can be given by [4]:

$$\hat{H}=-\hbar 22\Sigma\ NI=1\nabla I2MI-\hbar 22\Sigma\ ni=1\nabla i2mi-\Sigma\ N-1I=1\Sigma\ ni=1e2ZIrIi+\Sigma\ N-1I=1\Sigma\ NJ=I+1e2ZIZJRIJ$$

$$+\Sigma\ n-1i=1\Sigma\ nj=i+1e2rij \quad (2\text{-}5)$$

Where ZI and ZJ are the charges of the nucleus of atoms I and J; aIi is the distance between nuclei I and electron i; RIJ is the distance between nuclei I and J; and rij is the distance between electrons i and j.

The electron-electron interaction, the interaction with the external potential, and the kinetic energy are the three terms that make up the energy function, as the Schrodinger equation has demonstrated.

Equation (2-5) can be write using an atomic unit value (e2, ħ2and m =1) as follow:

A longstanding fundamental challenge in quantum mechanics has been the determination of molecular eigenfunctions. There are precise analytical solutions to the Schrodinger equation only for the hydrogen atom and the molecular hydrogen ion. Only for more complicated systems, using approximation approaches, can eigenfunctions be generated in an approximate manner. [48]

Approximation Methods Used in Quantum Computations

• Molecular Mechanics Methods (MM).

• Ab -initio Method.

• Semi-Empirical Methods (SE).

1.14 Molecular Mechanics Methods (MM)

Molecular mechanics (MM) is the term used to describe the use of Newtonian mechanics to explain molecular systems. Molecular dynamics simulations, ligand docking simulations, and molecular structure refinement all frequently employ molecular mechanics techniques. Material assemblies comprising dozens to millions of atoms, small compounds, and large biological systems can all be examined with MM. Using all-atomistic MM techniques, every atom is simulated as a single hard spherical particle with a radius and a constant net charge. Additionally, bound interactions are regarded as "springs," having equilibrium distances and harmonic force constants that match the vibrational frequencies and bond lengths predicted or determined through experimentation. [49]

By optimizing or modifying the spatial organization of the compounds under study, the MM approach determines energy dependencies that lead to the lowest energy. Without accounting for electrons, the particles are treated as if they were balls connected to one another by springs. The tensile and bending energies of the

new bond, as well as the true bond length and angle between each pair of atoms, must all be determined in order to calculate the energy value. [50]

1.15 Ab -Initio Methods

The Latin phrase "from first principles" or "from scratch," or ab-initio, describes calculations that are performed solely on the basis of theoretical concepts and do not require the application of empirical data. Most often, this corresponds to an approximate computation in quantum physics. Employing a simplified functional form of a function or estimating an approximate solution to a differential equation are two examples of popular mathematical approximations. [51]

The Hartree-Fock HF computation is the most common ab-initio calculation, and it uses a central field approximation as a first approximation. The approximate energy is typically less important than the energies from HF calculations. Because of the central field approximation, they gravitate to a particular value known as the Hartree Fock limit. For HF computations, the second approximation requires that the wavefunction be represented by a functional form, which is accurate for a limited number of electron systems.

However, new users often have problems regarding which basis set to use, if electron correlation corrections are necessary, and other relevant matters. To provide the essential information and respond to these queries is the aim of ab initio Molecular Orbital Theory (MOT). An overview of computational techniques and ab initio theories is provided at the outset. [52]

Due to the massive number of particles in the systems, computer programs are also used to carry out the necessary calculations to solve the Schrödinger

equation. These computations include numerous challenging integrals for complex systems. Using ab-initio arithmetic techniques, all of these integrals may be solved without rounding. The most dependable approaches are ab-initio ones for small and medium-sized systems, but they take a lot of time for larger systems.

1.16 Semi-Empirical Methods

In solid-state chemistry, semi-empirical methods have a lengthy and fruitful history dating back several decades. Approximate molecular orbital simulations provided the foundation for later ab initio methods when computational resources did not permit more exact procedures. The necessity of semi-empirical approaches is questioned in light of the increasing capacity of computers. [53]

The following techniques are categorized as semi-empirical methods:[54] Austin Model 1 (AM1), Modified Intermediate Neglect of Differential Overlap (MINDO), The Modified Neglect of Diatomic Differential Overlap (MNDO), Parametric Model number 3 (PM3), and Parametric Model number 6 (PM6). Zero-Differential Overlap (ZDO), Intermediate Neglect of Differential Overlap (INDO) & Complete Neglect of Differential Overlap (CNDO), The Neglect of Diatomic Differential Overlap (NDDO).

1.17 Density Functional Theory (DFT):

The theoretical basis for all computations of electronic structure can be used to determine a wide range of measurable solid properties. Density functional theory (DFT) is a highly potent theory that outperforms semi-empirical, Ab-initio, and Hartree-Fock theories in terms of accuracy. DFT can be used for solids, heavy atom-containing molecules, atoms, nuclei, quantum, and classical fluids. [55]

It gives a system's ground state features, and an important factor is the electrical density. Many different molecular features, including molecule structure, atomization energies, vibrational frequencies, electrical and magnetic properties, and ionization energies, are predicted by density functional theory.

The electron density has substantially lower dimensionality than the wave function, which is a benefit. As a result, DFT may now be used to analyze considerably bigger systems with hundreds or even thousands of atoms. DFT also has a low computational cost. Due to these factors, DFT is now frequently used in first-principles calculations intended to describe—or even predict—the characteristics of molecules and condensed matter systems [.56 - 57]

To find the energy for the electron density, one uses a density functional, which is a function defined by another function. Accordingly, the wave function and the electron density are functions, and the energy that depends on either of them is a functional. [58] Two articles summarized the early work on density functional theory: one by Pierre Hohenberg (Hohenberg and Kohn, 1964) [59]. and the other by Lu J. Sham (Kohn and Sham, 1965) [60].

1. The Hohenberg-KohnTheorem (HK):

The theorems that Hohenberg and Kohn developed in 1964 [61] serve as the formal foundation for DFT. Two of the Hohenberg–Kohn theorems (HK) gave DFT a solid theoretical foundation. The initial HK theorems were valid only for non-degenerate ground states in the absence of a magnetic field, but they have subsequently been included in their generalization. [62]

The two theorems that make up the theory state and demonstrate, respectively, what Hohenberg and Kohn

1st HK Theorem: According to the first HK theorem, an electron density that depends only on three spatial dimensions can determine a many-electron system's ground state features uniquely. By using the functional of the electron density, it establishes the foundation for reducing the many-body issue of N electrons with 3N spatial coordinates to 3 spatial coordinates.[63] Aside from an additive constant, the ground-state electron density ρo(r) uniquely determines the external potential Vext(r) for any system of interacting particles in an external potential Vext(r).

- **2nd HK Theorem*:*** The second HK theorem defines an energy functional for the system and proves that the correct ground state electron density minimizes this energy functional.

The Hohenberg-Kohn theorems, however, are not nearer to a practical method, also the exact evaluation of the Hohenberg-Kohn functional *F*HK would require us to solve the many-particles Schrödinger equation.[64] The Kohn-Sham (**KS**) scheme, a reformulation of the theory based on the **KS** orbitals instead of the mere density, is the starting-point of most of the actual calculations.

- **2. The Kohn-Sham Scheme:**

With the use of the Kohn-Sham formalism and density functional theory, one can effectively solve a single particle-like equation to precisely ascertain the ground-state properties of complicated systems of interacting particles.

In order to compute the ground state properties of atoms, molecules, and solids in a self-consistent manner, Kohn-Sham density theory is frequently employed.

The underlying principle of the Kohn-Sham approach is the creation of a fictional system of non-interacting particles, usually electrons, that produces the same density as any real system of interacting particles. The imaginary system is made up

of separate electrons that are all subjected to the identical external potential, or effective potential, Vext (r) .

The Kohn–Sham DFT (KS DFT) paradigm simplifies the unsolvable many-body issue of interacting electrons in a static external potential to a manageable problem of non-interacting electrons moving in an effective potential. Along with the effects of the Coulomb interactions—such as the exchange and correlation interactions—between the electrons, the effective potential also takes into account the external potential. KS DFT is a challenge for modeling the last two interactions.

Chapter Two

Experimental Part

2.1 Equipment

A variety of devices, all listed in Table (2-1), were utilized in this work to synthesize and characterize zinc selenide nanoparticles.

Table (2.1): Instrumentation

No	Instrumentation	Type, Company	Place
1	Spectrophotometer UV-Visible Double Beam-1800	UV-Vis 1800 Shimadzu-Japan	University of Kerbala "College of Science - Graduate Studies Laboratory"
2	Fourier transform infrared (FT-IR)	IRAffinity1S, SHIMADZU	University of Kerbala College of Science - Graduate Studies Laboratory
3	Centrifuge-Hettich	Universal -Germany	University of Kerbala College of Education for Pure Sciences / Department of Chemistry / Graduate Studies Laboratory
4	X-Ray Diffraction Spectrophotometer (XRD)	Analytical company	University of Tehran
5	Oven Me mort	LOD080+NLabtech, Korea	University of Kerbala College of Education for Pure Sciences / Department of Chemistry / Graduate Studies Laboratory
6	Field Emission Scanning Electron Microscope (FE-SEM)	Inspect of 50 femes FEI company	University of Tehran
7	Heater and magnetic motor -	ISO 9001 CERTIFIED	University of Kerbala College of Education for Pure Sciences / Department of Chemistry / Graduate Studies Laboratory
8	Raman spectroscopy	Tafsanj Fanavari Arnik	University of Tehran

2.2 Chemical Materials

Table (2-2) shows the chemical materials that were used in this work. All experiments were performed using deionized water as a solvent.

Table (2.2): Chemical materials and their formula

No	Chemicals	Chemical Formula	Purity %	Company supplied
1	Sodium hydroxide	NaOH	98 %	BDH chemicals Ltd Poole, England
2	Zinc acetate	$Zn(CH_3COO)_2.2H_2O$	99.5%	Sigma-Aldrich (now part of Millipore Sigma), Fisher Scientific, VWR International, Alfa Aesar, TCI Chemicals
3	Sodium Selenide	Na_2Se	≥99%	European Chemicals Agency (ECHA)
4	Ethylenediaminetetraacetic acid (EDTA)	$C_{10}H_{14}N_2O_8.H_2O$	80%	
5	Hydrochloric acid (HCl)	HCl	99%	SD Fine Chem limited, India

2.3 Method of Chemical Precipitation

2.3.1 Preparation the NaOH solution

To prepare (0.25) g (1) M of sodium hydroxide flakes were dissolved in 100 mL of deionized water while being continuously stirred for roughly 15 minutes at 25 °C.

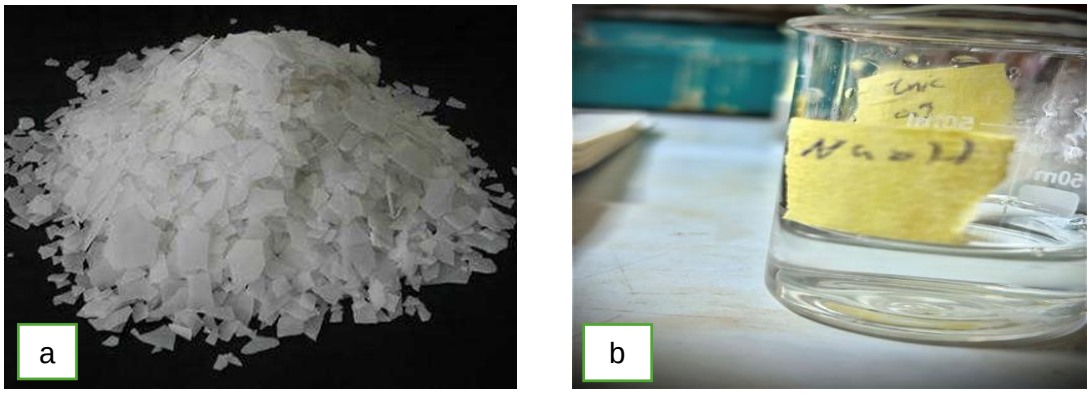

Figure (2.1): Images for sodium hydroxide flakes (a) and the NaOH solution (b)

2.3.2 prepared of Na_2Se solution

In the beginning (0.207) M of sodium selenium were dissolved in 150 milliliters of deionized water to create 0.5 M of Na_2Se Figure (2.2): It took 30 minutes to thoroughly mix the prepared solution.

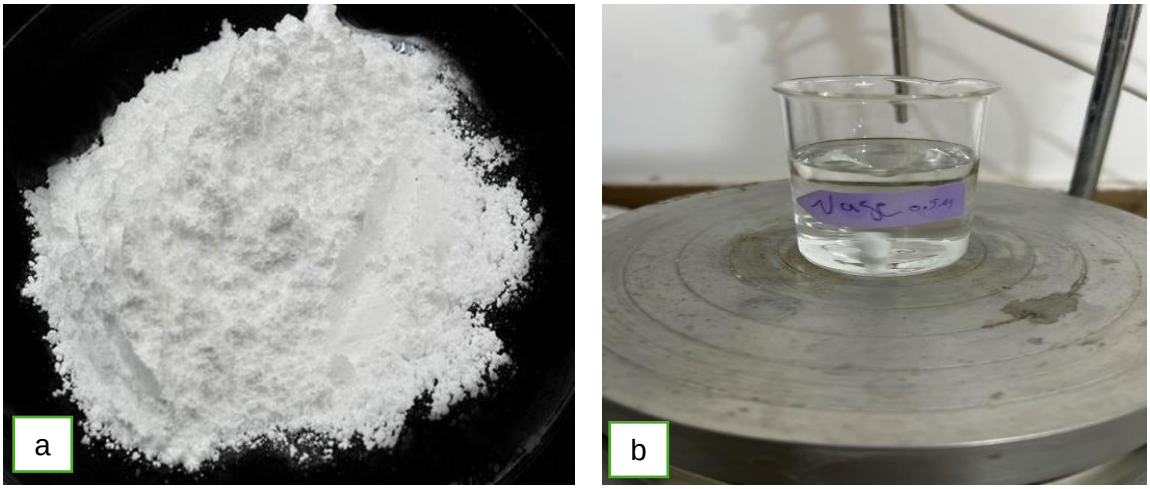

Figure (2.2): Images for sodium selenide prepare (a) and the Na_2Se solution (b).

2.3.3 Zinc acetate Preparation

in the binging (0.485) M of $Zn(CH_3COO)_2 \cdot 2H_2O$ was dissolved in 150 milliliters of deionized water to create 0.01 M $Zn(CH_3COO)_2 \cdot 2H_2O$ solution after dilution. The resultant solution was stirred for 30 minutes and then put somewhere dry.

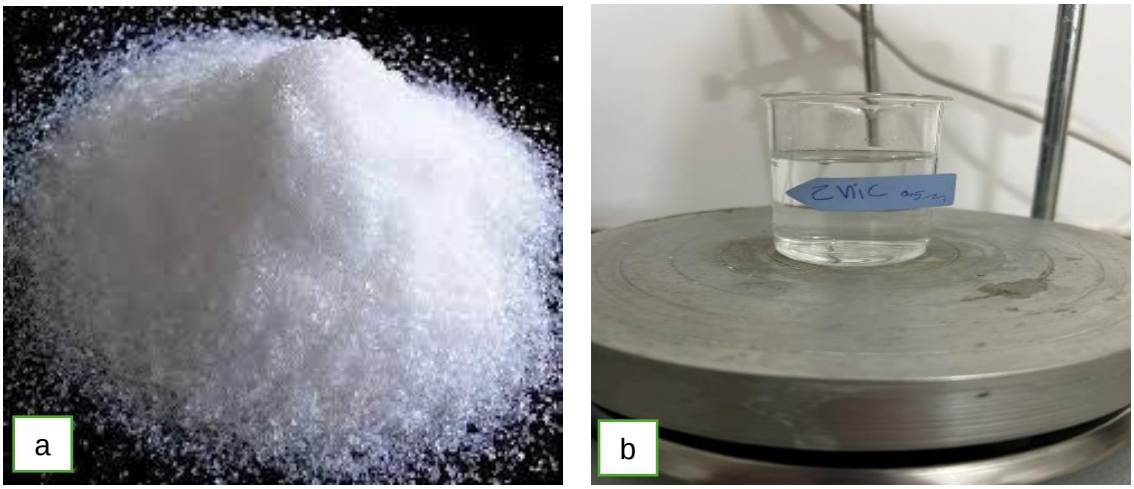

Figure (2.3): Images for Zinc Acetate prepare (a) and the Zinc Acetate solution (b).

2.3.4 Preparation of Ethylenediaminetetraacetic acid (EDTA)

In a beaker with 160 mL of deionized water, an appropriate quantity of ethylenediaminetetraacetic acid (EDTA) (4.67 g) was added to create the polymer solution. A magnetic stirrer was then used to shake the beaker for 15 minutes, or until no more particles were visible. In Figure (2.4)

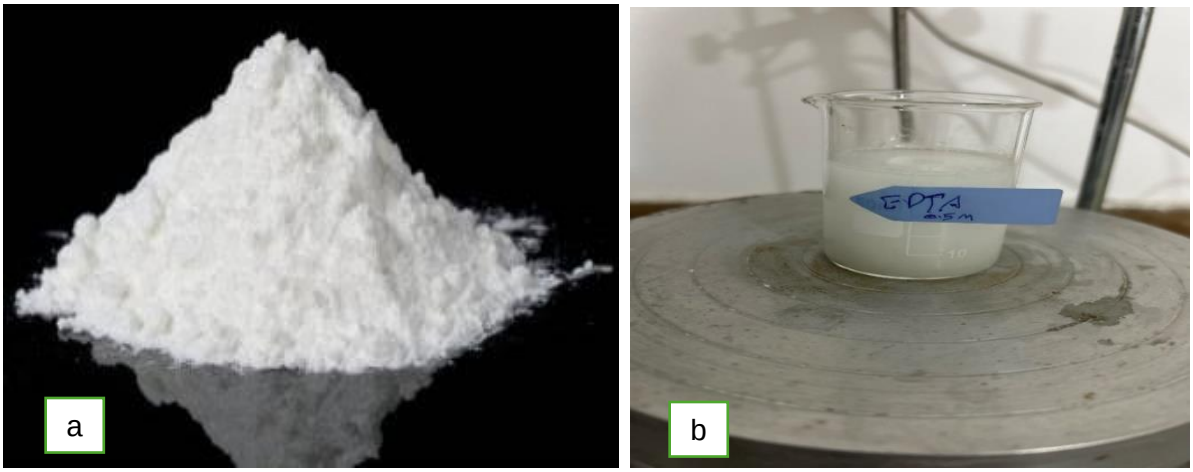

Figure (2.4): Images for EDTA prepare (a) and the EDTA solution (b).

2.4 Synthesis of ZnSe nanoparticles

The chemical precipitating approach was used to create ZnSe nanoparticles. The starting ingredients used were sodium selenide Na_2Se and zinc acetate, $Zn(CH3COO)_2.2H_2O$. (0.5 M) in the prepare quantity was dissolved in 100 ml of deionized water and vigorously agitated for approximately half an hour. Following a brief period of stirring at room temperature using a magnetic stirrer, 0.5 M sodium selenide was gradually added to the Solution of Zinc acetate. Zinc selenide nanoparticles were generated with the formation of a white solution after an hour. Three rounds of washing the precipitate with deionized water were employed to remove unwanted materials. We used a 4000-rpm centrifuge for 15 minutes in order to separate the precipitate. For three hours at 80 °C, the specimen was dried in a drying oven. Figure (2.5) summarizes the stages involved in the creation of ZnSe nanoparticles.

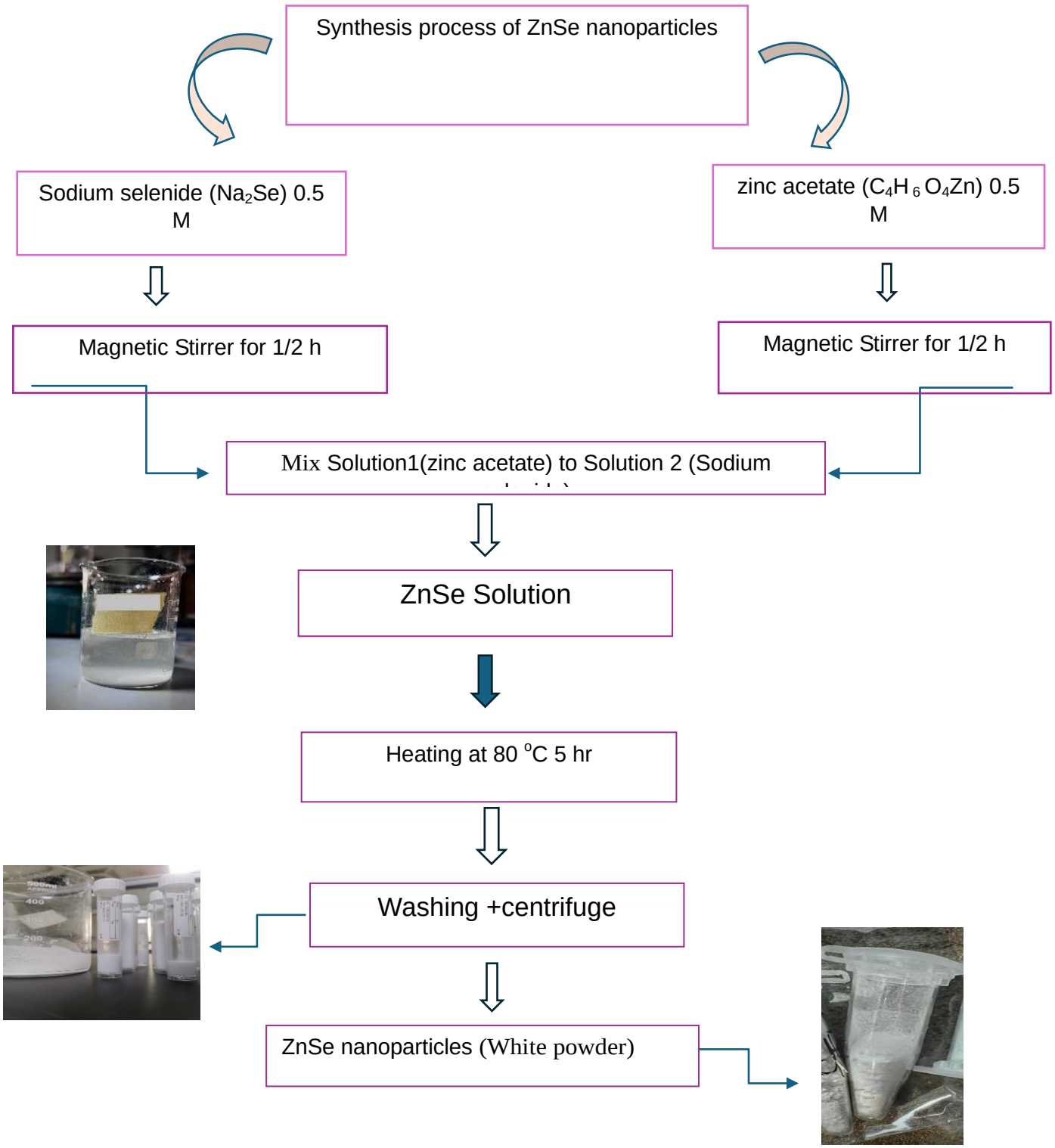

Figure (2.5): A schematic diagram showing the formation process of ZnSe nanoparticles by chemical precipitation method.

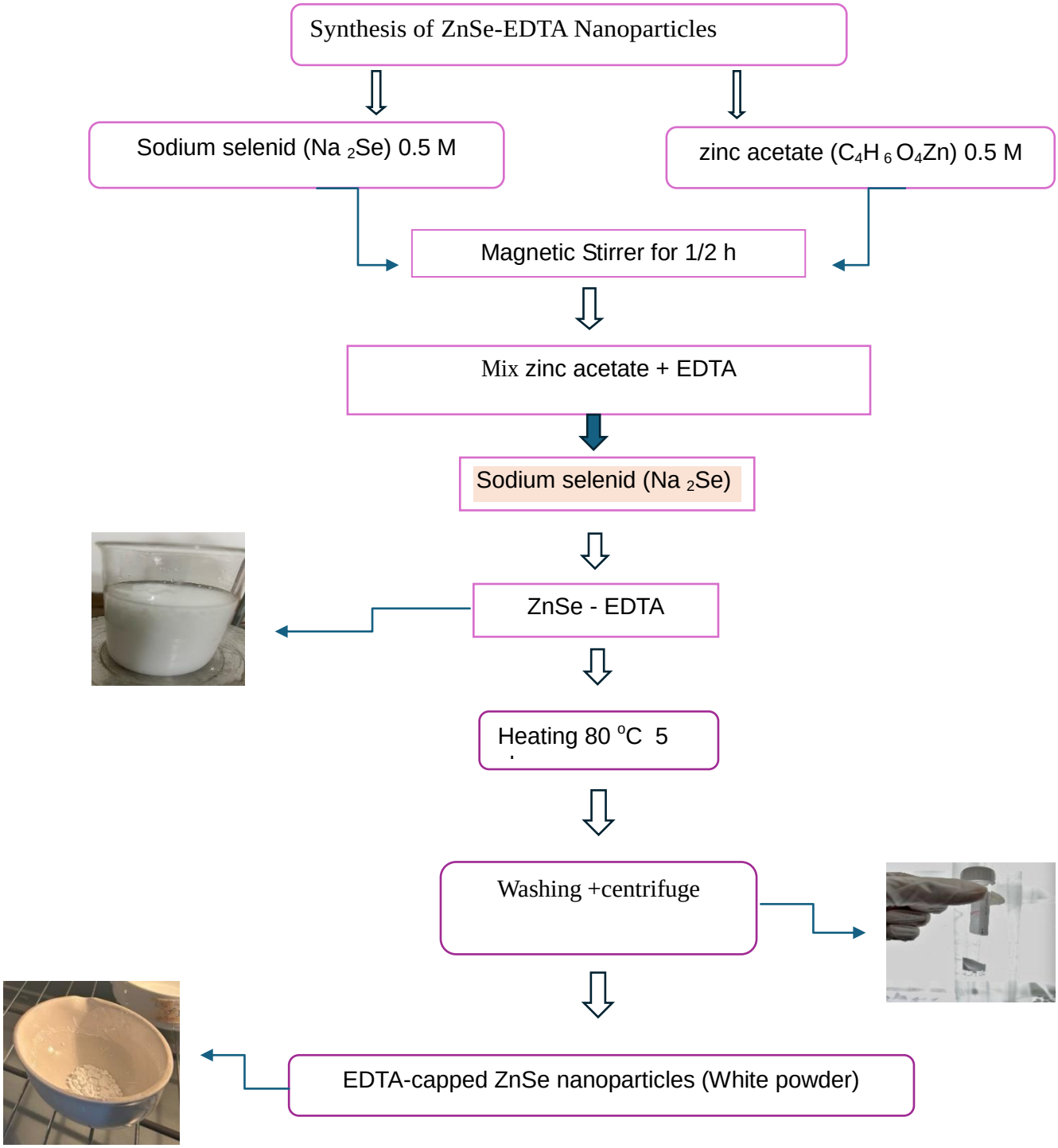

Figure (2.6): Diagram illustrating the stages involved in producing nanoparticles while is present.

2.5 Examination of nanostructure:

The production of both capped and uncapped ZnSe nanostructure can be confirmed using an easily technique (UV-visible spectroscopy). FT-IR spectrophotometer was used to determine the functional groups which are expected to be found on the surface of the ZnSe particle. This technique can also confirm the production of ZnSe particles. One of the most interesting things about this type of FTIR spectroscopy is that a little sample is used; instead of being combined with KBr like in conventional FTIR spectroscopy, the sample is placed on a tin selaned lens.

Field emission scanning electron microscopy (FESEM) was used to study the size and shape of the prepared particles. It provides a high resolving power estimated at nanometers due to the high energy of the electron beams. The extremely small size of the electron beam spot produces high-resolution images of the surface of the material when compared with the magnification of the optical microscope (500,000 times larger than the optical microscope. [65]

Finally, FESEM requires the sample chamber to operate in high vacuum, so it requires the preparation of a completely dry and solid sample. Energy dispersive X-ray spectroscopy (EDS) was used to identify the presence of elements in ZnSe sample.

XRD technique was used to determine crystal size and crystal structure. The XRD pattern is used as a kind of "thumbprint" to identify the material by comparing the sample's chart with the data in well-established global information repositories like the Center International Data Diffraction (ICDD). [66]

The basic principle of XRD technique is that the colliding of fast electrons with a target surface leads to producing an x-ray. The electrons of the atoms that are present in the crystal will interact with this ray. The atomic planes permit some

of the beam to pass while reflecting the remainder. The incidence angle (θ) is equal to the reflected angle, which is also referred to as the Bragg angle which can be calculated from Bragg's law nλ =2dsin θ, where θ is Bragg angle; λ is the wavelength of x-ray; n is an integer called the order of reflection (n=1, 2, 3); and D is the distance between the set of levels.[67]

For the rays to interfere constructively, this path difference must be an integral number of wavelengths. The possible d-spacing defined by the indices h, k, l are determined by the shape of the unit cell. Rewriting Bragg 's law we get:

n λ =2dsin θ

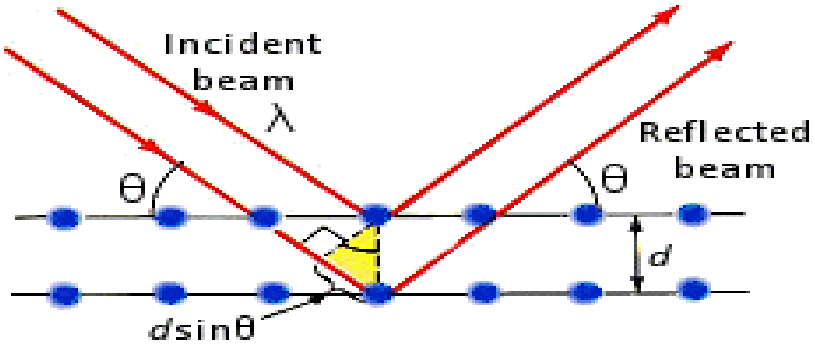

Figure (2.7): Schematic diagram of X-ray diffraction process.

An efficient technique for differentiating between capped and uncapped nanoparticles is Raman spectroscopy, which examines the variations in vibrational spectra. Peak changes, intensities, and the emergence of new peaks can be used to help researchers better understand the chemistry and characteristics of nanoparticle surfaces. Raman affect can be seen in molecules that have no net dipole moment and so no pure rotational spectrum, but it also depends on the polarizability of the molecule. Through this technique, details regarding the molecule's structure and moment of inertia can be discovered. There is very little impact from light scattering by molecules or crystal lattices. Spectral analysis shows the presence of a strong line that corresponds to the wavelength of the light source when monochromatic light is dispersed by molecules or crystal lattices. Furthermore,

lines with lower intensity can be seen at wavelengths that differ from the wavelength of the light source. These lines are known as Raman lines, named for the Indian physicist Chandrasekhara Venkata Raman. Though these lines were known to exist in theory, Raman was the first to really demonstrate them in 1928[.68)]

2.6 Theoretical part

2.7 Functional Hybrids

Hybrid functions are a class of approximations to the exchange and correlation energy function in density functional theory (DFT) that incorporate a part of the exact exchange from Hartree-Focke theory. The core of the hybrid functionals is a GGA correlation functional with an exchange contribution that was obtained partially from the HF theory, which accurately calculated the exchange energy, and partially from an exchange functional. [(69)] Different hybrid approaches have different ratios for the two GGA functionals and the HF exchange energy, which are frequently changed to fit a set of experimental data. Although hybrid approaches are the most accurate, they have the disadvantage of calculating the HF exchange energy requires the use of four-center integrals. The result is GGA calculations are less expensive computationally than hybrid DFT calculations. [(70)]For instance, the common BLYP functional combines the gradient-corrected exchange functional developed by Becke and the gradient-corrected correlation functional developed by Lee, Yang, and Parrs (Becke, 1986; Lee et al., 1988). For molecular simulations with basis sets of at least 6-31G(d), the B3LYP hybrid functional, also known as Becke3LYP, is most frequently used. For many organic molecule calculations, the B3LYP methodology is the go-to method due to its often-high accuracy vs. CPU time trade-off. [(71)] Due to its youth and ongoing

evolution as new functionals are created, DFT performance is unclear. Depending on the amount of theory used, Cramer provides a comprehensive overview of the applications and effectiveness of DFT. A thorough evaluation of the advantages and disadvantages of DFT versus MO theory is also given. This issue would be avoided by hybrid functionals, which combine DFT and HF and group the exchange and correlation components of each approach. [72]

2.8 Introductory

Density functional theory is one of the most well-known and frequently applied theories that have been developed to study and understand the electrical characteristics of molecules. Nowadays, DFT is widely acknowledged as an effective technique for calculating ab-initio molecular dynamics as well as the quantum states of atoms, molecules, and solids. Thomas and Fermi devised an early, approximative variant of density functional theory in 1927, not long after the development of quantum mechanics. A density functional theory of the quantum ground state was later developed by Hohenberg, Kohn, and Sham, which outperformed the theories of Thomas-Fermi and Hartree-Fock and allowed for a wide range of applications for real physical systems. [73]

2.9 Density Functional Theory (DFT)

Density Functional Theory (DFT) is known for being an effective research instrument for verifying experimental findings or describing unexplored possibilities. [74]

Electronic structure is found in the chemical and physical domains by the application of DFT, a quantum mechanical modeling technique.[75] Computational approaches that provide precisely superior scales in chemical interactions and combinations phenomena, such the DFT method, are not only affordable but also

theoretically predictive of material design through geometrical structures.[76] Furthermore, the greater the number of quantitative predictions of phenomena that are made and validated by experiment, the more a theory is accepted overall when it comes to a specific experiment that is "confirmed" by theoretical study. In. [77] Some theoretical studies have been mentioned and taken into consideration, nevertheless, as gas sensors in practical applications. ([78] In recent times, ZnSe DFT theory has been used to study the structural and electrical characteristics of molecules as nanotubes with different concentrations of ZnSe atoms.

2.10 The Technique of Density Functional Theory (DFT)

This technique, known as DFT, has been more and more common since the late 1980s. Functions whose solution yields another function, i.e., the function of the function, are referred to as functional [2].

The Schrödinger equation is the foundation of this approach, as it is of the ab initio and semi-empirical approaches. Except that it uses the electronic density function in place of the wave function. DFT's fundamental tenet is that a system's density can be used to determine its energy:

$$E = E(\rho) \qquad (2.1)$$

The DFT theory reformulates the quantum issues by using an electronic density function, which reduces the many-particle system problem to a single-particle problem. The latter minimizes the number of variables utilized as a foundation for measurement in the calculation by only requiring three variables to be calculated.

Quantum mechanics has many applications, and DFT is one of the most popular. These days, chemistry and physics frequently employ it to compute things like the band structure of materials and the binding energy of molecules. First applications are emerging in domains like biology and mineralogy, which are typically thought to be further removed from quantum mechanics. DFT has been applied to the study of relativistic effects in heavy elements and atomic nuclei, superconductivity, atoms in the center of intense laser pulses, classical liquids, and alloy magnetic properties. [79-80]

2.11 The Roothaan – Hall Equations and the Linear Combination of Atomic Orbitals (LCAO) Theoretically

The Roothaan – Hall equations can be derived by applying linear summation of atomic orbitals (LCAOS) and the principle of variation to the high frequency equation. On the other hand, in order to solve problems related to HF with respect to atoms. This can be done by using any traditional technique to solve the differential integration equations, and through the integration of the number, the HF limit can be achieved.

2.11.1 Slater-Type Orbitals (STOs):

When linear combination of atomic orbitals (LCAOs) are used to calculate molecular properties, slater type orbitals (STOs) for multiple atoms have been widely used. The STO approach relies primarily on the basis functions used for the patterns on the electronic distribution they provide. Slater calculations take enormous time but are more accurate than Gaussian calculations in this way (Pople and Beveridge 1970). The wave function is given by the spherical polar coordinates:

$$\Psi_{nlm}{}^{S}(r, \theta,\phi) = R_{nl}(\vec{r})Y_{lm}(\theta, \Phi) \qquad (2.2)$$

$\Psi_{nlm}{}^{S}(r, \theta, \phi)$: Total wavefunction. Represents the probability of finding an electron at a given point in space.

Variables: Depends on spherical coordinates ($r\ \theta, \phi$).

n: Principal quantum number.

l: Azimuthal (orbital) quantum number.

m: Magnetic quantum number.

S: Spin quantum number.

$R_{nl}(\vec{r})$: Radial wavefunction. Describes how the electron density changes with the radial distance r from the nucleus. Depends on the radial distance r.

n: Determines the energy level of the electron.

l: Defines the shape of the orbital

Where $Yl(\theta, \Phi)$ is a spherical harmonic, n, l, and m represent the principal, orbital, and magnetic quantum numbers, respectively and R (r) is the radial part of the atomic functions $Rnl(\vec{r})$ for (STOs) is expressed as:

$R_{nl}(r) = Nnr\ n-1\ \exp(-\zeta r)$ (2.3)

And:

$Y(\theta, \phi) = \theta l\ (\theta)\phi m(\phi)$ (2.4)

Where N normalization constant, and ζ is the orbital exponent and given by:

$\zeta = z-s/\ n*$ (2.5)

Where:

1: s is a protection parameter

2: z is the number of atoms

3: n* is active principal quantum number

4: The shielding parameter s, is offer an empirical value based on n and l.

2.11.2 Gaussian-Type Orbitals (GTOs):

Since Gaussian orbits (GTOs) are calculated much faster than Slater's calculations, i.e., they do not take much time, therefore Gaussian orbits are used in molecular and atomic calculations at the present time, and because Gaussian orbits (GTOs) do not have a limit in the first place, therefore they are considered representations of atomic orbits and are less satisfactory than orbits (STOs). The general shape of GTOs is the same as that of STOs, but alpha is the normal coefficient difference instead of zeta (r) in GTOs raised to the square. That is, the orbits of STOs depend on exp(-(r)) opposite in GTOs. This type of orbit depends on the radial type on exp (-(r^2)) and it is known that solving electron-electron integrals is difficult, but the limit of exp ((-(r^2)) It makes the solution of these integrals analytically possible. While in STOs it can only be solved numerically:

$\Psi nlm\ G(r, \theta, \phi) = Rnl(r)Ylm(\theta, \Phi)$ (2.6)

$Rnl(r) = Nnr\ n-1\ \exp(-\zeta r\ 2\ )$ (2.7)

The radial type in GTO depends on exp($-\zeta r2$) rather than exp($-\zeta r$). As aresult whereas with STOs they can only be solved numerically, the electron-electron repulsion can now be calculated analytically as integrals.

The fundamental drawback of GTOs is that they lack the correct "cusp" near the nucleus, as illustrated in Figure (2.8), and the exponent goes to zero extremely quickly as r increases.

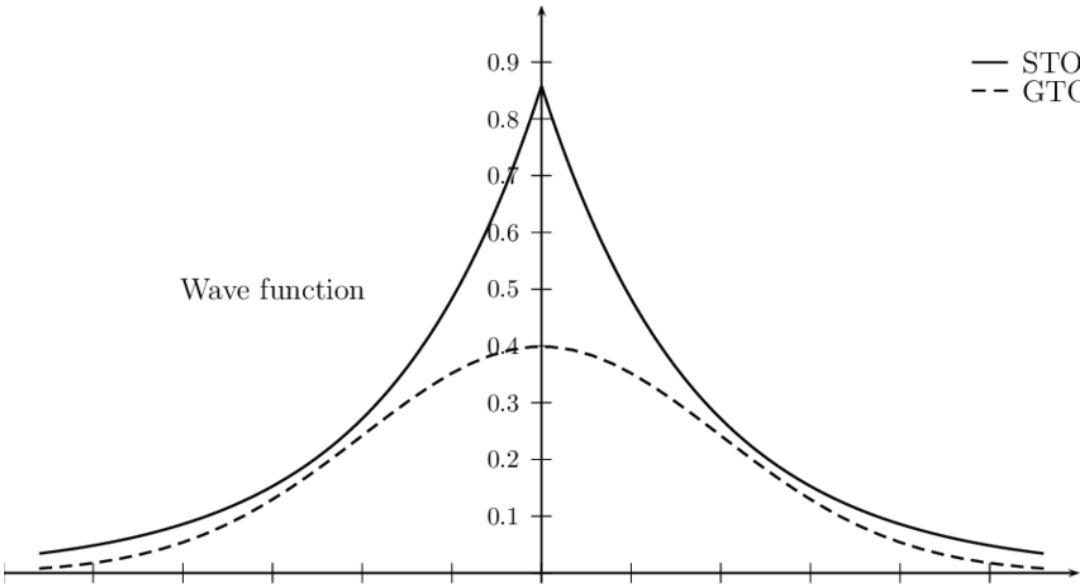

Figure (2.8): Comparison of the wave of a STO and GTO functions. [79]

2.12 Basis Sets

A basis set is a group of mathematical operations that are utilized to build a system's quantum mechanical wavefunction. [80]

The electron distribution surrounding each atom is represented by a variety of basis functions, which are frequently focused on atomic nuclei. The electron distribution across the molecule is obtained by integrating the atomic basis functions. A Slater-type orbital (STO) basis function is a specific kind of basis function that approximates atomic orbital wavefunctions with good accuracy. Yet, is challenging to evaluate; as a result, most basis sets approximate the STOs using different combinations of Gaussian-type orbitals (GTOs). To fully characterize every electron on every atom in a minimal basis set, only the bare minimum of basic functions is needed. [81]

Base groups are a set of fundamental functions used to describe both molecular and atomic orbitals. In order to obtain valuable results from chemical

calculations, the appropriate base set must be selected. The basic criterion for choosing the base set depends on its flexibility to evaluate a specific problem, the cost of calculating the required integrals, and other computational factors. [82] The following are some of the several basic set types:

2.12.1 Minimal Basis Sets

It is the basic set that contains a few basic functions and provides less accurate results compared to the rest of the other base sets. [83] STO_3G This symbol indicates a base set that utilizes one reduction of three Gaussian functions to approximate the STO orbit. The minimum baseline groups (Al-Adley) are used for qualitative results and for very large results, where accuracy is affected. The minimum group is computationally inexpensive compared to its counterparts from other base groups.

2.12.2 Split Valence Basis Sets

In this type of base group, the electrons are divided into two groups, the first group is the group of electrons, the inner layer, and the second group is the layer of electrons, the outer layer or valence electrons, this permits the alteration in orbital size that takes place during bonding. The common split-valence 6-31G basis defines the contraction scheme. [84] The dash marks the separation between the valence (on the right) and the core (on the left).

2.12.3 Polarized Basis Sets

An important basic concept that is still being used is the polarized basis set, which is a nominal function with a higher angular number. The basis group is remarkably close to the exact electronic energy in the phase modulation of the wave function. At least one set of (d) functions is included in the base set.

Polarization functions have additional functions added to the base to strengthen its flexibility, especially in the bonding regions, to provide a better description of the electron density. Can be added as (d) or * type: d-type functions added on to atoms other than hydrogens. It can be introducing as (d, p) or ** type: p-type functions added on to Hydrogens. [85]

Ex: 6-31G(d) or 6-31G*.

2.12.4 Diffuse Basis Sets

The conventional valence-size functions are opposed to diffuse functions. The s- and p-type functions are enlarged in this function. They make it possible for orbitals to cover more space. Basis sets with diffuse functions are beneficial for systems in which have electrons that are spread out from the nucleus, such as anions, effective negative charge systems, lone pair molecules, excited states systems, low ionization potential systems, and so on. For instance, in addition to the 6-31G+ + (d) basis set, the 6-31+ G(d) basis set includes plus diffuse functions for heavy atoms. [86]

2.13 Electronic Properties

2.13.1 Total Energy (Et)

The kinetic and potential energy terms of the Kohn-Sham Hamiltonian together make up the molecule's total electronic energy. The energy of a system with no interacting electrons is represented by the first term, while the effective potential energy (Kohn-Sham potential) is represented by the second. There are three terms in it; the first is electrostatic repulsion. The exchange-correlation term comes third, it precedes it to be in second place the classical coulomb interaction between the nuclei (see Eq. 2. below). This indicates that the energy needed to

combine all of the atoms and electrons is what accounts for the energy's extremely negative value. Geometry optimization is the process of determining the equilibrium positions of atomic nuclei within a specific symmetry restriction. Geometric improvements that take into account both computations. [87]

$$[\rho] = \int v\text{ext}(\vec{r})\rho(\vec{r})d\text{r} + Ts\,[\rho] + J[\rho] + E\text{xc}[\rho] \qquad (2.8)$$

Where: $E\text{xc}[\rho]$ is the exchange-correlation energy.

Ts[ρ]: is the kinetic energy of the KS pseudo particle system.

$[\rho]$: is the Coulomb energy which is a known functional of the density.

The big advantage of the KS approach is now, that $T[\rho] - Ts\,[\rho]$ is small, this means, $Ts\,[\rho]$ accounts for most of the kinetic energy contributions of the many body system, the remaining fractions of the exact kinetic energy are contained in $E\text{xc}[\rho]$.

2.13.2 Energy Gap (Eg)

The difference between the highest occupied molecular orbital (HOMO) and the lowest unoccupied molecular orbital (LUMO), as per the Koopmans theorem, is known as the energy gap. [88]

$Eg = E_{LUMO} - E_{HOMO}$

The energy differential that LUMO and HOMO produce has an impact on the molecule's kinetic stability, chemical reactivity, and interactions with other species. High levels of chemical reactivity and polarizability are exhibited by molecules with narrow energy gaps.

2.13.3 Ionization potential (IE):

For a molecule is the amount of energy needed to extract an electron from a molecule or isolated atom, and it is represented by the energy difference between the neutral (E(n)) and positive charged (+E), or the HOMO energy needed to within the context of Koopman's theorem, compute (IE) as follows [89- 90].

IE= - EHOMO

2.13.4 Electron affinity (EA)

A molecule or atom's electron affinity (EA) is the energy change that occurs when an electron is added to a neutral atom to form a negative ion. EA is expressed as the energy difference between the neutral energy (En) and the negatively charged energy (-E). Koopman's theorem uses the LUMO energy to calculate EA. [91]

$E_A = - E_{LOMO}$

2.13.5 Chemical Potential (Cp)

The energy that can be released or absorbed during a chemical interaction or phase change is known as chemical potential, and it is contingent upon the number of electrons in the molecule. When an electron system reaches absolute zero temperature, it's also known as the ferry energy in a semiconductor. $Cp = -\chi$

2.13.6 Global Hardness (η)

Determines how resistant an atom is to a charge transfer. According to IE and EA, the hardness is equal to half of the energy difference between two frontier orbitals, as expressed by the following formula:

$\eta = IP-EA/2$

2.13.7 Chemical Softness (S)

Chemical softness of molecules, which has a smaller energy gap than hardness, is a feature that indicates the degree of a chemical reaction. We thus have modest excitation energies in softness. It follows that the soft molecule's electron density varies more readily than that of the hard molecule, and we observe that the ion is the inverse of hardness based on the equation that determines softness.

$S = 1/\eta$

2.13.8 Electronegativity (χ)

One of a material's fundamental characteristics is its electronegativity, or the molecular capacity to draw electrons to itself. It is a measurement of an atom's capacity to draw electrons into chemical bonds.

$\chi = IP+EA/2$ (2.9)

2.13.9 Electrophilicity (ω)

When electrons are added to a chemical system to bring it closer to saturation, the system's electrophilicity is determined by thermodynamic properties as well as an assessment of the favorable energy shift. It can be calculated using the equation below. $\omega = -\chi\, 2/\, 2\eta$

2.13.10 Nucleophilicity (ε)

It is known as the antithesis of electrophilicity and is represented by the equation below [92]

$\varepsilon = 1/\omega$

2.13.11 Molecular Electrostatic Potential (MEP) Surface

The Minimum Energy Potential (MEP) is the energy required to transfer a single positive charge from infinity to any given location.[93] It is a local three-dimensional attribute that can be assessed anywhere in the system's space. It can show the charge distributions inside the molecule in three dimensions. Using color grading, can be specify the size, shape, and electrostatic potential of molecules.[94] The relationship between molecular structure and the physicochemical properties of compounds like biomolecules and medications has been shown to be incredibly helpfully examined using the MEP surface. It can be utilized to differentiate between the regions on the surface where there are fewer electrons (nucleophilic attacks) more electrons (electrophilic attacks). [95]High electrostatic potential energy indicates a relative lack of electrons, while low electrostatic potential energy indicates an abundance of electrons.[96]

2.14 Infrared Spectrum (IR)

The emergence of the infrared spectrometer was the reason for the emergence of spectral data processing techniques, Recently, methods of rapid analysis of spectra have become increasingly important due to ease of measurement, speed and accuracy, as the digitization of the spectra allows spectral analyzers to extract information within a period of time that does not exceed a few seconds Through infrared spectroscopy, we can know the functional groups present in the sample. The sample can vibrate in different patterns, each pattern of which is related to a distinct energy. The number of patterns in the molecule is determined by the number N of its constituent atoms. If the molecules are linear, the number of patterns is known through the relationship (3N-5), In the case of the non-linear molecule, it is determined through the relationship(3N-6).[97] For a molecule to be effective in infrared spectroscopy, it has a spectrum, it must possess a second pole

moment. [98] The compounds and their functional groups can be identified as shown in the figure (2.9).

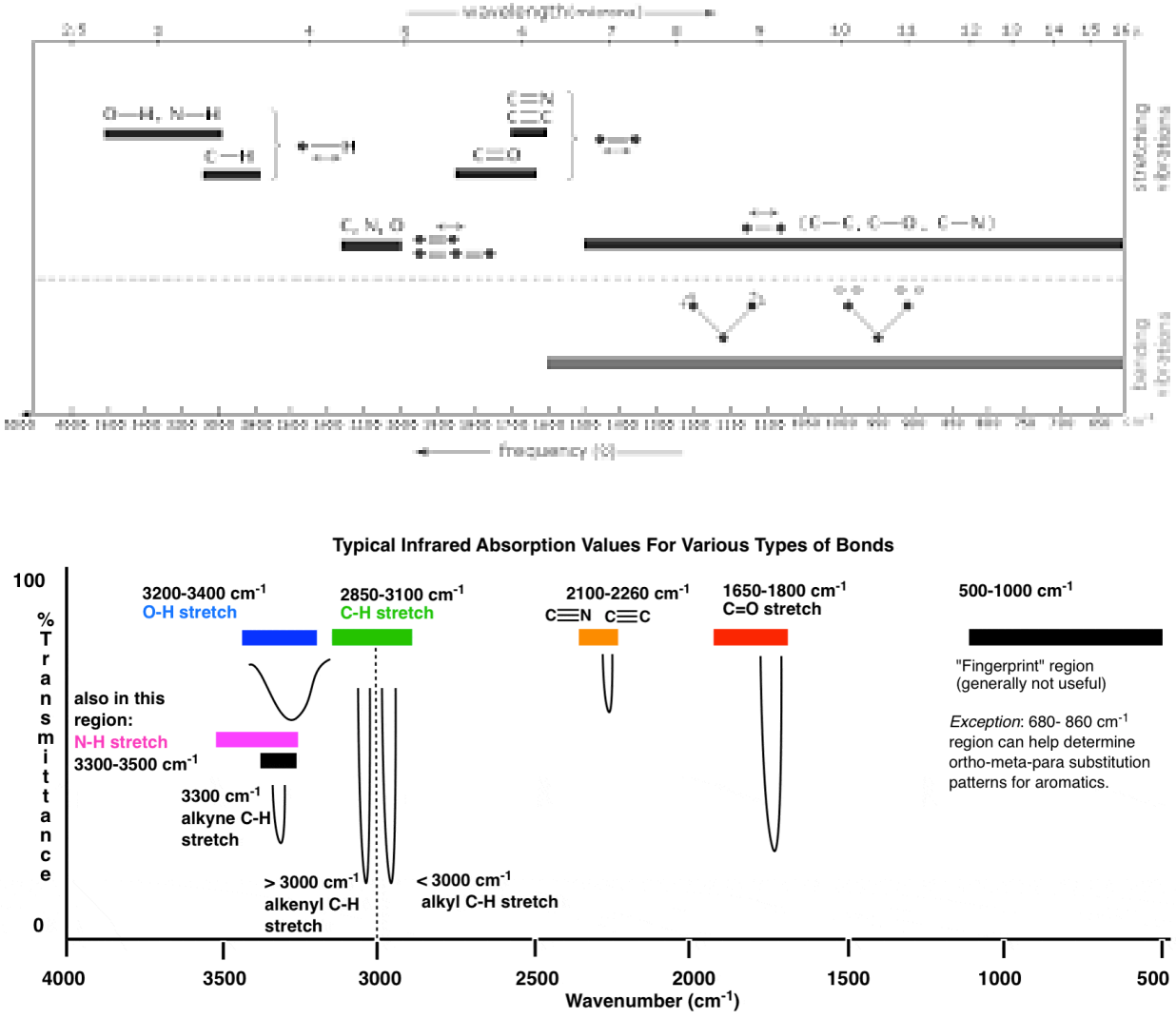

Figure (2.9): The compounds and their functional groups

2.15 Vibrational Frequencies

Vibrational modes of active molecules in infrared or Raman spectra correspond to specific bends or stretches that can be determined by their frequency. The characteristics of these modes can vary depending on whether they are vibrational patterns that are stretching or bending. Bending modes change the bond angles while keeping the bond length constant, whereas stretching modes change the bond length while maintaining the bond angles. In addition to a variety of bending modes, such as scissoring, wagging, twisting, and rocking, there are two types of stretching modes: symmetric and asymmetric stretching. These modes are illustrated in Figure (2.10). [(99)]

Bending modes, which are frequently used in IR spectroscopy in various materials or chemical compounds, may be able to discriminate between amino acids in what is referred to as the fingerprint region. Stretching modes are much more common than terminating modes. In Raman spectroscopy, bending modes are rarely observed because they do not change the bond length or polarizability. For the same reason, asymmetric spans are also rare. Because the bond length varies, but does so uniformly for both molecules, indicating that the overall distance does not vary, Raman spectroscopy has been able to see these phenomena. In the symmetric stretching modes, the variation of both bond lengths affects the polarizability of the molecule. Due to the fact that numerous vibrational modes observed in Raman spectroscopy appear to be symmetric stretching modes. [100]

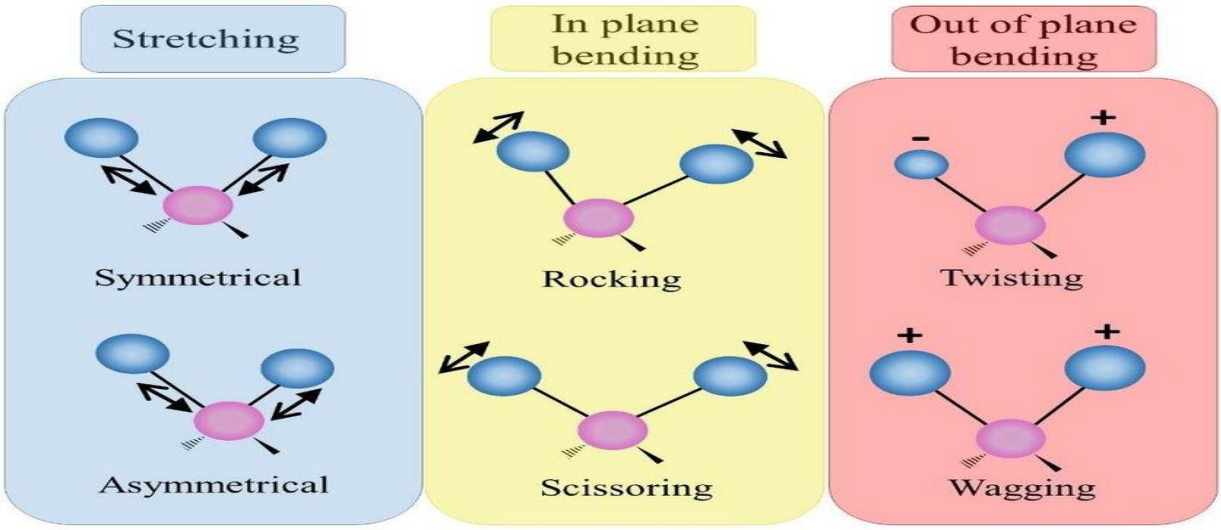

Figure (2.10): The Bending modes

2.16 Theoretical part:

2.16.1 Computer used

1. Laptop Think pad
2. System: Windows 10 - 64-bit
3. Hard disk: 500 GB
4. RAM: 8.00 GB
5. Intel Core i7-5600U CPU @ 2.60GHz 2.59 GHz

2.16.2 Programs

Gaussian 09W and Gauss View 6.0 are computational programs used in physical chemistry to study and analyze molecules using quantum mechanics. Gaussian 09W calculates molecular properties such as energy, shapes, and vibrational frequencies, while Gauss View 6.0 provides a graphical interface for visualizing molecular structures and analyzing computational results in an easy-to-understand way.

2.16.2.1 Gaussian 09W

Numerous chemists and chemical engineers utilize this computer program in physical biochemistry, fundamental applications of quantum mechanics to forecast energies, compositions, and elemental combinations of the ultraviolet and infrared resonance spectra, and Gaussian This computer program has being continuously updated and developed by a research group at the University of The phrases orbital and gaussian are the sources of the name Carnegie-Mellon, which was first used in advertising in 1970. Starting with the basic concepts of quantum mechanics, Gaussian predicts the energies, molecule shapes, and vibrational frequencies of molecular systems in addition to many other molecular attributes derived from these core computation types.

It can be applied to investigate molecules and processes in various contexts, such as those involving compounds and difficult stable species. The Gaussian program, which is based on solving the Roothaan-Hull equation, can be used to determine the most elements in the periodic table. The basis set or quantity of wave functions used determines how accurate the calculations in this program are. [101]

2.16.2.2 Program Gauss View 6.0

Gauss View application interface was used to construct a graphic depiction of the chemical structures after extensive experimentation with the program's interface. The major functions of Gauss View 6.0 are used in conjunction with the routine works. A visual depiction of molecular structures can be obtained as a result. The input files were exported into Gauss View to provide an example. the dimensional photo's output files for the Gaussian software. In addition to the Gaussian calculations, which are not utilized as calculation steps, the Gaussian view is a software that makes the Gaussian program's work easier. The main goals of the Gaussian perspective are [(102)], First, molecules—especially large ones—are easily drawn. This allows for fast rotation, transfer, and modification of atomic bonds and angles.

Second, the Gaussian view makes it possible to use geometrical methods, such as balanced molecular patterns, molecular orbitals, and electronic surface density, to verify the outcomes of Gaussian calculations.

Third: Several Gaussian computations can be accomplished with the help of the Gaussian perspective, simplifying the complicated input required for both common tasks and sophisticated techniques. [(103)]

2.17 Energy Gap, LUMO, and HOMO

Within the molecular orbitals, the two most significant ones are the lowest unoccupied orbital (LUMO) and the highest occupied orbital (HOMO). Located near the outermost limits of the molecules' electrons, these orbitals are known as the frontier orbitals. Acting as an electron donor is the orbital with the highest energy (outermost) containing electrons, or HOMO. Within the theory of molecular orbitals, the most significant are the highest occupied molecular orbital (HOMO) and the lowest unoccupied molecular orbital (LUMO). Conversely, the

Lowest Energy Orbital (LUMO) is the innermost orbital with the least amount of space for electrons to enter. In terms of the band gap, the difference in energies between the HOMO and LUMO levels ($Egap = ELUMO - EHOMO$) and the resulting energy gap not only dictate how the molecule interacts with other species, but also helps characterize its kinetic stability and chemical reactivity.

More polarizable and typically linked to strong chemical reactivity and low kinetic stability, a molecule with a tiny frontier orbital gap is also known as a soft molecule. Figure 2.11 represents the band gaps and energy levels of (HOMO) and (LUMO) interactions between two different molecules. However, Figure 2.12 clearly illustrates the movement of electrons from the ground state to the excited state—also referred to as the excited state—through the filling of open molecular orbitals.[104]

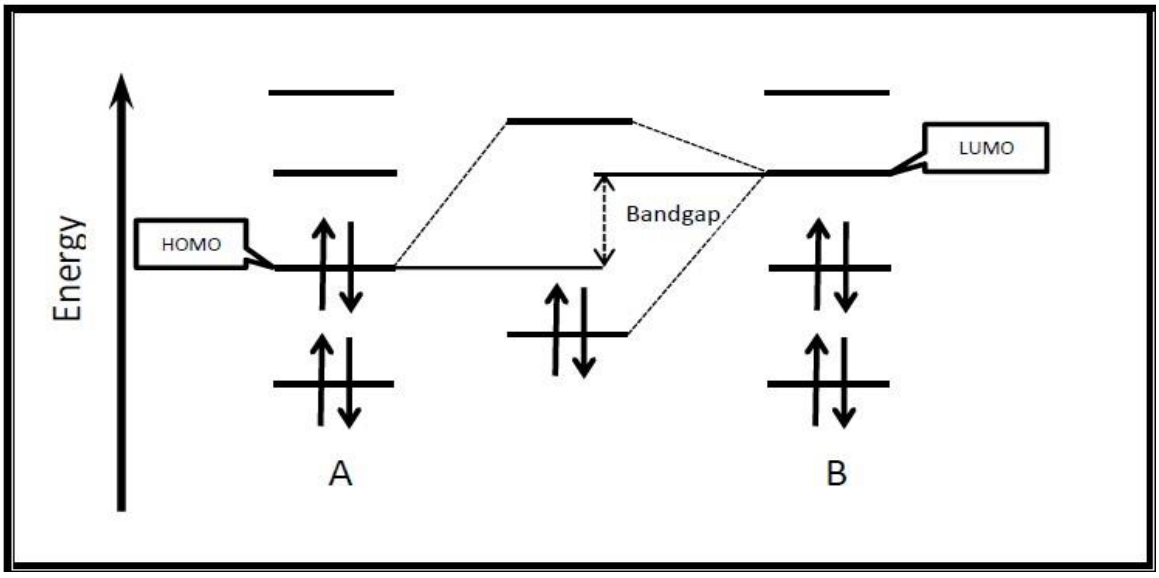

Figure (2.11): The band gap diagram and HOMO-LUMO of two interacting molecules

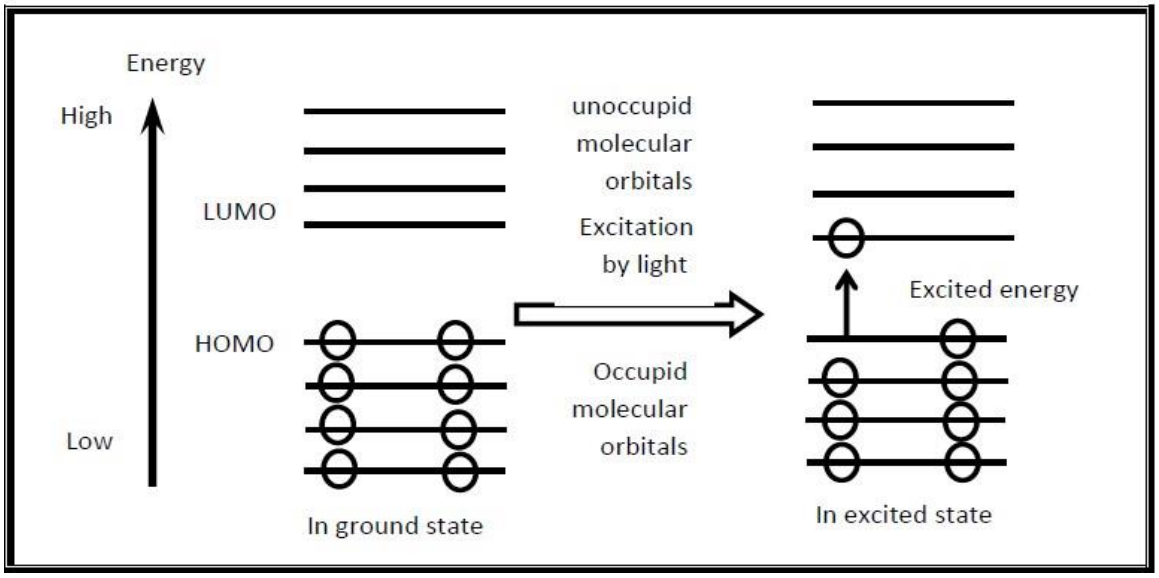

Figure (2.12): The ground state and excited states' HOMO-LUMO diagram.[105]

Chapter Three

Results and Discussion

3.1 Structural properties of ZnSe Nanoparticles

3.1.1 Field Emission Scanning Electron Microscopy

3.1.1.1 FE-SEM of uncapped ZnSe

Figure 3.1 shows an insight into the surface morphology of uncapped ZnSe nanostructures. Short, elongated structures with large spherical particles were seen when the ZnSe formed without the addition of the capping agents. A possible explanation for the formation of these structures derives from the agglomeration of some nanoparticles. In other words, the additional atoms of Zn and Se will approach the existence ZnSe particles and agglomerate to form irregular elongated structures [106].

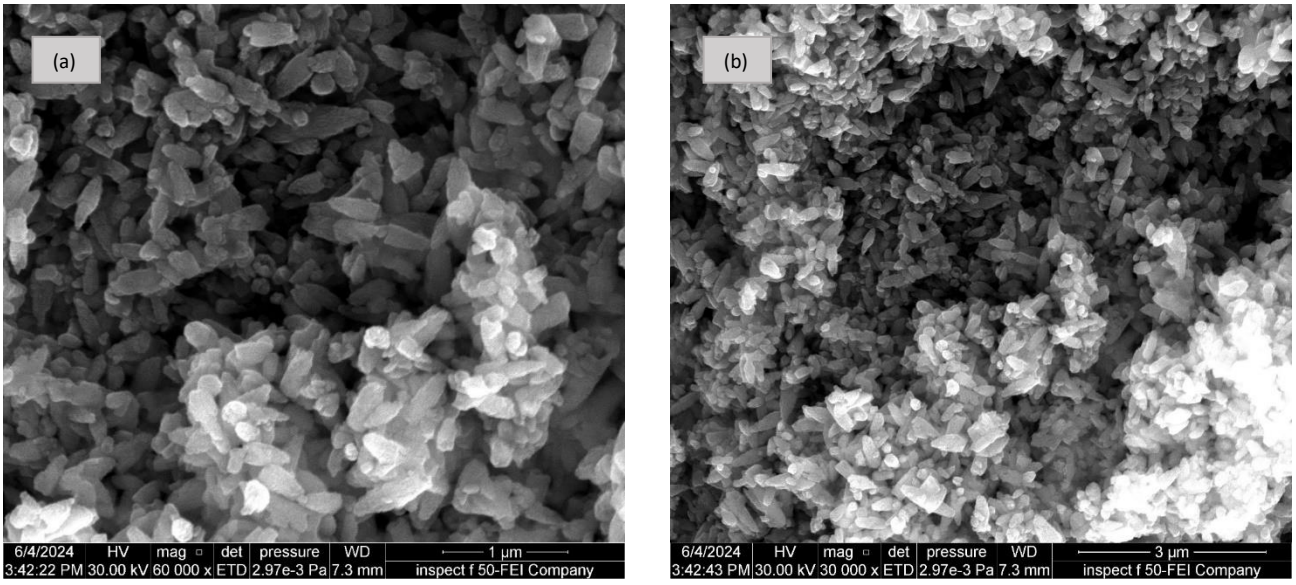

Figure (3.1): FE-SEM images for uncapped ZnSe nanostructures. The scale bar for images (a) and (b) are 1 μm and 3 μm, respectively.

3.1.1.2 Surface morphology of EDTA-capped ZnSe nanostructures

It is clear from the FE-SEM images in Figure 3.2 that EDTA plays a role in changing the shape of the prepared structures. ZnSe structures formed without the addition of EDTA have an elongated shape with few spherical particles (see section 3.1.1.1). It was thought that these elongated structures could be formed as a result of particles agglomeration. However, by introducing EDTA to the formation process, the shape was altered and became quasi-spherical. Our explanation is that the EDTA molecules prevent additional atoms from being attached to the already formed ZnSe particles. By lowering the surface energy and enabling electrostatic repulsion between the particles, this is accomplished[107]. In other words, EDTA acts as a stabilizing agent, which reduces the coalescence of ZnSe particles.

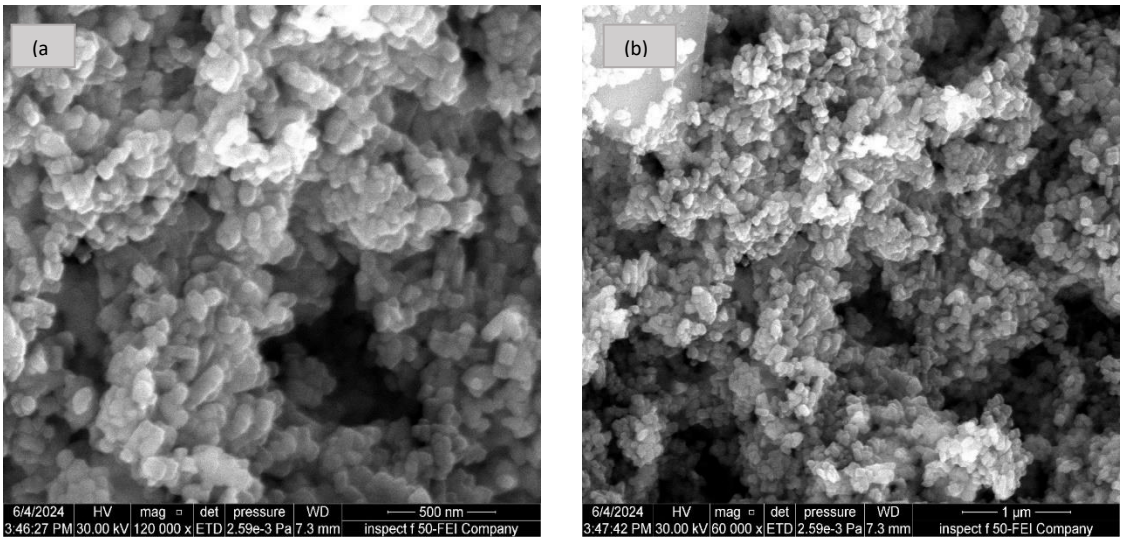

Figure (3.2): FESEM images for ZnSe nanoparticles formed in the presence of EDTA (capping agent). The scale bars of image (a) and image (b) are 500 nm and 1µm.

3.1.2 Energy-dispersive-X-ray (EDX) analysis

3.1.2.1 EDX for uncapped ZnSe nanostructures

The elemental analysis of ZnSe formed in the absence of EDTA was studied using EDX. Figure 3.3 (a) conforms the presence of Zn and Se in the sample in addition to the appearance of small peak for carbon atoms which has probably come from the coating process of our sample in order to make the sample conductive.

Elemental mapping was used to confirm the elemental analysis of the sample. It seems from Figure 3.3 (b and c) that the majority of a sample is composed of zinc (Zn) and selenium (Se) atoms suggests that these two elements are the main constituents of the substance under study. According to the statement, the sample is composed of the combined concentration of Zn and Se, which are both probably present in considerable levels.

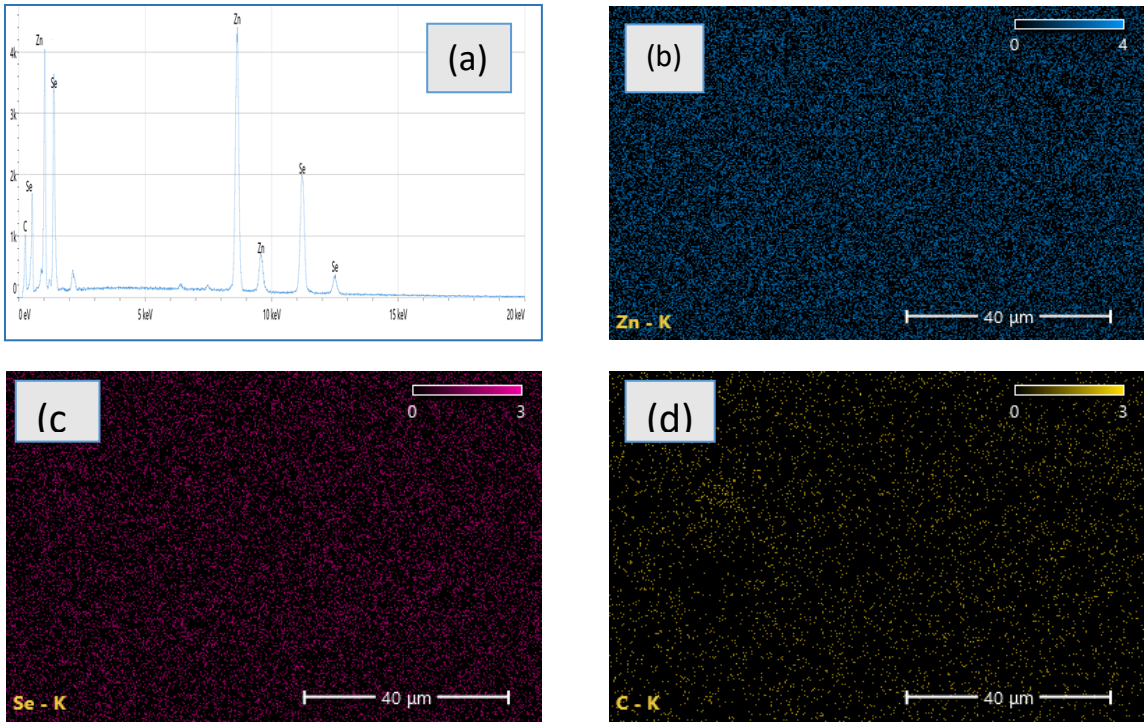

Figure (3.3): EDX chart for ZnSe nanoparticles in the absence of EDTA (a), elemental map of Zn, Se, and C of ZnSe nanostructures (b-d)

3.1.2.2 EDX of EDTA-capped ZnSe

The EDX chart for ZnSe structures capped with EDTA shows that in addition to the presence of expected elements (Zn and Se) in the sample, there are two peaks for oxygen and nitrogen elements, which are properly raised from the EDTA components. As seen in Figure 3.4 (a) there is a peak for carbon element, which is attributed to the coating of the sample with carbon element to make it conductor.

The elemental map for each element distributes inside EDTA-capped ZnSe particles is represented in Figure 3.4 (b-f). Each color in the map represents a distinct element. The element's concentration in that area of the sample determines how intense the color is. Accordingly, the Zn and Se atoms are the dominant components in EDTA-capped ZnSe sample.

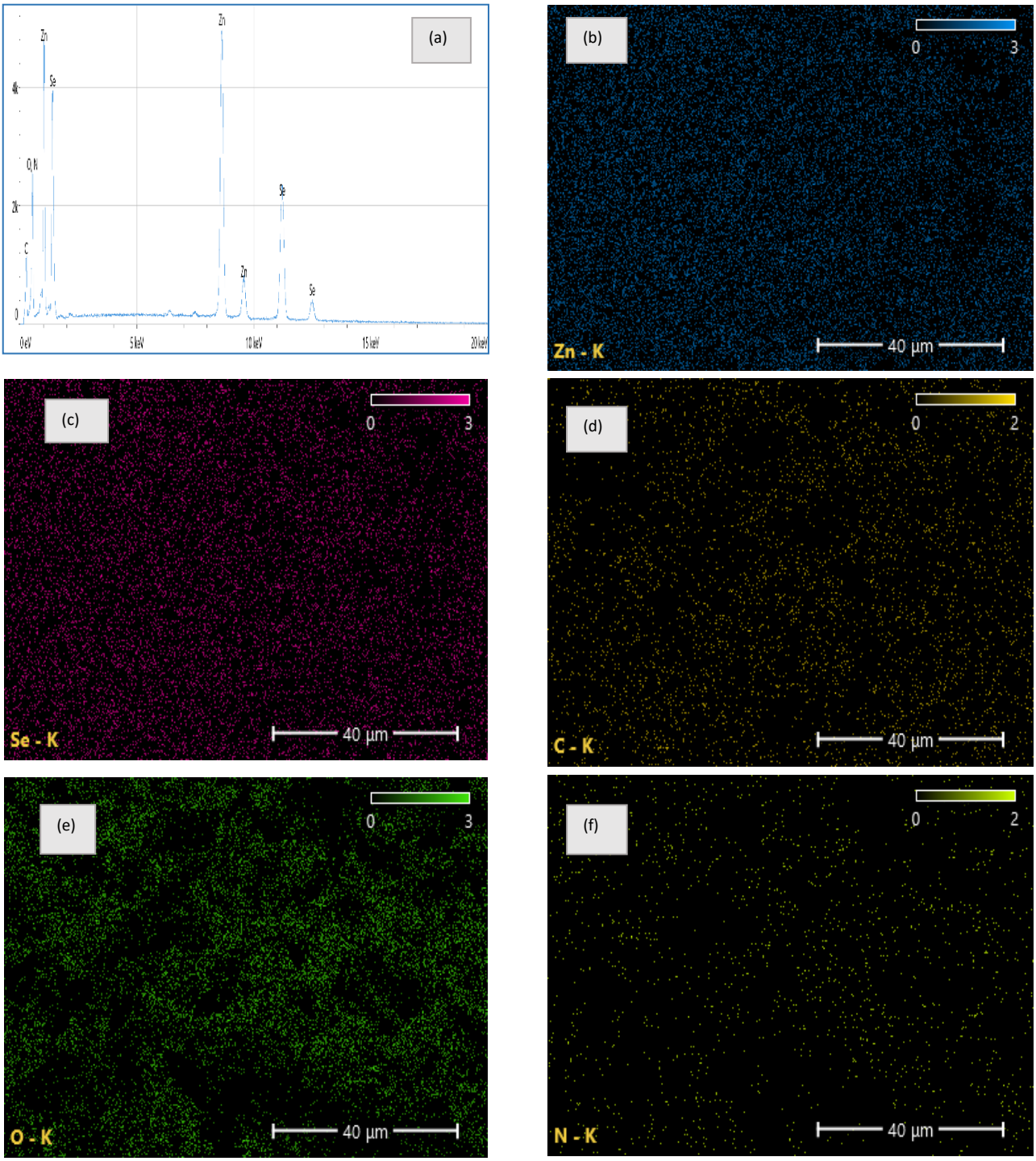

Figure (3.4): EDX for EDTA-capped ZnSe (a) and EDX mapping which shown the distribution and concentration of of Zn, Se, C, O, and N inside the sample (b-f).

3.1.3 FTIR characterization

3.1.3.1 FTIR for uncapped ZnSe nanoparticles

FTIR spectra for ZnSe nanoparticles formed without any addition of capping agent was recorded in the range 500- 4000 cm^{-1} and shown in Figure 3.5. The peaks that appear in the region between 500 -600 cm^{-1} can be assigned to the Zn-Se stretching vibration bond,[108] conforming to the formation of zinc selenid.

Additionally, several other absorption peaks appear at different wavenumber values, which may be attributed to residual materials from the synthesis process or interactions with other functional groups. The decrease in transmittance at these peaks indicates high absorption by these bonds in their respective spectral regions.

Overall, this spectrum confirms the formation of ZnSe nanoparticles without capping agents, as indicated by the characteristic Zn-Se bond absorption in the expected region.

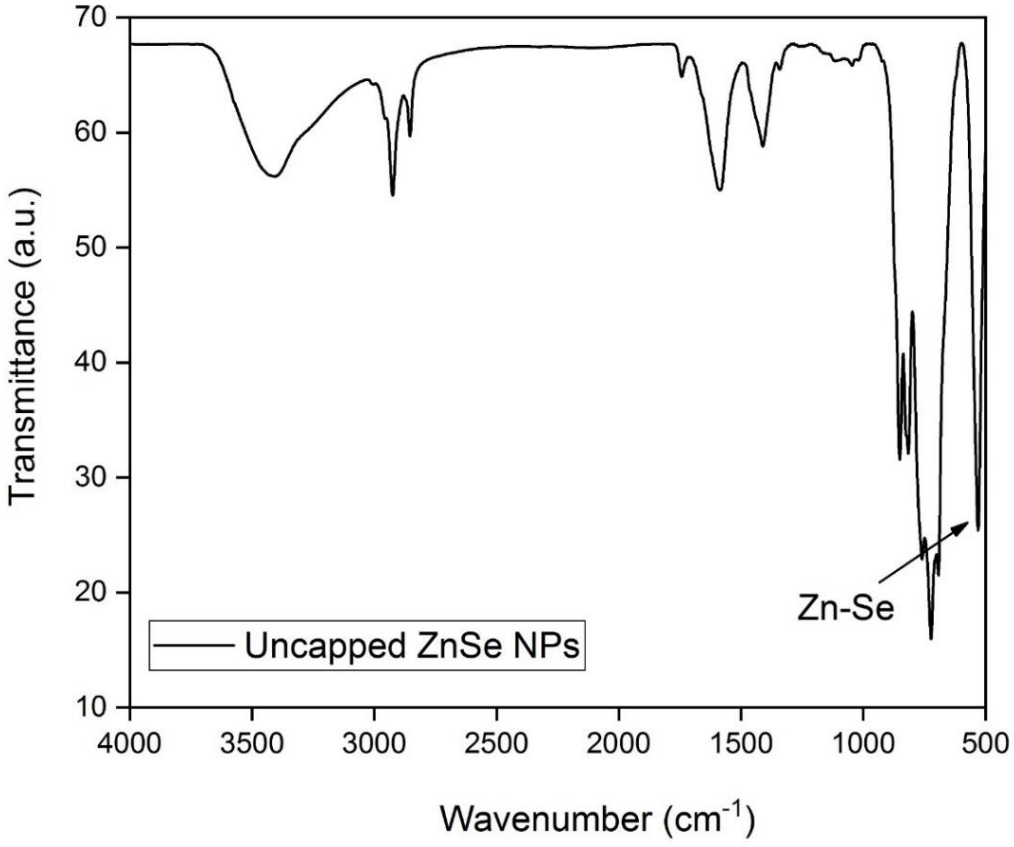

Figure (3.5): FTIR spectrum of uncapped ZnSe nanostructures

A broad absorption peak centered at 3415 cm^{-1} representing the stretching mode of O-H, which probably comes from the present of water on the surface of ZnSe nanoparticles [109]. The peak appears at 2927 cm^{-1}, suggesting the asymmetric stretching mode of C-H bond.[4] The appearance of additional peaks in the region of 700 to 900 cm^{-1} could be attributed to the surface defects phenomenon which can be observed in the FTIR spectrum of nanosized materials due to their high surface-to-volume ratio.[110]

3.1.3.2 FTIR for EDTA-capped ZnSe nanostructures

The FTIR spectra for EDTA-capped ZnSe nanoparticles was also recorded in the range 500- 4000 cm^{-1} as shown in Figure 3.6. Same peaks were observed as in uncapped ZnSe spectrum. However, the peaks at 1563 cm^{-1} and 1400 cm^{-1} are attributed to the presence of C=O stretching vibrations and the intensity in the case of capped sample is high compared to uncapped sample which could be from the presence of carboxylate anion in ETDA molecules. (111) Peak appear at 535 cm^{-1} is assigned to Zn-Se vibrations, indicating the formation of ZnSe.(112)

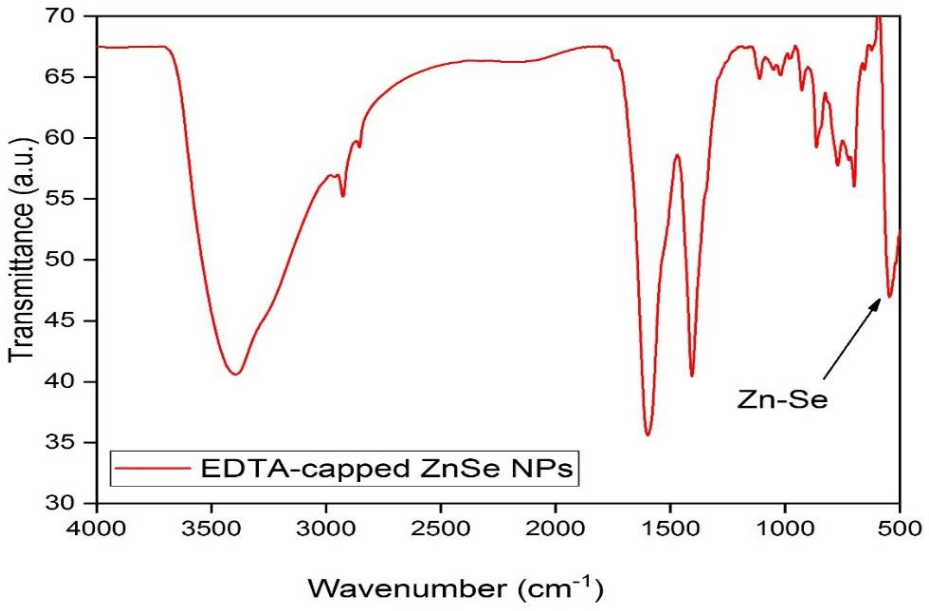

Figure (3.6): FTIR spectrum of ZnSe nanoparticles formed in the presence of EDTA.

3.1.4 X-Ray Diffraction of uncapped and EDTA-capped ZnSe nanostructures

The crystal structure of the synthesized zinc selenide was investigated using X-ray pattern (see Figure 3.7, upper panel)). The appearance of sharp and intense peaks at 2θ positions of 24°, 28°, and 29.5°, indicating the formation of well-crystallized ZnSe nanostructures. According to the most dominant Bragg peaks in the XRD chart and especially at 2theta angle of 29.5°, which corresponds to 111 plane, the prepared zinc selenide has zinc blend structure. The crystallite sizes of ZnSe particles were obtained via Scherrer equation [113] using the high intensity peaks at a diffraction angle of 29.5°.

$D=K\lambda/\beta\cos\theta$ ……. 3.1

Here, the wavelength of the Cu Kα is 0.15406 nm, θ is the diffraction angle, k is a constant (equal to 0.9), and β is the full width half maximum of the peak. The crystallite size is reported to be 22.124 nm.

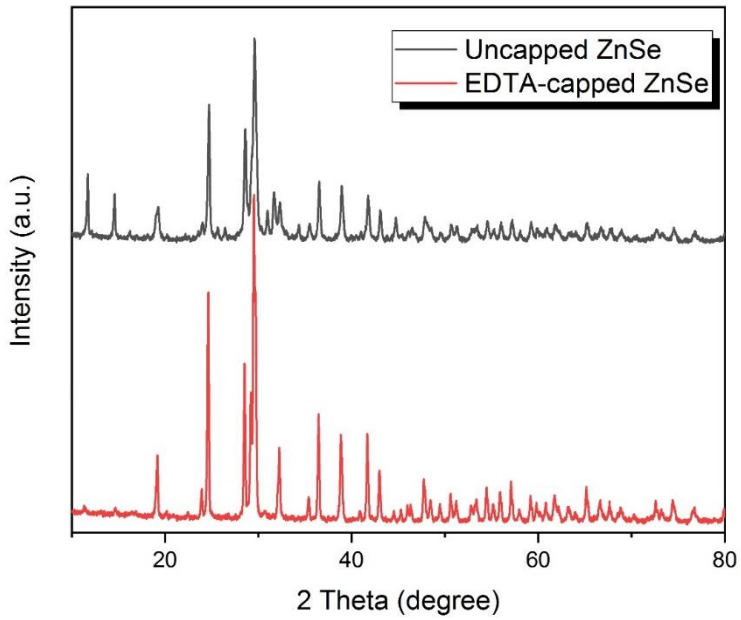

Figure (3.7): XRD pattern for uncapped ZnSe nanoparticles (upper panel) and EDTA-capped ZnSe nanoparticles (lower panel).

In order to see if the EDTA has an effect on the crystal structure of ZnSe, the XRD chart of ZnSe in the presence of EDTA was recorded in the range of 10^{o} to 80^{o}. As can be seen in figure 3.7 (lower panel) the diffraction peaks for EDTA-capped ZnSe nanoparticles are consistent with those of cubic structure, according to JCPDS Card no. 01-088-2345. [114] Capping ZnSe nanocrystals with EDTA leads to enhance the intensity of the diffraction peaks, suggesting the formation of more crystal structure of ZnSe. This finding which is quite similar to the previous work reported in the literature when the researchers capped ZnSe particles with mercaptopropionic acid (MPI). [115] The crystallite size was also calculated using Scherrer equation and it was 22.23 nm.

3.1.5 Raman Spectroscopy

The vibrational properties of the uncapped and EDTA-capped ZnSe nanostructures were studied using Raman spectroscopy at room temperature. It is known that the Raman spectrum of bulk ZnSe has two sharp peaks: Longitudinal Optical (LO) mode at 250 cm^{-1} and Transverse Optical (TO) mode at 200 cm^{-1}.[116] Moving to the nanoscale levels, the peak position, width and intensity could be altered due to the size effect. A notable shift was seen in both spectra in Figure 3.8 with respect to the bulk ZnSe, because the phonon modes may change to lower or higher frequencies as the particle size decreases. In uncapped ZnSe spectrum, a strong peak appears at 140 cm^{-1} could relate to TO phonon mode, another wide peak was observed at 478 cm^{-1}. These peaks were shifted towards higher wavenumbers (blue shift) when the particles capped with EDTA. This can be explained by the fact that smaller particles have distinct phonon modes. The Raman peaks for EDTA-capped ZnSe nanoparticles exhibit broadening compared to uncapped ZnSe nanoparticles. The reasons for this broadening are phonon scattering, size effects, and a higher surface-to-volume ratio.

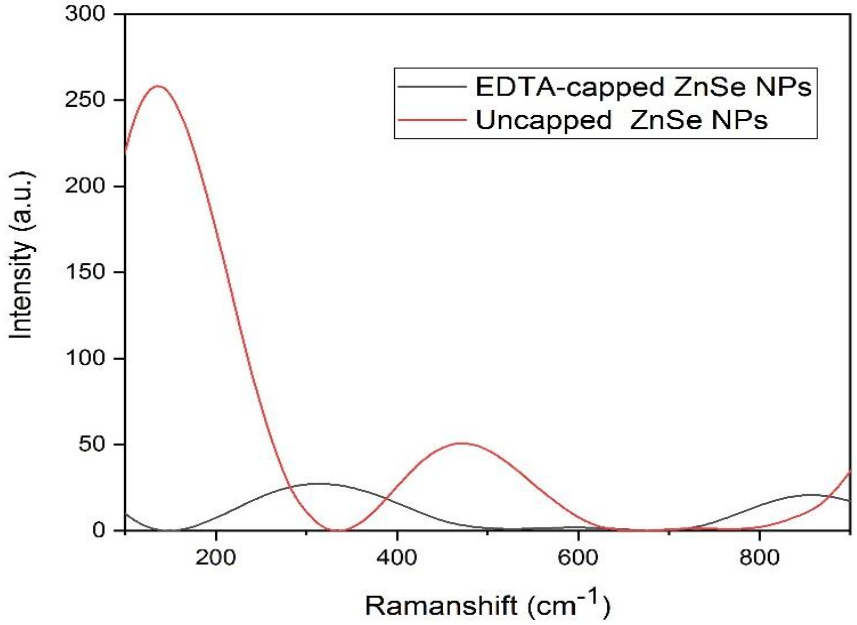

Figure (3.8): Raman spectra for ZnSe formed without the addition of EDTA and with the addition of EDTA.

3.2 Optical properties of ZnSe nanostructures

3.2.1 The absorption spectrum of uncapped ZnSe nanostructures

It is well known that the properties of nanomaterials can be easily changed by altering their shape and size. Therefore, in this section we amid to study the optical properties of ZnSe nanomaterials in the absence and presence of the capping agent (EDTA). After mixing the precursors, the color of the solution changed from colorless to white, which can be attributed to the formation of ZnSe nanoparticles. The UV-Visible spectrum of uncapped ZnSe nanomaterial was shown in Figure 3.9(a). A notable peak at 363.8 nm can be seen, which is in a blue shift with respect to the bulk ZnSe (460 nm),[117] suggesting the formation of nano-sized ZnSe structures.

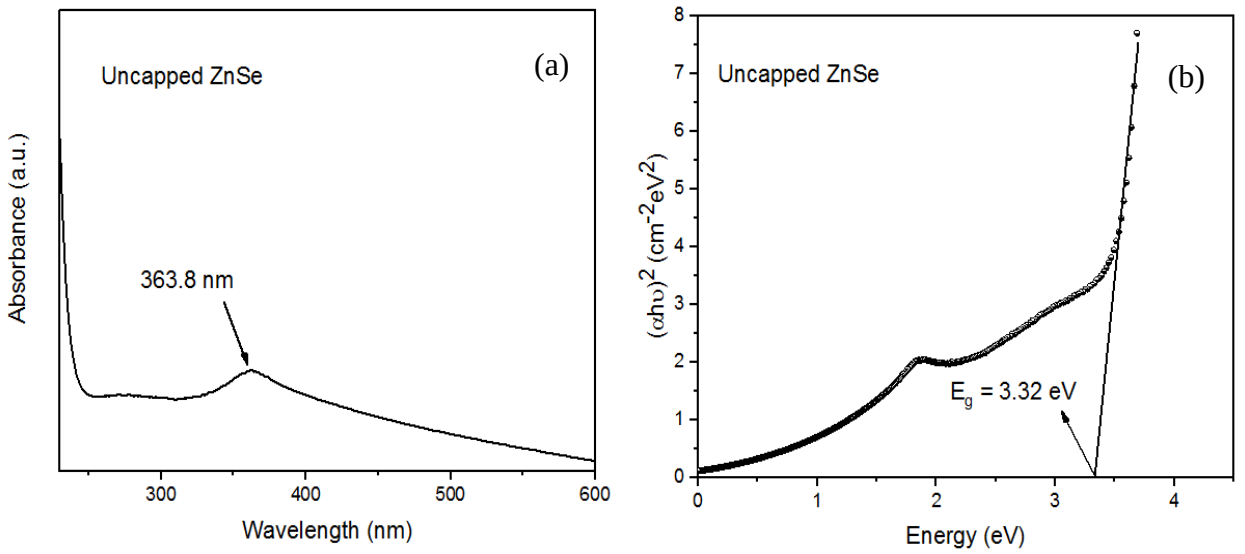

Figure (3.9): The absorption spectrum of zinc selenide nanoparticles before the addition of EDTA (a) and the optical band gap energy of ZnSe nanoparticles (b).

The band gap energy for the prepared samples was calculated using Tauc equation:[118]

$$\alpha h\nu = C\,(h\nu - Eg)^n \quad \ldots\ldots\ldots 3.2$$

The direct electronic transition (n) is equal to 0.5.[119], where (α) is the absorption coefficient, (h) is planks constant (6.626×10^{-34}), (E_g) is the band gap energy and C is the constant. The value of band gap energy was estimated from the extrapolation of the linear part of UV-Visible curve[120, 121] and it is 3.32 eV. Generally, the band gap energies of uncapped ZnSe nanoparticles are larger than that of bulk ZnSe (2.7 eV), confirming the quantum size effect.

3.2.2 UV-Vis spectroscopy for EDTA-capped ZnSe nanoparticles

The effect of introducing EDTA (capping agent) on the optical properties of ZnSe nanostructures was studied using UV-Vis spectroscopy. The UV-Visible absorption band in the EDTA-capped ZnSe nanoparticles spectrum (see Figure 3.10 (a)) is shifted towards shorter wavelengths (~360.61 nm) compared with pure ZnSe nanoparticles (~363.8 nm) and bulk ZnSe (460 nm). This shift can be attributed to the dependence of the absorption band on the size and shape of the prepared particles. In other words, EDTA plays a role in reducing the agglomeration of ZnSe particles because they prevent further atom from being add to the exist parts, leading to the reducing and stabilizing their morphology and size.

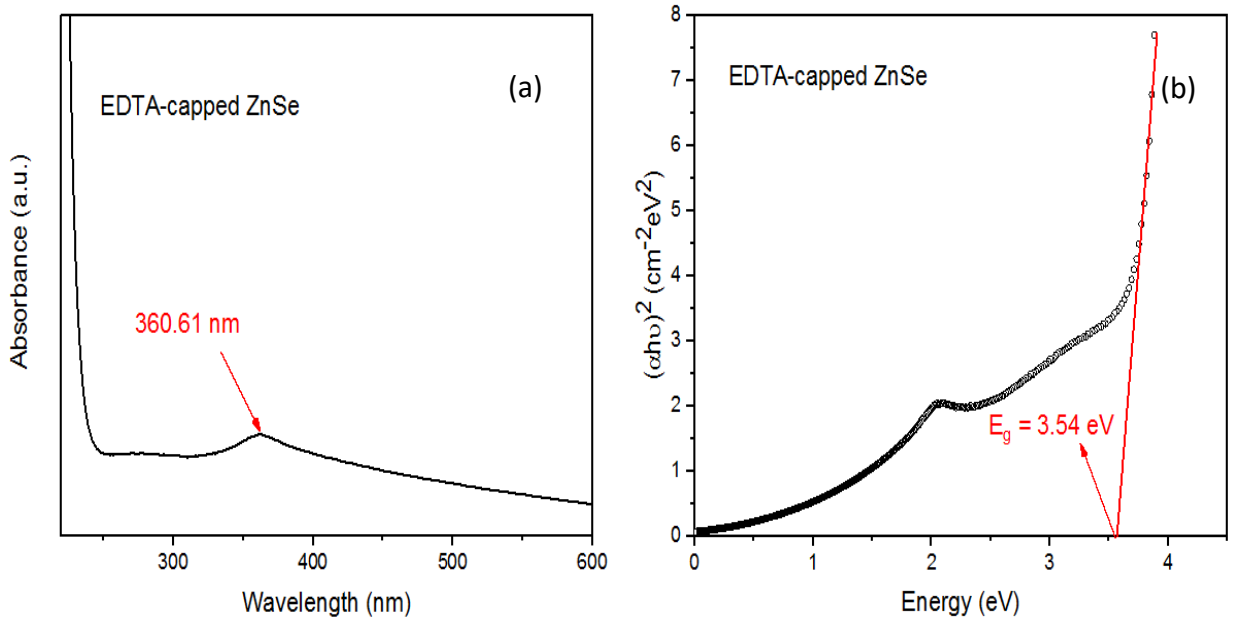

Figure (3.10): The absorption spectrum of zinc selenide nanoparticles in the presence of EDTA (a) and the optical band gap energy of EDTA-capped ZnSe nanoparticles (b).

From the UV-Visible curve, one can estimate the value of band gap energy be extrapolating the linear portion of the curve via the energy axis as shown in Figure 3.10 (b). The band gap energy of EDTA-capped ZnSe was found to be 3.54 eV, which is larger than that of pure and bulk ZnSe. A proper explanation for the formation of small nanoparticles in the presence of EDTA is that the EDTA has the ability to bind to Zn^{+2} ions via amine and carboxylate groups, leading to form stable compound. The binding zinc ions exhibit lower reactivity in comparison to free Zn^{+2} ions. This can potentially attenuate the rate of ZnSe nanoparticle nucleation and growth, resulting in a more regulated particle size.

As a result, by introducing capping agent into the growth process of nanoparticles, one can be able to tuning the band gap energy according to the desired applications.

Second part Theoretical Results

The second part in this work involving theoretical investigation using DFT calculations with hybrid B3LYP (Becke, three-parameters, Lee-Yang-Parr) and a basis set with 6-311G**, where the first asterisk above basis G represents the polarization set d – function for heavy atoms. However, the second sign indicates the polarization of p-functions of hydrogen atoms or sometimes has to be written as 6-311G (d, p) [122]

3.3 Computational details

The density functional theory (DFT) has been used to examine the electronic structure and behavior of many-electron systems, and this has had an impact on the development of the quantum mechanical approach. To comprehend the electron density distribution, functional analysis is being used by physics and chemical disciplines. This study illustrates how DFT can be used to determine the ground state (GS) and other properties of a many-electron system. In the fields of computational chemistry and physics, DFT is by far the most widely used and flexible approach. It has also shown to be quite effective at estimating the ground state characteristics of materials. The method used in this work is a basis set with 6-311G** and DFT theory with hybrid B3LYP (Becke, three-parameters, Lee-Yang-Parr). Everyone who Gaussian 09 and Gaussian View 6.0 involved equations and theories.

3.3.1 Minimize Energy

To achieve accurate results, the geometries of molecules were optimized precisely to lower the convergence thresholds. Furthermore, Frequencies of normal vibrations were calculated to confirm the minimal energy at geometric optimization by solving the equation of self-consistent field (SCF).

Figure 3.11 (-a) demonstrates the complete optimization of the geometric structure of the model of a cluster of three Zn atoms and three Se atoms (Zn3Se3), either (-b) clarifies the cluster of Zn_3Se_3 after adding EDTA, as adsorption process of EDTA on Zn_3Se_3 surface.

(a) (b)

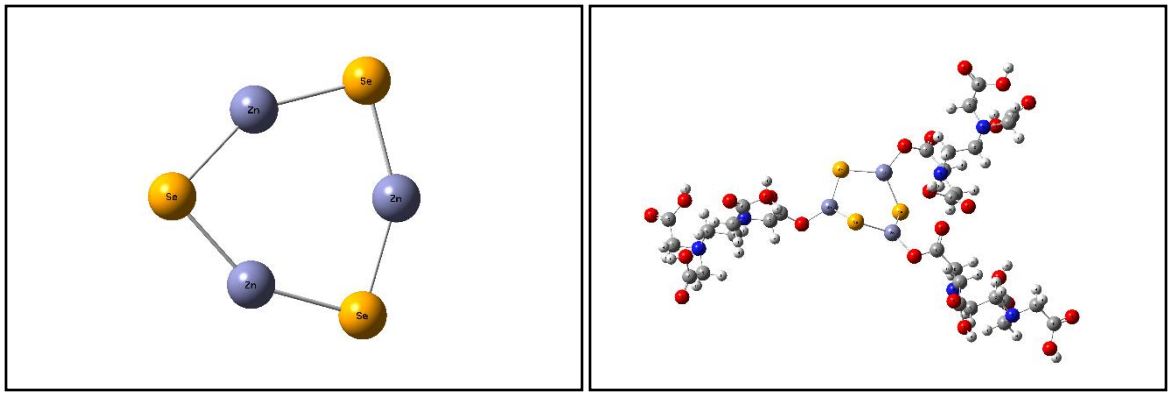

Figure (3.11): The optimized structures of (Zn_3Se_3) before adding EDTA (a), and after adding EDTA (b) using the DFT method with basis set 6-311G**.

3.3.2 Total Energy

Using the B3LYP method, the electronic energy was obtained. The value of the total electronic energy of the Zn_3Se_3NPs and Zn_3Se_3NPs/EDTA are found to be (-12542.628and -15846.135) Hartree, respectively indicating that the second value to a stronger structure. This is due to the complexity of structure and the overlap of orbitals between the O atom and Zn atom. Furthermore, Tables (3.1) and (3.2) present the properties summary of Gaussian calculations for mentioned two molecules involving electronic and thermal characterizations at the stable structure conditions.

Table (3.1): Overview properties of Zn_3Se_3 composite by RB3LYP method and 6-311G (d,p) basis set.

Properties	Numerical values	Unit
Calculation Type	FREQ	
Calculation Method	RB3LYP	
Basis Set	6-311G(d,p)	
Charge	0	
Spin	Singlet	
Solvation	sctf=check	
Electron Energy	-12542.628	Hartree
RMS Gradient Norm	0.000138	Hartree/Bohr
Imaginary Freq	0	
Dipole Moment	0.003297	Debye
Polarizability (α)	140.0223	a.u
Imaginary Freq	0	
Temperature	298.150	Kelvin
Pressure	1.00000	Atm

Table (3.2): Overview properties of Zn_3Se_3/EDTA composite by RB3LYP method and 6-311G (d,p) basis set.

Properties	Numerical values	Unit
Calculation Type	FREQ	
Calculation Method	RB3LYP	
Basis Set	6-311G(d,p)	
Charge	0	
Spin	Singlet	
Electron Energy	-15846.135	Hartree
RMS Gradient Norm	0.000	Hartree/Bohr
Imaginary Freq	0	
Dipole Moment	12.4488	Debye
Polarizability (α)		a.u
Temperature	298.150	Kelvin

3.4 Electronic Properties

3.4.1 HOMO–LUMO Energy Gab

Their significance as quantum mechanical descriptors stems from their ability to regulate a wide range of chemical reactions. The base set B3LYP 6_31G** was used to compute the Homo Lumo energies for the PC. The polarization set d-function for large atoms is represented by the first asterisk above basis G. The polarization of hydrogen atoms' functions is indicated by the second sign, which is sometimes required to be represented as 6-311G (d,p). The electrons in the lumo orbitals are vacant because they are inherently preserved in the homo ground state. The reason for this is that lumino orbitals have greater energy than homo orbitals. There are two electrons with alpha (ms = 1 /2) or beta (ms = − 1 /2) spin in the electron-occupied MO orbitals, which results in Zero net spin Since all of the alpha and beta electrons are located in the same orbital, the lack of unpaired electrons serves as evidence that there is zero multiplicity and zero total spin. The energy gap (Eg), as shown in Table (3.3), is determined using the following formula:[123].

$$E\boldsymbol{g} = E_{LUMO} - E_{HOMO} \qquad (3.3)$$

Table (3.3): HOMO-LUMO energy values of B3LYP 6_31G** (dp).

Property	Total energy (eV) B3LYP
	Zn_3Se_3
EHOMO	-0.0087404518 Hartree = -0.23784 eV
ELUMO	-0.0073318514 Hartree = -0.19951 eV
Eg	-0.0014086004 Hartree = 0.03833 eV
	Zn_3Se_3/EDTA
EHOMO	-0.0089422 Hartree = -0.19543 eV
ELUMO	-0.00435148 Hartree = -0.05746 eV
Eg	0.00459072 Hartree = 0.13797 eV

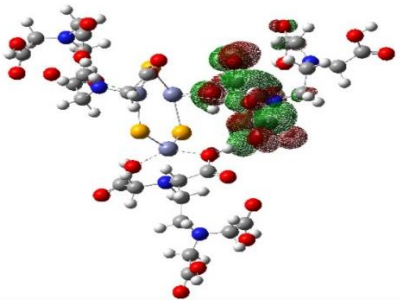

LUMO

E_{LUMO}= -0.0073318514 Hartree

= -0.19951 eV

LUMO

E_{LUMO}= -0.00435148 Hartree

= -0.05746 eV

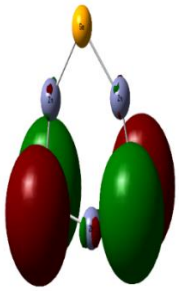

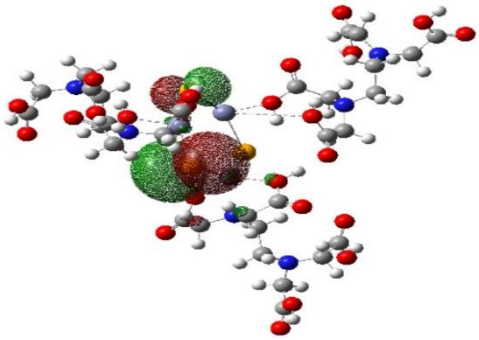

E_{HOMO} = -0.0087404518 Hartree

= -0.23784 eV

E_{HOMO} = - 0.0089422 Hartree

= -0.19543eV

HOMO

Eg = -0.0014086004 Hartree = 0.03833 eV

HOMO

***Eg* = 0.00459072 Hartree = 0.13797 eV**

Figure (3.12): Frontier molecular (HOMO&LUMO) orbitals and E***g*** of Zn_3Se_3cluster (on left), for Zn_3Se_3-EDTA (on right). An increase in E***g*** around eV with adding EDTA polymer indicates the enhancement for nano features.

Figure (3.12) clarifies HOMO and LUMO MOs for mentioned molecules, where the a energy gap E***g*** increases with adding polymer indicating the effect of the EDTA molecule on the ZnSe particles as a capping agent indicating the quantum confinement concept strongly, the greater value for the band gap (the smallest nanoparticle diameter). Fig. (3.13) demonstrates a schematic of molecular orbitals that are filled with electrons (pair of electrons at each level) and the empty levels. Also, Frontier molecular (HOMO&LUMO) orbitals were determined with yellow colour and E***g*** by green dashed lines for Zn_3Se_3-EDTA (a) and Zn_3Se_3 (b)

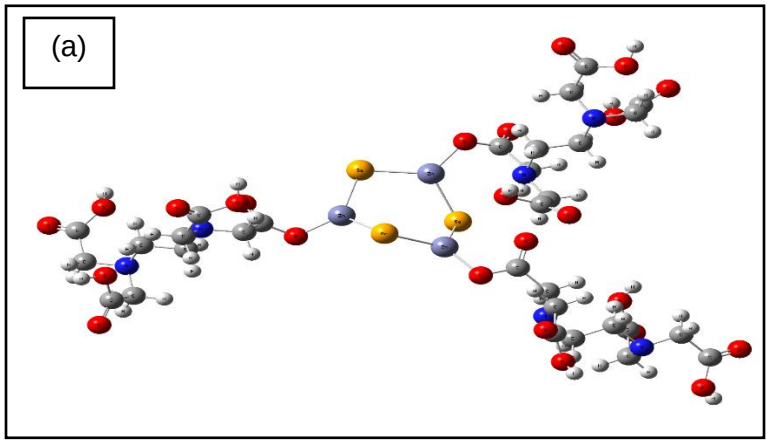

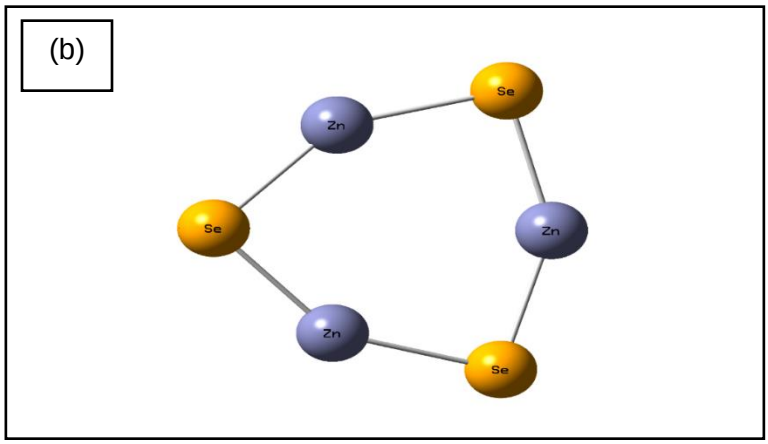

Figure (3. 13): A schematic of molecular orbitals that are filled with electrons and empty levels for Zn3Se3- EDTA (a) and Zn3Se3 (b).

3.4.2 Ionization Potential (IP) and Electron Affinity (EA):

The Homo orbital energy, or Ionization Potential (IP), is a measure of the amount of energy required to break the structural unit of the weakest electron connection to the nucleus. Increasing the ionization energy makes it more challenging to extract the electron, while electron affinity (EA) is related to the Lumo orbital energy which is the amount of energy discharged when an electron is added to a gaseous atom, after identifying the Highest Occupied (HOMO) and Lowest Unoccupied (LUMO) molecular orbitals energies , According to the equations, the values of IP and EA were lower for Zn_3Se_3 0.23784 eV and 0.19951 eV respectively, while the IP and EA values for ZnSe - EDTA were within 0.19543eV and 0.05746eV respectively.

3.4.3 Electronegativity(χ), Electrophilicity(ω)

Electronegativity is a property that describes the ability of molecules, ions, or atoms to attract electrons to them through chemical bonds. The nucleophilic and electrophilic properties of molecules are determined by electrophilicity which is a

measurement of the energy lost during the transfer of an electron from a source to an acceptor. A higher electrophilicity value indicates electron (acceptor) properties. While the low value electronegativity indicates higher capacities of electron donors (donor), the electronegativity values of Zn_3Se_3 and Zn_3Se_3_EDTA with respect to B3LYP were within the limits of 0.21867, 0.126445 eV respectively. The electrophilicity values of Zn_3Se_3 and Zn_3Se_3_EDTA with respect to B3LYP were within the limits of -1.247, - 0.115882 eV.

3.4.4 Global Hardness (η) and Chemical Softness (S)

The concepts of hardness and softness have made it simple to comprehend how chemical systems behave. Hardness controls a molecule's ability to polarize, while softness measures the degree of charge transmission inside that molecule. In terms of interaction, when the arithmetic value of hardness is high, the molecules are fewer interactive and stronger than the delicate molecules. The arithmetic value of hardness and ductility is calculated using B3LYP according to the following equations. the arithmetic value of hardness was for Zn_3Se_3 (0.01917) ,Zn_3Se_3_EDTA (0.068985) While the arithmetic value for ductility was Zn_3Se_3 (52.164) , Zn_3Se_3_EDTA(14.495).

3.4.5 Chemical Potential($\boldsymbol{Cp}$)

It is the energy that can be emitted or absorbed when a change in the number of particles, and Cp can also be known as ferry energy in semiconductors when the system is at a temperature of absolute zero, according to the following equations, the arithmetic value of Chemical Potential was for Zn_3Se_3 (- 0.21867), Zn_3Se_3_EDTA (- 0.126445) The arithmetic value of Chemical Potential is calculated as per the equation given below.

Table (3.4) demonstrates the electronic properties of ZnSe–NPs clusters before and after adding EDTA at room temperature. It was observed an agreement of E$\boldsymbol{g}$ experimentally and theoretically around (3.32) (grey shaded) and (3.54)

eV respectively for the Zn_3Se_3 cluster. In the same manner, concerning Zn_3Se_3 - EDTA, are (eV - Exp) and (eV - DFT), where the experimental findings were obtained from the first part of this work.

Table (3.4): Computed electronic features of Zn_3Se_3 before and after adding EDTA polymer at lab temperature.

Properties	**Zn_3S_3 (DFT)**	**Zn_3S_3 – PEG (DFT)**
EHOMO	- 0.23784	- 0.19543
ELUMO	-0.19951	- 0.05746
Ef / eV	- 0.218675	- 0.126445
E$\boldsymbol{g}$/ eV	0.03833	0.13797
E$\boldsymbol{g}$ / eV	(Exp) 3.32	(Exp) 3.54
IP / eV	0.23784	0.19543
EA / eV	0.19951	0.05746
$\boldsymbol{Cp}$ / eV	- 0.21867	- 0.126445
χ / eV	0.21867	0.126445
η / eV	0.01917	0.068985
S / $(eV)^{-1}$	52.164	14.495

ω / eV	-1.247	- 0.115882

3.4.6 Molecular Electrostatic Potential (MEP) Surface

In order to assess the relationships and non-covalent interactions between molecules at a distance from one another and to look into repulsive or attractive interactions Density of the electron with charge, the molecular electrostatic potential (MEP) diagram [124] ,B3LYP calculations using basis set 6-311G(d,p), and nonlocalized dispersion among the structure's reactions were used . Figure provided a description of these interaction zones for the molecule to depict three areas of contacts based on the electron density function. Blue zones illustrate the nature of hydrogen bonding. Green zones denote the Van der Waals bonding (VdW), while red areas represent repulsive interactions [125]. Moreover, the benefit the molecular electrostatic potential scheme is a helpful instrument to look into how responsive the systems under study are to either nucleophilic or electrophilic assaults, depending on the charge distribution. The color-coded system for two regions is represented by the colored line in Fig. (3.13) supper border: the red and blue regions between -8.065×10-2 and 8.065×10_{-2}, and the Zn3Se3 cluster's range from -4.036×10-4 to 4.036×10-4. The red-colored negative charge concentrations indicate the acceptor of an H-bonding molecule. In contrast, the second zone shows the donor of the H-bonding's positive charge densities in the blue ruler [126]. The MEP diagram (as shown in Figure 3.13) provides a visualization of interaction zones within the molecule, categorizing them based on electron density distribution:

- Blue zones: Represent hydrogen bonding interactions.
- Green zones: Indicate Van der Waals (VdW) bonding.

• Red zones: Correspond to repulsive interactions due to high electron density.

Additionally, the MEP scheme is a valuable tool for examining the system's reactivity to nucleophilic or electrophilic attacks, depending on charge distribution.

The red regions indicate negative charge concentrations, representing H-bond acceptor sites, whereas the blue regions correspond to H-bond donor sites, where positive charge densities are concentrated.

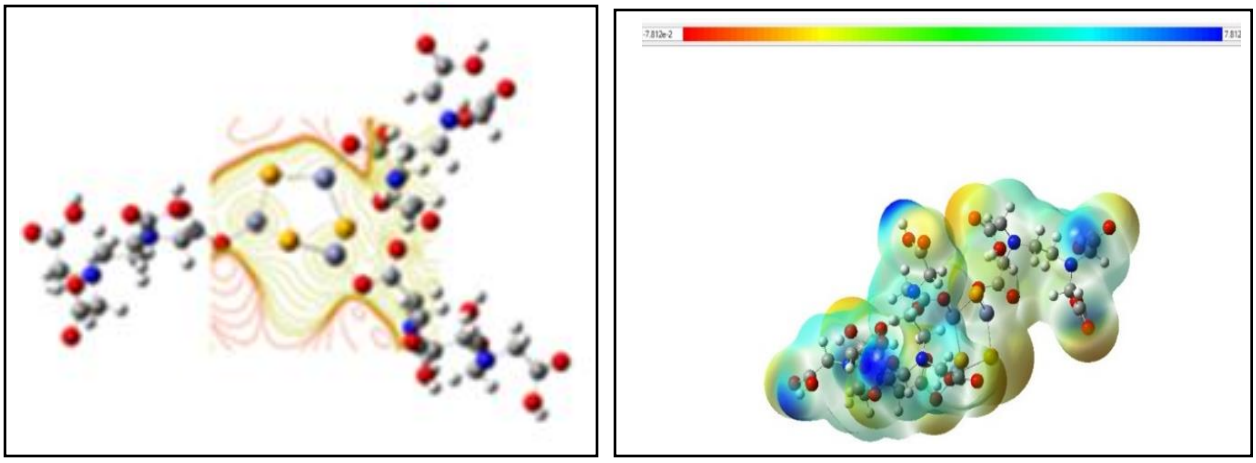

2D-Zn_3Se_3-EDTA 3D-Zn_3Se_3-EDTA

Figure (3.14): charge densities distribution as colour-coded ruler in upper adage (red colour for negative charge and blue for positive), MEP is surface surfaces diagram of Zn_3Se_3 (a) Zn_3Se_3_EDTA.

3.5 Vibrational frequencies

3.5.1 Modes of Vibration of Zn_3S_3 molecule

The number of normal vibration modes of non-linear molecules can be computed using the equation (3N-6), where N is the number of atoms. As a result, for the six-atom Zn3Se3 molecule, twelve vibrational modes were found From the pattern's lowest frequency to its highest mode, these frequencies are shown in Table 3.5. In the range (290.94_291.62) cm-1.

Table (3.5): The range of normal vibrational modes for Zn_3Se_3 from lowest to highest frequency.

No. Mode	Frequency/ cm^{-1}
MODE 1	61.27
MODE2	61.35
MODE3	85.42
MODE4	85.42
MODE5	93.55
MODE6	152.67
MODE7	169.10
MODE8	169.64
MODE9	174.18
MODE10	271.59

MODE11	290.94
MODE12	291.62

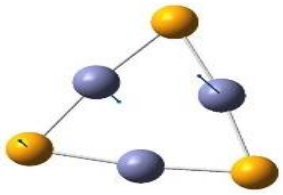

MODE 1

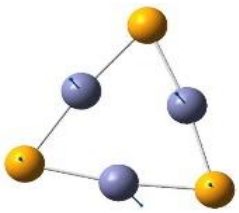

MODE2

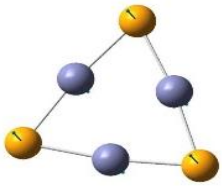

MODE3

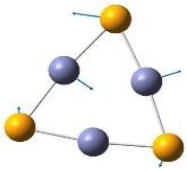

MODE4

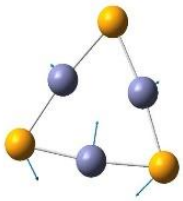

MODE5

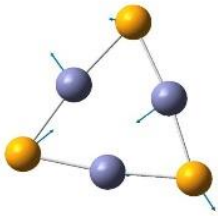

MODE6

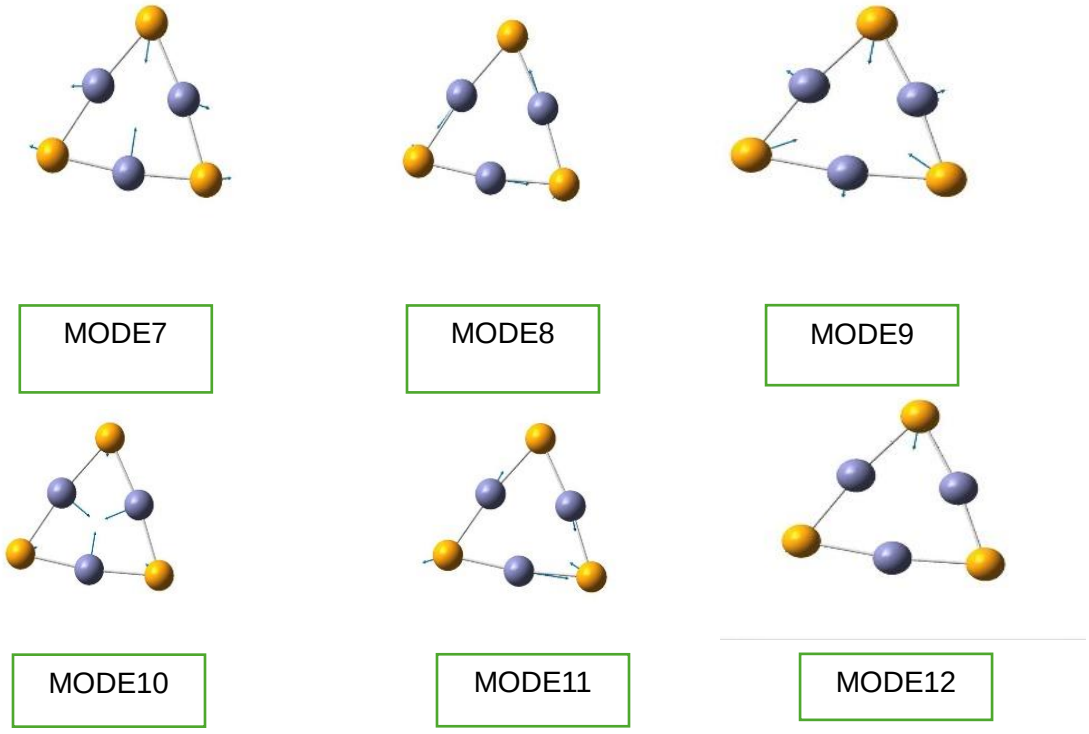

3.5.2 Modes of Vibration of Zn_3Se_3-EDTA molecule

All connections to the polymer of ethylene diamine tetra acetic acid are planar, forming the C1 point symmetry group. The number of normal vibration modes for non-linear molecules can be computed using the equation (3N-6), where N is the number of atoms [127].Therefore, for the 111-atom (Zn_3Se_3-EDTA) molecule, 327 vibrational modes were found. From the lowest frequency of the patterns to the highest mode, these frequencies are displayed in Table 3.5. The frequency range of 3818.35–3852.17 cm^{-1} contains the highest frequency modes (320 and 327). The DFT-B3LYP levels with the 6-311G** .

Table (3.6): Some range of normal vibrational modes for Zn_3Se_3_EDTA from lowest to highest frequency

No. Mode	Frequency/cm-1	No. Mode	Frequency/cm-1	No. Mode	Frequency/cm-1

MODE 1	5.79	MODE 120	555.44	MODE 240	1351.30
MODE 2	6.57	MODE 121	557.89	MODE 241	1351.52
MODE 3	7.56	MODE 122	569.93	MODE 242	1357.48
MODE 4	10.76	MODE 123	576.53	MODE 243	1358.33
MODE 5	11.38	MODE 124	583.65	MODE 244	1361.67
MODE 40	111.44	MODE 160	942.20	MODE 280	1993.10
MODE 41	117.72	MODE 161	943.01	MODE 281	2025.57
MODE 42	121.48	MODE 162	947.37	MODE 282	2035.52
MODE 43	125.56	MODE 163	950.46	MODE 283	2805.25
MODE 44	130.38	MODE 164	952.78	MODE 284	2822.15
MODE 80	368.84	MODE 200	1161.73	MODE 323	3845.21
MODE 81	373.82	MODE 201	1175.70	MODE 324	3845.28
MODE 82	379.83	MODE 202	1179.82	MODE 325	3846.55
MODE 83	384.51	MODE 203	1186.51	MODE 326	3850.51
MODE 84	398.70	MODE 204	1188.44	MODE 327	3852.17

Interpretation of Frequency Ranges

• Low-Frequency Modes:

• Example: MODE 1 (5.79 cm^{-1}), MODE 2 (6.57 cm^{-1}), MODE 3 (7.56 cm^{-1}), etc.

• These low values typically correspond to collective or large-scale movements of the molecule, such as torsions or bends.

• Intermediate-Frequency Modes:

• Example: Modes around MODE 120 (555.44 cm^{-1}) to MODE 244 (1361.67 cm^{-1}).

• These frequencies generally relate to moderate-energy vibrations that might involve bending or stretching of certain bonds.

• High-Frequency Modes:

• Example: The highest frequency modes, such as MODE 323 (3845.21 cm^{-1}) through MODE 327 (3852.17 cm^{-1}).

• These modes are associated with very high energy vibrations, often corresponding to strong bond stretching (like X–H bonds) or other localized, high-frequency vibrations.

Significance in Molecular Analysis

• Spectroscopic Analysis:

• The complete spectrum of 327 vibrational modes provides a detailed fingerprint of the molecule. Each mode can be associated with specific movements within the molecule, which can be observed in vibrational spectroscopy (e.g., IR or Raman spectroscopy).

• Understanding Molecular Dynamics:

• Analyzing these modes helps in understanding the dynamics, stability, and chemical behavior of the Zn_3S_3-EDTA molecule. It provides insight into which bonds are more flexible and which are more rigid, and how the molecule might interact with light or other molecules.

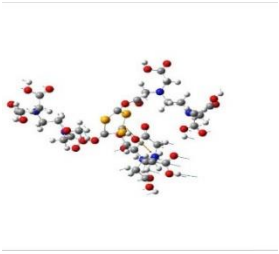

MODE1

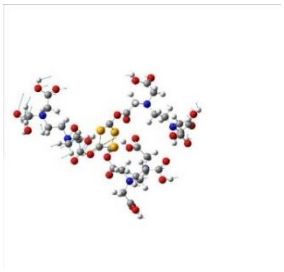

MODE2

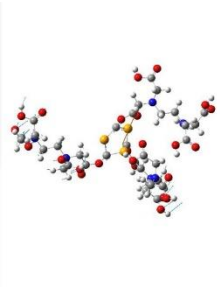

MODE3

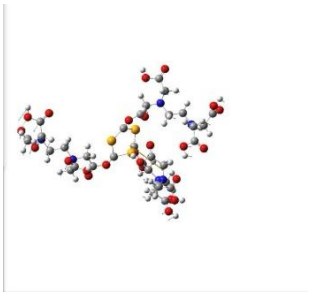

MODE4

MODE5

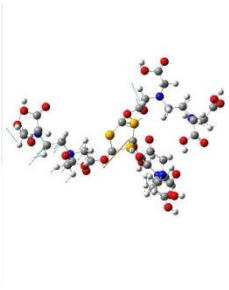

MODE40

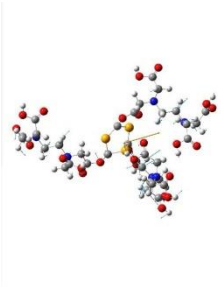

MODE41

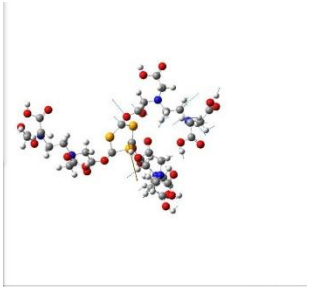

MODE42

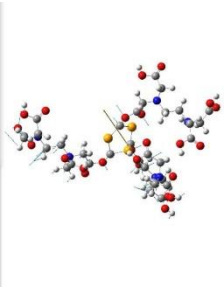

MODE43

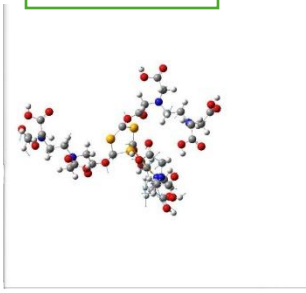

MODE44

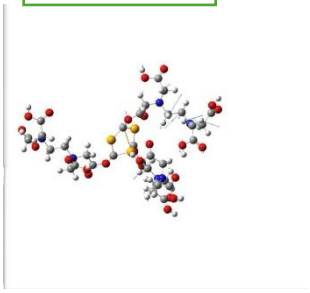

MODE45

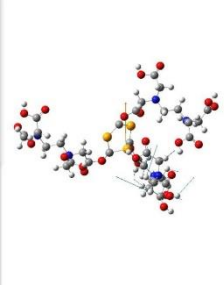

MODE80

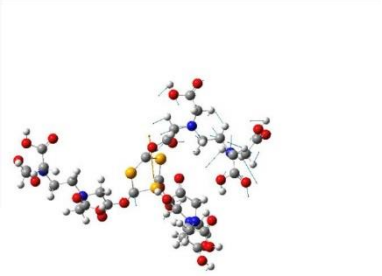

MODE81

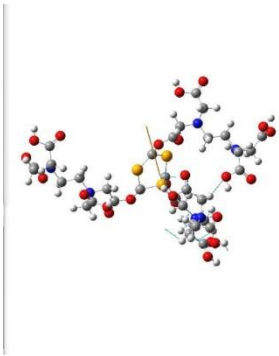

MODE82

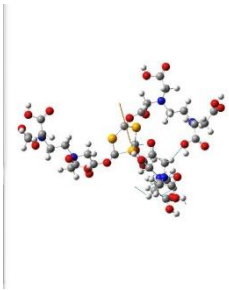

MODE83

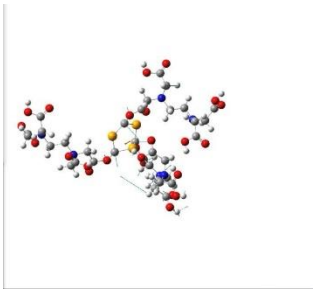

MODE84

MODE120

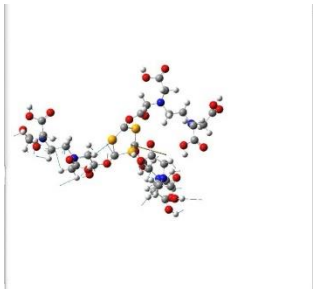

MODE121

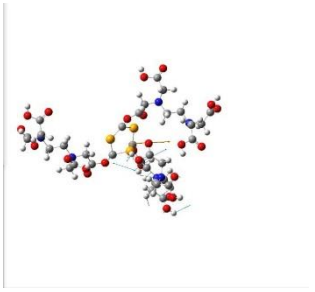

MODE122

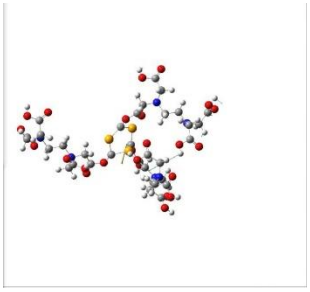

MODE123

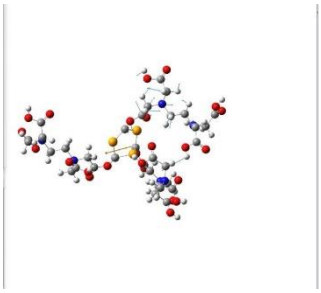

MODE124

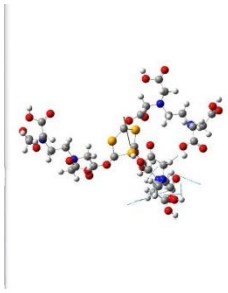

MODE160

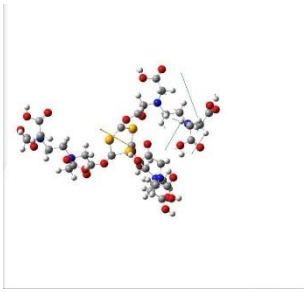

MODE161

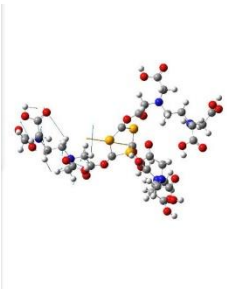

MODE162

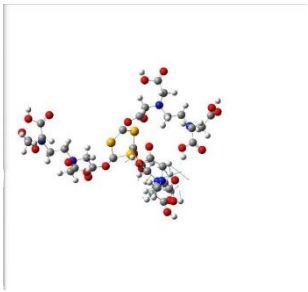

MODE163

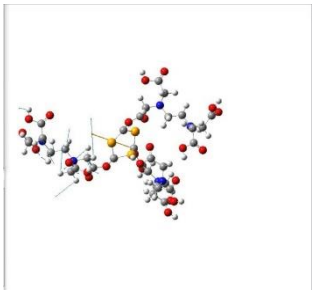

MODE164

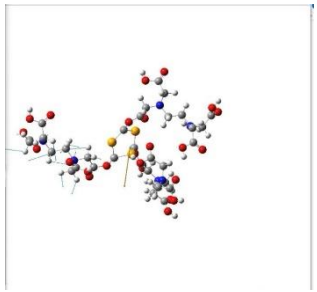

MODE200

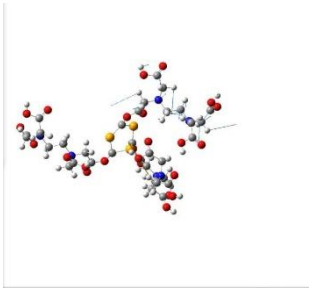

MODE201

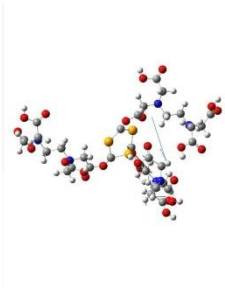

MODE202

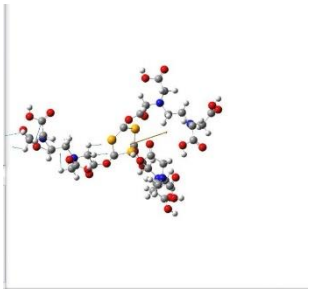

MODE203

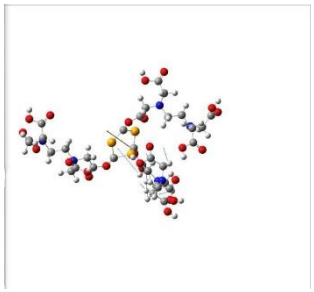

MODE204

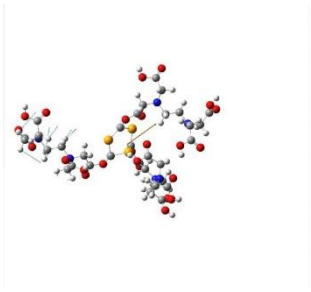

MODE240

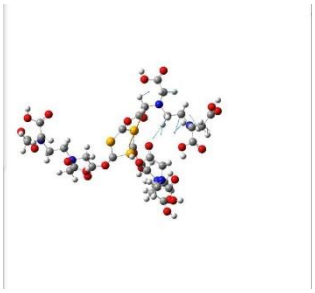

MODE241

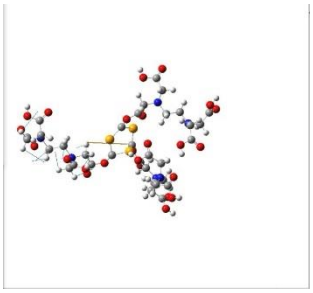

MODE242

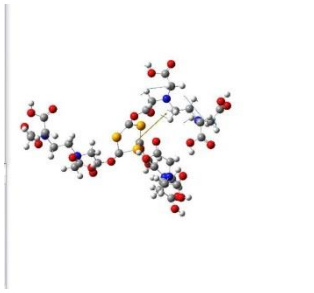

MODE243

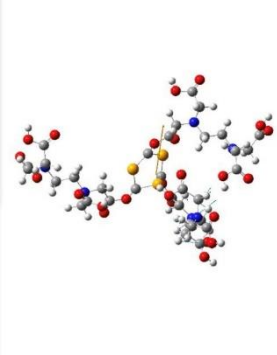

MODE7244

MODE280

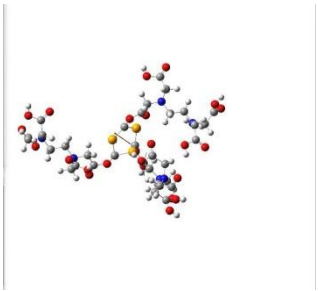

MODE281

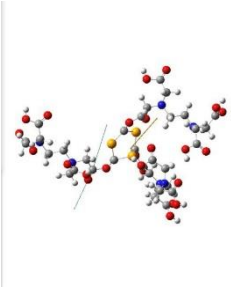

MODE282

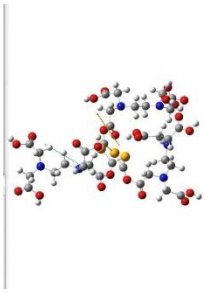

MODE315

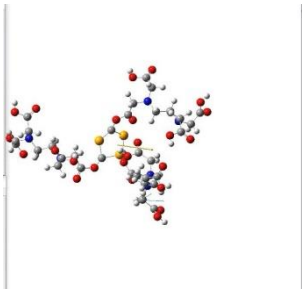

MODE316

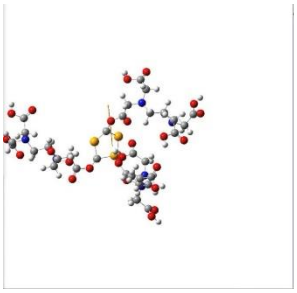

MODE317

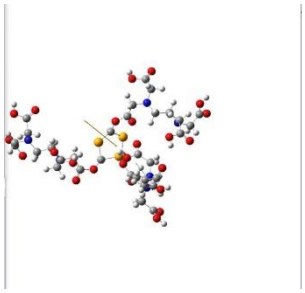

MODE318

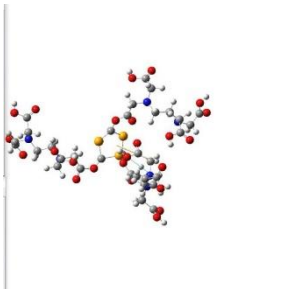

MODE319

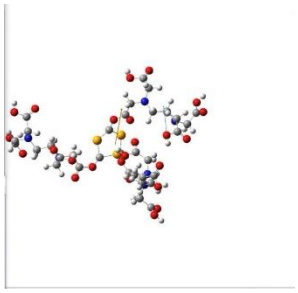

MODE320

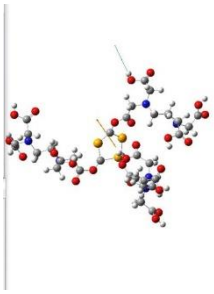

MODE321

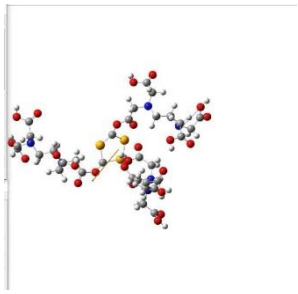

MODE322

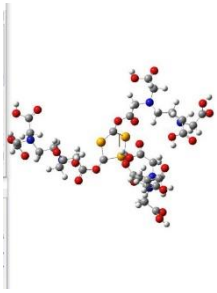

MODE323

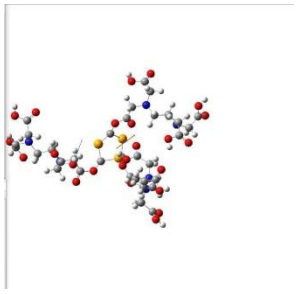

MODE324

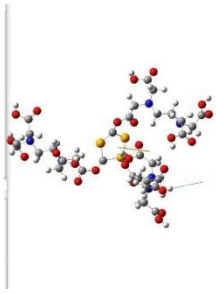

MODE325

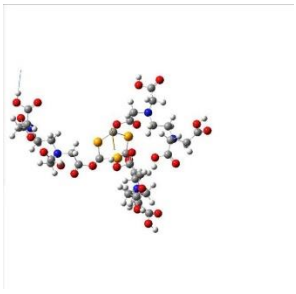

MODE326

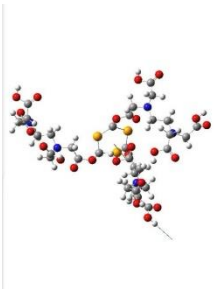

MODE327

3.6 Fourier Trans form Infrared Spectroscopy IR Spectra Analysis

IR spectra of the studied structure were calculated at the range (500 – 4000) cm^{-1} using DFT- B3LYP levels with the 6-311G** basis set. The comparison of the FTIR spectra between theoretical and experimental spectra is illustrated in Figure (3.14) for Zn3Se3 and Zn_3eS_3-EDTA, observing a strong agreement between them.

Zn_3Se_3 (Red Spectrum): The low intensity in the red spectrum indicates a lack of active or functional groups on the surface of the material, which are typically detected in the FTIR range. The absence of prominent absorption peaks suggests the material has a limited number of polar bonds, resulting in weak spectral activity.
Zn_3Se_3-EDTA (Black Spectrum): The distinct absorption peaks are attributed to the addition of EDTA, a chelating agent with functional groups. Prominent Absorption Peaks: 3500–3200 cm^{-1}: Correspond to O-H and N-H stretching vibrations from EDTA groups. 1700–1600 cm^{-1}: Represent carbonyl (C=O) stretching vibrations in EDTA carboxyl groups.1500–500 cm^{-1}: Reflect changes due to interactions between Zn and Se and new bonds formed due to EDTA addition, such as Zn-O or Zn-N. Comparison Between Zn_3Se_3 and Zn_3Se_3-EDTA:
The peaks observed in Zn_3Se_3-EDTA indicate chelation between Zn_3Se_3 and EDTA, where EDTA's carboxyl and amine groups form bonds with Zn.The spectral changes highlight that EDTA addition increases the material's complexity and enriches it with active groups, enhancing absorption in the FTIR range.

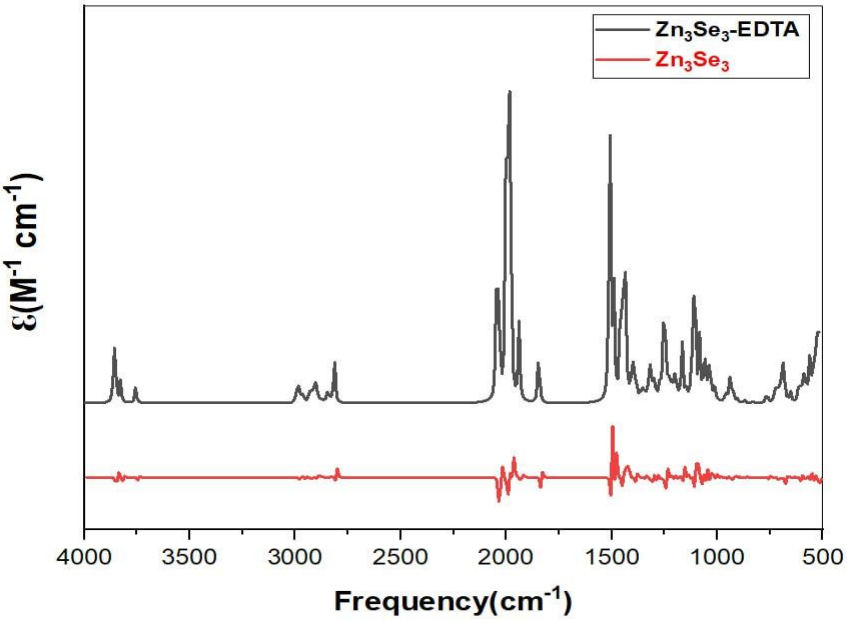

Figure (3.15): Theoretical comparison of IR spectra for Zn_3Se_3 before and after adding EDTA.

3.7 Conclusions

This study focused on the synthesis and comprehensive characterization of both uncapped and EDTA-capped ZnSe nanoparticles, examining their optical, structural, and electronic properties. The main conclusions are summarized as follows:

1. Synthesis of Nanoparticles:

• ZnSe nanoparticles, both uncapped and capped with EDTA, were successfully synthesized using the chemical precipitation technique.

• The introduction of EDTA as a capping agent significantly reduced nanoparticle aggregation, leading to the formation of distinct individual particles as observed in microscopic images.

2. Enhanced Optical Properties:

• The presence of EDTA improved the optical properties of the ZnSe nanoparticles by widening the band gap, indicating an enhancement in their optical performance.

3. Theoretical Investigations:

• For the first time, the structural and electronic features of a Zn_3Se_3 cluster (consisting of three Zn atoms and three Se atoms) were theoretically investigated

using density functional theory (DFT) with the hybrid B3LYP functional and the 6-311G(d,p) basis set.

• These theoretical findings provide a deeper understanding of the molecular structure and electronic behavior of the ZnSe nanoparticles.

4. Spectral Analysis:

• FTIR spectral analysis was conducted, and a detailed comparison was made between the experimental spectra and the theoretical predictions.

• The agreement between experimental data and computational models confirms the reliability of the theoretical approach used.

5. Energy Gap Evaluation:

• The energy gap (E_9) was assessed by calculating the energies of the highest occupied molecular orbital (HOMO) and the lowest unoccupied molecular orbital (LUMO).

• These calculations provide valuable insights into the electronic properties of the synthesized nanoparticles.

3.8 Future Studies:

Some future studies can be suggested:

1. To Study the photo catalytic activity of ZnSe nanoparticles.
2. Possibility of preparing nanofilm from ZnSe and studying its electronic properties
3. To Studying the bioactivity of ZnSe nanoparticles.
4. To show the nonlinear properties of a ZnSe solution using the Z_scan technique.
5. To Study the possibility of using ZnSe nanoparticles in the medical field including cancer treatment or bacterial infections.

References

References:

1. Bayda, S., Adeel, M., Tuccinardi, T., Cordani, M., & Rizzolio, F. (2019). The history of nanoscience and nanotechnology: from chemical–physical applications to nanomedicine. *Molecules*, *25*(1), 112

2. Freestone, I., Meeks, N., Sax, M., & Higgitt, C. (2007). The Lycurgus cup—a roman nanotechnology. *Gold bulletin*, *40*, 270-277.

3. Wagner, F. E., Haslbeck, S., Stievano, L., Calogero, S., Pankhurst, Q. A., & Martinek, K. P. (2000). Before striking gold in gold-ruby glass. *Nature*, *407*(6805), 691-692.

4. Srivastava, S., & Bhargava, A. (2022). *Green nanoparticles: the future of nanobiotechnology* (pp. 1-13). Singapore: Springer.

5. Habibullah, H. (2020). 30 years of atomic force microscopy: creep, hysteresis, cross-coupling, and vibration problems of piezoelectric tube scanners. *Measurement*, *159*, 107776.

6. Li, A., Tyson, J., Patel, S., Patel, M., Katakam, S., Mao, X., & He, W. (2021). Emerging nanotechnology for treatment of Alzheimer's and Parkinson's disease. *Frontiers in Bioengineering and Biotechnology*, *9*, 672594.

7. Raj, S., Khurana, S., Choudhari, R., Kesari, K. K., Kamal, M. A., Garg, N., ... & Kumar, D. (2021, February). Specific targeting cancer cells with nanoparticles and drug delivery in cancer therapy. In *Seminars in cancer biology* (Vol. 69, pp. 166-177). Academic Press.

8. Scodeller, P., & Asciutto, E. K. (2020). Targeting tumors using peptides. *Molecules*, *25*(4), 808.

9. Saeed, N. A., Hamzah, I. H., & Mahmood, S. I. (2021, March). The applications of nano-medicine in the breast cancer therapy. In *Journal of Physics: Conference Series* (Vol. 1853, No. 1, p. 012061). IOP Publishing.

10. Gupta, N., & Malviya, R. (2021). Understanding and advancement in gold nanoparticle targeted photothermal therapy of cancer. *Biochimica et Biophysica Acta (BBA)-Reviews on Cancer*, *1875*(2), 188532.

11.M. B. Tahir, M. Sohaib, M. Sagir and M. Rafique, Encyclopedia of smart materials, 2022, 578.

12. Effiong, D. E., Uwah, T. O., Jumbo, E. U., & Akpabio, A. E. (2019). Nanotechnology in cosmetics: basics, current trends and safety concerns—A review. *Advances in nanoparticles*, *9*(1), 1-22.

13. Motelica, L., Ficai, D., Oprea, O. C., Ficai, A., & Andronescu, E. (2020). Smart food packaging designed by nanotechnological and drug delivery approaches. *Coatings*, *10*(9), 806.

14. Rahman, M. A., Abul Barkat, H., Harwansh, R. K., & Deshmukh, R. (2022). Carbon-based nanomaterials: carbon nanotubes, graphene, and fullerenes for the control of burn infections and wound healing. *Current Pharmaceutical Biotechnology*, *23*(12), 1483-1496.

15. Samykano, M. (2021). Progress in one-dimensional nanostructures. *Materials Characterization*, *179*, 111373.

16. Rahman, B. A., Viphavakit, C., Chitaree, R., Ghosh, S., Pathak, A. K., Verma, S., & Sakda, N. (2022). Optical fiber, nanomaterial, and thz-metasurface-mediated nano-biosensors: A Review. *Biosensors*, *12*(1), 42.

17. Devatha, C. P., & Thalla, A. K. (2018). Green synthesis of nanomaterials. In *Synthesis of inorganic nanomaterials* (pp. 169-184). Woodhead Publishing.

18. Yadav, T. P., & Awasthi, K. (2022). Carbon nanomaterials: fullerene to graphene. *Transactions of the Indian National Academy of Engineering*, *7*(3), 715-737.

19. Abid, N., Khan, A. M., Shujait, S., Chaudhary, K., Ikram, M., Imran, M., ... & Maqbool, M. (2022). Synthesis of nanomaterials using various top-down and bottom-up approaches, influencing factors, advantages, and disadvantages: A review. *Advances in Colloid and Interface Science*, *300*, 102597.

20. Shiltagh, N. M., Ridha, N. J., Hindawi, A. M. A., Tahir, K. J., Madlol, R. A., Alesary, H. F., ... & Watkins, M. J. (2020, December). Studying the optical properties of silver nitrates using a pulsed laser deposition technique. In *AIP Conference Proceedings* (Vol. 2290, No. 1). AIP Publishing.

21. Abed, A. Q., Al Hindawi, A. M., & Alesary, H. F. (2022). Green synthesis of zinc sulfide nanoparticles for the removal of methylene blue dye from aqueous solution. *Nano World J*, *8*, 79-84.

22. Al Hindawi, A. M., Joudah, I., Hamzah, S., & Tarek, Z. (2019, July). Plant extract: safe way for fabrication silver nanoparticles. In *IOP Conference Series: Materials Science and Engineering* (Vol. 571, No. 1, p. 012069). IOP Publishing.

23. GTaka, G., & Das, T. D. (2022, July). Synthesis of ZnO nanoparticles through a simple wet chemical precipitation method. In *IOP Conference Series: Earth and Environmental Science* (Vol. 1042, No. 1, p. 012017). IOP Publishing.

24. Nipa, S. T., Akter, R., Raihan, A., Rasul, S. B., Som, U., Ahmed, S., ... & Rahman, W. (2022). State-of-the-art biosynthesis of tin oxide nanoparticles by chemical precipitation method towards photocatalytic application. *Environmental Science and Pollution Research*, *29*(8), 10871-10893.

25. Baig, N., Kammakakam, I., & Falath, W. (2021). Nanomaterials: A review of synthesis methods, properties, recent progress, and challenges. *Materials advances*, *2*(6), 1821-1871.

26. Ahmed, S., Ahmad, M., Swami, B. L., & Ikram, S. (2016). A review on plants extracts mediated synthesis of silver nanoparticles for antimicrobial applications: a green expertise. *Journal of advanced research*, *7*(1), 17-28.

27. Smith, A. M., & Nie, S. (2010). Semiconductor nanocrystals: structure, properties, and band gap engineering. *Accounts of chemical research*, *43*(2), 190-200.

28. Abed, H., Abduljalil, H. M., & Abdulsattar, M. A. (2020). Analysis of electronic, Raman and UV-vis spectra for Zn11Se11, Zn11S11, and ternary alloys Zn11SnSe11-n (n= 1-11) A DFT/TDDFT study. *Egyptian Journal of Chemistry*, *63*(11), 4235-4241.

29. Bao, Z., Jiang, Z. F., Su, Q., Chiu, H. D., Yang, H., Chen, S., ... & Liu, R. S. (2020). ZnSe: Te/ZnSeS/ZnS nanocrystals: an access to cadmium-free pure-blue quantum-dot light-emitting diodes. *Nanoscale*, *12*(21), 11556-11561.

30. Gao, M., Yang, H., Shen, H., Zeng, Z., Fan, F., Tang, B., ... & Du, Z. (2021). Bulk-like ZnSe quantum dots enabling efficient ultranarrow blue light-emitting diodes. *Nano Letters*, *21*(17), 7252-7260.

31. Elsaeedy, H. I., Hassan, A. A., Yakout, H. A., & Qasem, A. (2021). The significant role of ZnSe layer thickness in optimizing the performance of ZnSe/CdTe solar cell for optoelectronic applications. *Optics & Laser Technology*, *141*, 107139.

32. Boschker, J. E., Spengler, U., Ressel, P., Schmidbauer, M., Mogilatenko, A., & Knigge, A. (2022). Stability of ZnSe-passivated laser facets cleaved in air and in ultra-high vacuum. *IEEE Photonics Journal*, *14*(3), 1-6

33. Zhang, Q., Li, H., Ma, Y., & Zhai, T. (2016). ZnSe nanostructures: synthesis, properties and applications. *Progress in Materials Science*, *83*, 472-535.

34. Jankiewicz, B. J., Jamiola, D., Choma, J., & Jaroniec, M. (2012). Silica–metal core–shell nanostructures. *Advances in colloid and interface science*, *170*(1-2), 28-47.

35. Javed, R., Sajjad, A., Naz, S., Sajjad, H., & Ao, Q. (2022). Significance of capping agents of colloidal nanoparticles from the perspective of drug and gene delivery, bioimaging, and biosensing: An insight. *International Journal of Molecular Sciences*, *23*(18), 10521.

36. Rahal, H. T., Awad, R., Abdel-Gaber, A. M., & Bakeer, D. E. S. (2017). Synthesis, Characterization, and Magnetic Properties of Pure and EDTA-Capped NiO Nanosized Particles. *Journal of Nanomaterials*, *2017*(1), 7460323.

37. Kovács, A., Nemcsok, D. S., & Kocsis, T. (2010). Bonding interactions in EDTA complexes. *Journal of Molecular Structure: THEOCHEM*, *950*(1-3), 93-97.

38. Lee, J. W., Lee, S. M., Huh, Y. D., & Hwang, C. S. (2010). EDTA surface capped water-dispersible ZnSe and ZnS: Mn nanocrystals. *Bulletin of the Korean Chemical Society*, *31*(7), 1997-2002.

39. Rosli, A. N., Zabidi, N. A., & Kassim, H. A. (2014, March). Ab initio calculation of vibrational frequencies of ZnSe and the Raman spectra. In *AIP Conference Proceedings* (Vol. 1588, No. 1, pp. 265-270). American Institute of Physics.

40. Hong, H. S., Kim, M. S., Byun, E. K., & Lee, Y. L. (2020). Facile synthesis and characterization of zinc selenide nanoparticles in aqueous solution at room temperature. *Journal of Crystal Growth*, *535*, 125523.

41. Vijai Anand, K. (2021). Improved structural, optical and photoluminescence properties of EDTA capped zinc sulfide nanoparticles for optoelectronic applications. *Journal of Cluster Science*, *32*(1), 155-161.

42. Wang, X., Zhu, Y., Liu, M., Jiang, G., Hou, G. L., Zhang, M., & Yu, K. (2021). Effect of One-Coordinated Atoms on the Electronic and Optical Properties of ZnSe Clusters. *ACS omega*, *6*(29), 18711-18718.

43. Sridevi, D. V., Ramesh, V., & Sundaravadivel, E. (2021). Ultraviolet light induced dye degradation of methylene blue in the presence of photocatalytic CdSe and ZnSe nanoparticles. *Materials Today: Proceedings*, *42*, 1244-1250.

44. Gupta, P., Solanki, R. G., Patel, P., & Sujata, K. M. (2024). Conversion of ZnSe nanorods to ZnSe/ZnO nanoparticles via air annealing. *MRS Advances*, 1-10.

45. Al-Owaedi, O. A. A. (2016). *Electronic Properties of Nano and Molecular Quantum Devices*. Lancaster University (United Kingdom).

46. Pople, J. A., & Beveridge, D. L. (1970). Molecular orbital theory. *C0., NY*.

47. Capelle, K. (2006). A bird's-eye view of density-functional theory. *Brazilian journal of physics*, *36*, 1318-1343.

48. Hameka, H. F. (2004). *Quantum mechanics: a conceptual approach*. John Wiley & Sons.

49. Röthlisberger, U. (2015). Introduction to electronic structure methods. *EPFL, Lausanne*.

50. Lewars, E. G., & Lewars, E. G. (2016). Semiempirical calculations. Computational Chemistry: Introduction to the Theory and Applications of Molecular and Quantum Mechanics, 421-482.

51.Selman, S.R., The Electronic Structure of Cubic Silicon Carbide Nanocrystals using Ab-initio Large Unit Cell Method. University of Babylon, 2010

52. Wiberg, K. B. (1986). Ab Initio Molecular Orbital Theory by WJ Hehre, L. Radom, P. v. R. Schleyer, and JA Pople, John Wiley, New York, 548pp. Price: $79.95 (1986).

53. Profeta, S., Molecular Modeling. Kirk-Othmer Encyclopedia of Chemical Technology, 2000: p. 1-46

54. Young, D. (2004). *Computational chemistry: a practical guide for applying techniques to real world problems*. John Wiley & Sons.

55. Ziesche, P. (1994). Pair density functional theory—a generalized density functional theory. *Physics Letters A*, *195*(3-4), 213-220.

56. Kohn, W., Becke, A. D., & Parr, R. G. (1996). Density functional theory of electronic structure. *The journal of physical chemistry*, *100*(31), 12974-12980.

57. Capelle, K. (2006). A bird's-eye view of density-functional theory. *Brazilian journal of physics*, *36*, 1318-1343.

58. Young, D. C. (2001). A practical guide for applying techniques to real-world problems. *Computational Chemistry, New York*, *9*, 390.

59. Hohenberg, P., & Kohn, W. (1964). Inhomogeneous electron gas. *Physical review*, *136*(3B), B864.

60. Kohn, W., & Sham, L. J. (1965). Self-consistent equations including exchange and correlation effects. *Physical review*, *140*(4A), A1133.

61. Hohenberg, P., & Kohn, W. (1964). Inhomogeneous electron gas. *Physical review*, *136*(3B), B864.

62. Levy, M. (1979). Universal variational functionals of electron densities, first-order density matrices, and natural spin-orbitals and solution of the v-representability problem. *Proceedings of the National Academy of Sciences*, *76*(12), 6062-6065.

63. Vignale, G., & Rasolt, M. (1987). Density-functional theory in strong magnetic fields. *Physical review letters*, *59*(20), 2360.

64. S. Laricchia, New Developments in Subsystem formulation of Density Functional Theory, Italian: Salento University, 2013

65. Ahmed, T., Noman, M., Manzoor, N., Shahid, M., Abdullah, M., Ali, L., ... & Li, B. (2021). Nanoparticle-based amelioration of drought stress and cadmium toxicity in rice via triggering the stress responsive genetic mechanisms and nutrient acquisition. *Ecotoxicology and Environmental Safety*, *209*, 111829.

66. Sayab, A. A. (2024). *Semiconductor Nanoparticles: Synthesis, Characterization, and Theoritical Analysis of Electronic and Structural Properties* (Doctoral dissertation, University of Kerbala).

Hirvonen Grytzelius, J. (2006). Atomic Force and Scanning Tunneling Microscopy Studies of Single Walled Carbon Nanotubes.

68. Young, H. D., Freedman, R. A., & Ford, A. L. (2020). *University physics with modern physics* (Vol. 191). San Francisco: Pearson.

69. Rahimkhani, P., Ordokhani, Y., & Sabermahani, S. (2023). Hahn hybrid functions for solving distributed order fractional Black–Scholes European option pricing problem arising in financial market. *Mathematical Methods in the Applied Sciences*, *46*(6), 6558-6577.

70. Gasteiger, J., & Engel, T. (Eds.). (2006). *Chemoinformatics: a textbook*. John Wiley & Sons.

71. Cohen, R. D., Wood, J. S., Lam, Y. H., Buevich, A. V., Sherer, E. C., Reibarkh, M., ... & Martin, G. E. (2023). DELTA50: a highly accurate database of experimental 1H and 13C NMR chemical shifts applied to DFT benchmarking. *Molecules*, *28*(6), 2449.

72. Munshi, M. R., Sen, S. K., & Rana, M. Z. Computational Condensed Matter.

73. Al-Owaedi, O. A. A. (2016). *Electronic Properties of Nano and Molecular Quantum Devices*. Lancaster University (United Kingdom).

74. Rahimi, R., & Solimannejad, M. (2022). Empowering hydrogen storage performance of B4C3 monolayer through decoration with lithium: A DFT study. *Surfaces and Interfaces*, *29*, 101723.

75. Huang, E. W., Lee, W. J., Singh, S. S., Kumar, P., Lee, C. Y., Lam, T. N., ... & Liaw, P. K. (2022). Machine-learning and high-throughput studies for high-entropy materials. *Materials Science and Engineering: R: Reports*, *147*, 100645..

76. Adekoya, O. C., Adekoya, G. J., Sadiku, R. E., Hamam, Y., & Ray, S. S. (2022). Density functional theory interaction study of a polyethylene glycol-based nanocomposite with cephalexin drug for the elimination of wound infection. *ACS omega*, *7*(38), 33808-33820.

77. Huang, B., von Lilienfeld, O. A., Krogel, J. T., & Benali, A. (2023). Toward DMC accuracy across chemical space with scalable Δ-QML. *Journal of Chemical Theory and Computation*, *19*(6), 1711-1721.

78. Hussein, T. A., Shiltagh, N. M., Alaarage, W. K., Abbas, R. R., Jawad, R. A., & Nasria, A. H. A. (2023). Electronic and optical properties of the BN bilayer as gas sensor for CO2, SO2, and NO2 molecules: A DFT study. *Results in Chemistry*, *5*, 100978.

79. Tao, Y., Li, Y., & Li, C. (2023). Is there a better way of representing stationary wave functions than basis expansion? *International Journal of Quantum Chemistry*, *123*(9), e27083.

80. Slov, A. C. (2003). Book Review: Exploring Chemistry with Electronic Structure Methods, James B. Foresman and AEleen Frisch. Published by Gaussian, Inc., Pittsburgh, PA, 15106 USA. 354 pages. Soft cover: $42.00 ISBN 0-9636769-3-8, Hard cover: $100.00 ISBN 0-9636769-4-6 Abraham F. Jalbout. *Acta Chim. Slov*, *50*, 159-160.

81. Reel, J. (2016). *A comparative review of computational methods as applied to gold (I) complexes and mechanisms* (Master's thesis, Duke University).

82. Picelli, S., Björklund, Å. K., Reinius, B., Sagasser, S., Winberg, G., & Sandberg, R. (2014). Tn5 transposase and tagmentation procedures for massively scaled sequencing projects. *Genome research*, *24*(12), 2033-2040.

83. Kato, A. S., Burris, K. D., Gardinier, K. M., Gernert, D. L., Porter, W. J., Reel, J., ... & Witkin, J. M. (2016). Forebrain-selective AMPA-receptor antagonism guided by TARP γ-8 as an antiepileptic mechanism. *Nature medicine*, *22*(12), 1496-1501.

84. Müller, M., Hansen, A., & Grimme, S. (2023). ωB97X-3c: A composite range-separated hybrid DFT method with a molecule-optimized polarized valence double-ζ basis set. *The Journal of Chemical Physics*, *158*(1).

85. Rassolov, V. A., Ratner, M. A., Pople, J. A., Redfern, P. C., & Curtiss, L. A. (2001). 6-31G* basis set for third-row atoms. *Journal of Computational Chemistry*, *22*(9), 976-984.

86. Foresman, J., & Frish, E. (1996). Exploring chemistry. *Gaussian Inc., Pittsburg, USA*, *21*.

87. Rana, D., Narbaitz, R. M., Garand-Sheridan, A. M., Westgate, A., Matsuura, T., Tabe, S., & Jasim, S. Y. (2014). Development of novel charged surface modifying macromolecule blended PES membranes to remove EDCs and PPCPs from drinking water sources. *Journal of Materials Chemistry A*, *2*(26), 10059-10072.

88. Zarrouk, A., Zarrok, H., Salghi, R., Hammouti, B., Al-Deyab, S. S., Touzani, R., ... & Hadda, T. B. (2012). A theoretical investigation on the corrosion inhibition of copper by quinoxaline derivatives in nitric acid solution. *International Journal of Electrochemical Science*, *7*(7), 6353-6364.

89. Parida, S. K., Behera, D., & Sahu, S. (2021). A computational quantum chemical and polarizability calculations of liquid crystal 4-cyano-4-pentylbiphenyl with water molecule (H2O). *Journal of Molecular Structure*, *1227*, 129568.

90. Mizera, A., Dubis, A. T., & Łapiński, A. (2022). Density functional theory studies of polypyrrole and polypyrrole derivatives; substituent effect on the optical and electronic properties. *Polymer*, *255*, 125127.

91. Mueller, M. (2002). Fundamentals of Quantum Chemistry.

92. Kantek, F., Kaya, A., & Gezer, N. (2017). The effects of nursing education on professional values: A longitudinal study. *Nurse Education Today*, *58*, 43-46.

93. Pinkerton, E. (2003). Toward specificity in complexity: understanding co-management from a social science perspective. In *The fisheries co-management experience: Accomplishments, challenges and prospects* (pp. 61-77). Dordrecht: Springer Netherlands.

94. Murray, P. J., & Wynn, T. A. (2011). Protective and pathogenic functions of macrophage subsets. *Nature reviews immunology*, *11*(11), 723-737.

95. Chand, P., & Sharma, M. C. (2015). Glacier changes in the Ravi basin, North-Western Himalaya (India) during the last four decades (1971–2010/13). *Global and Planetary Change*, *135*, 133-147.

96. Lingam, C. B., & Tewari, S. P. (2013). Theoretical studies on aminoborane oligomers. *Computational and Theoretical Chemistry*, *1020*, 151-156.

97. Segneanu, A. E., Gozescu, I., Dabici, A., Sfirloaga, P., & Szabadai, Z. (2012). *Organic compounds FT-IR spectroscopy* (Vol. 145). Romania: InTech.

98. Ayala, P. Y., & Schlegel, H. B. (1998). Identification and treatment of internal rotation in normal mode vibrational analysis. *The Journal of chemical physics*, *108*(6), 2314-2325.

99. Hokenek, S. (2009). Characterization of conductive polycarbonate films.

100. Shen, W. K., Sheldon, R. S., Benditt, D. G., Cohen, M. I., Forman, D. E., Goldberger, Z. D., ... & Yancy, C. W. (2017). 2017 ACC/AHA/HRS guideline for the evaluation and management of patients with syncope: a report of the American College of Cardiology/American Heart Association Task Force on Clinical Practice Guidelines and the Heart Rhythm Society. *Journal of the American College of Cardiology*, *70*(5), e39-e110.

101. Frisch, M. J., Trucks, G. W., Schlegel, H. B., Scuseria, G. E., Robb, M. A., Cheeseman, J. R., ... & Foresman, J. B. (2016). 16, Revision C. 01, Gaussian. *Inc., Wallingford CT*, *2016*.

102. Hiscocks, J., & Frisch, M. J. (2009). *Gaussian 09: IOps Reference*. M. Caricato, & M. J. Frisch (Eds.). Wallingford, CT, USA: Gaussian.

103. R. Gaussian, G. Trucks, H. Schlegel, G. Scuseria, M. Robb, J. Cheeseman, G. Scalmani, V. Barone, B. Mennuci, G. Petersson, H. Nakatsuji, M. Caricato, X. Li, H. Hratchian, A. Izmaylov, J. Bloino, G. Zheng, J. Sonnenberg, M. Hada, D. Fox, Gaussian, Inc., Wallingford CT (2004).

104. Ahmed, J.T.m., Density Function Theory Calculations For donor-bridge-accepter molecular systems. University of Babylon, 2014.

105. Kim, B. G. (2010). *Mercury-containing species and carbon dioxide adsorption studies on inorganic compounds using density functional theory*. The University of Arizona.

106. Kovács, A., Nemcsok, D. S., & Kocsis, T. (2010). Bonding interactions in EDTA complexes. *Journal of Molecular Structure: THEOCHEM*, *950*(1-3), 93-97.

107. Sultana, S., Alzahrani, N., Alzahrani, R., Alshamrani, W., Aloufi, W., Ali, A., ... & Siddiqui, N. A. (2020). Stability issues and approaches to stabilised nanoparticles-based drug delivery system. *Journal of drug targeting*, *28*(5), 468-486.

108. Gupta, T., & Chauhan, R. P. (2021). Structural, morphological, and electrical properties of ZnSe nanostructures: Effects of Zn precursors. *Surfaces and Interfaces*, *25*, 101196.

109. Nguyen, V. K., Pham, D. K., Tran, N. Q., Dang, L. H., Nguyen, N. H., Nguyen, T. M., ... & Luong, B. T. (2022). Effect of stabilizers on Mn ZnSe quantum dots synthesized by using green method. *Green Processing and Synthesis*, *11*(1), 327-337.

110. Matras-Postołek, K., Sovinska, S., & Węgrzynowicz, A. (2019). Synthesis and characterization of ZnSe and ZnSe: Mn nanosheets and microflowers with high photoactive properties by microwave-assisted method. *Chemical Engineering and Processing-Process Intensification*, *135*, 204-216.

111. Vijai Anand, K. (2021). Improved structural, optical and photoluminescence properties of EDTA capped zinc sulfide nanoparticles for optoelectronic applications. *Journal of Cluster Science*, *32*(1), 155-161.

112. Ahamed, A. J., Ramar, K., & Kumar, P. V. (2016). Journal of Nanoscience and Technology. *Journal of Nanoscience and Technology*, *2*(3), 148-150.

113. Abed, A. Q., Al Hindawi, A. M., & Alesary, H. F. (2022). Green synthesis of zinc sulfide nanoparticles for the removal of methylene blue dye from aqueous solution. *Nano World J*, *8*, 79-84.

114. Senthilkumar, K., Kalaivani, T., Kanagesan, S., & Balasubramanian, V. (2012). Synthesis and characterization studies of ZnSe quantum dots. *Journal of Materials Science: Materials in Electronics*, *23*, 2048-2052.

115. Varma, V. R., Sanjeev, G., Hegde, S., Shruthi, K. N., Kumar, M., Sahana, G. K., & Sushma. (2024). Synthesis and optimization of MPA-capped ZnSe quantum dots for photo-activation based applications. *Journal of Materials Science: Materials in Electronics*, *35*(21), 1474.

116. Shi, L., Wang, C., Wang, J., Fang, Z., & Xing, H. (2016). Temperature-dependent Raman scattering of ZnSe nanowires. *Advances in Materials Physics and Chemistry*, *6*(12), 305-317.

117. Toufanian, R., Zhong, X., Kays, J., Saeboe, A., & Dennis, A. (2020). ZnSe Quantum Dots: Determination of Molar Extinction Coefficient for UV to Blue Emitters.

118. Jubu, P. R., Yam, F. K., Igba, V. M., & Beh, K. P. (2020). Tauc-plot scale and extrapolation effect on bandgap estimation from UV–vis–NIR data–a case study of β-Ga2O3. *Journal of Solid-State Chemistry*, *290*, 121576.

119. Ji, J., Ge, Y., Balsam, W., Damuth, J. E., & Chen, J. (2009). Rapid identification of dolomite using a Fourier Transform Infrared Spectrophotometer (FTIR): A fast method for identifying Heinrich events in IODP Site U1308. *Marine Geology*, *258*(1-4), 60-68.

120. Turki, Z. T., Al Hindawi, A. M., & Shiltagh, N. M. (2022). Green synthesis of CdS nanoparticles using avocado peel extract. *NanoWorld Journal*, *8*, 73-78.

121. Turki, Z. T., Hindawi, A. M. A., & Shiltagh, N. M. (2023, December). Fabrication and characterization of cadmium sulfide nanoparticles using chemical precipitation method. In *AIP Conference Proceedings* (Vol. 2834, No. 1). AIP Publishing.

122. Becke, A. D. (1988). 5648;(c) C. Lee, W. Yang, RG Parr. *Phys. Rev. B*, *37*, 785.

123. Cremer, D. (1988). Pros and cons of σ-aromaticity. *Tetrahedron*, *44*(24), 7427-7454.

124. Shamim, M., Perveen, M., Nazir, S., Hussnain, M., Mehmood, R., Khan, M. I., & Iqbal, J. (2021). DFT study of therapeutic potential of graphitic carbon nitride

(g-C3N4) as a new drug delivery system for carboplatin to treat cancer. *Journal of Molecular Liquids*, *331*, 115607.

125. Noureddine, O., Issaoui, N., Medimagh, M., Al-Dossary, O., & Marouani, H. (2021). Quantum chemical studies on molecular structure, AIM, ELF, RDG and antiviral activities of hybrid hydroxychloroquine in the treatment of COVID-19: Molecular docking and DFT calculations. *Journal of King Saud University-Science*, *33*(2), 101334.

126. Adekoya, O. C., Adekoya, G. J., Sadiku, E. R., Hamam, Y., & Ray, S. S. (2022). Application of DFT calculations in designing polymer-based drug delivery systems: An overview. *Pharmaceutics*, *14*(9), 1972.

127. Huang, B., von Lilienfeld, O. A., Krogel, J. T., & Benali, A. (2023). Toward DMC accuracy across chemical space with scalable Δ-QML. *Journal of Chemical Theory and Computation*, *19*(6), 1711-1721.

الخلاصة

يُحضَّر سيلينيد الزنك (ZnSe) باستخدام طريقة الترسيب الكيميائي. وقد تم تأكيد تكون جسيمات ZnSe النانوية في غياب وحضور مادة EDTA باستخدام مجهر المسح الإلكتروني بالانبعاث الميداني(FE-SEM) ، وتحليل الطيف بالأشعة السينية المشتتة للطاقة(EDX) ، وتقنية تحويل فورييه للأشعة تحت الحمراء(FT-IR) ، وحليل حيود الأشعة السينية(XRD) ، وتحليل مطياف رامان. كما تم استخدام الطيف المرئي-الأشعة فوق البنفسجية لتقدير طاقة فجوة الحزمة، وتبين أنها (3.32 eV و3.54 eV) لكلٍ من جسيمات ZnSe غير المُغطاة وتلك المُغطاة بـ .EDTAوتم دراسة الخصائص البصرية للمواد النانوية المحضرة سواء كانت مغطاة بالبلمرة أم لا. ثم تم الانتقال إلى الجزء النظري من العمل باستخدام البرامج المتخصصة مثل Gaussian View 6.0 و Gaussian 09Wو15.0 ChemDraw Professional، بهدف مقارنة نتائج الجزء العملي مع النتائج النظرية.

في هذه الدراسة، تعمل مادة EDTA كعامل تغليف. وقد تم إعداد العينات وتحليلها باستخدام مجموعة متنوعة من التقنيات التحليلية، حيث أظهرت النتائج أن EDTA يعمل كعامل تغليف فعال ينظم حجم الجسيمات النانوية ويمنع تكتلها، مما يؤدي إلى زيادة استقرار مادة .ZnSe وكشفت قياسات مطياف UV-Vis عن فجوة بصرية مناسبة للتطبيقات الكهرضوئية، مع تأثير EDTA على الخصائص البصرية للمادة. كما أظهر تحليل XRD تكون بنية بلورية مرتبة مع تقليل ملحوظ في حجم البلورة نتيجة لتأثير خصائص EDTA على سيلينيد الزنك.

وقد تحسنت نقاوة المادة بفضل عملية التغليف، التي منعت أيضاً تكون الملوثات غير المرغوب فيها، كما تبين من بيانات FT-IR ومطياف رامان التي أظهرت بوضوح وجود تفاعل بين ZnSe و .EDTAوعندما خضعت العينة المحضرة لتحليلEDS ، تبين توزيع العناصر بشكل متجانس.

تمت أيضًا دراسة إعدادات الطاقة الحدية منخفضة الميل بدقة في التكوينات الهندسية الجزيئية لمجموعة Zn_3Se_3، قبل وبعد إضافة حمض الإيثيلين ديامين تترأأسيتك .(EDTA) وقد تم فحص نظرية الدوال الكثيفة والخصائص الهيكلية والإلكترونية لمركب Zn_3Se_3-EDTA باستخدام حسابات DFT/B3LYP مع مجموعة الأساس 6-113 .(d, p) Gكما تم فحص ترددات أوضاع الاهتزاز الشاملة بطريقة منهجية باستخدام توزيع الطاقة الكامنة كأساس للتحليل. وتم تقييم الاستنتاجات النظرية الخاصة بالقمم النشطة للمجموعات الوظيفية O–H و N–Hو C=Oو Zn–Seباستخدام أطياف FT-IR للمركبات المحددة. وتم حساب فجوة الطاقة (Eg) الناتجة عن الفرق بين هذه المدارات ورسمها باستخدام المدارات الجزيئية الأمامية (HOMO) والمدارات الجزيئية الخلفية .(LUMO) وقبل وبعد إضافةEDTA ، تم تحقيق مؤشر واعد بزيادة قيمة Eg من 0.03833 eV إلى 0.13797eV ، مما يبرز تأثير عامل التغليف للمركب العضوي على سطح .Zn_3Se_3 بالإضافة إلى ذلك، تم تحديد شكل وتوزيع الجهد الكهروستاتيكي الجزيئي (سطح وتوزيع الكنتور) لكل من Zn_3S_3 وZn_3S_3_EDTA، إلى جانب الخصائص الإلكترونية للهياكل المذكورة، والتي شملت القدرة التأيين(IP) ، والألفة الإلكترونية (EA)، وEf، وفجوة الطاقة(Eg) ، والجهد الكيميائي(Cp) ، والكهربية(χ) ، والصلابة العالمية(η) ، والمرونة الكيميائية(S) ، والكهربائية(ω) ، والنيوكليوفيلية.(ε)
خلصت الدراسة إلى أن خصائص المادة النانوية، مثل الاستقرار والتحكم في الحجم، تتحسن بشكل كبير عند استخدام EDTA كعامل تغليف أثناء تصنيع.ZnSe

جامعة كربلاء

كلية التربية للعلوم الصرفة

قسم الكيمياء

الدراسة النظرية والتجريبية لخصائص الهياكل النانوية لمادة شبه الموصلة ZnSe

رسالة مُقدمة إلى مجلس كلية التربية للعلوم الصرفة / جامعة كربلاء وهي جزء من متطلبات نيل درجة الماجستير في الكيمياء

كُتبت بواسطة

شرمين صاحب حسين عواد

بإشراف

أ. م. د. عــلا مهدي الهنداوي

أ. م. د. جهان حميد عبد الامير

1446 هـ

2024 م